Westinghouse

Westinghouse Electric Company
Nuclear Plant Projects
P.O. Box 355
Pittsburgh, Pennsylvania 15230-0355
USA

U.S. Nuclear Regulatory Commission
ATTN: Document Control Desk
Washington, D.C. 20555

Direct tel: 412-374-5355
Direct fax: 412-374-5456
e-mail: corletmm@westinghouse.com

Your ref: Project 711
Our ref: DCP/NRC1510

June 6, 2002

Subject: Reference for AP1000 Probabilistic Risk Assessment

Attached please find the report titled "Quantification of Limits to Coolability in ULPU-2000 Configuration IV," CRSS-02.05.3 dated May 23, 2002. An earlier version of this report was referenced in Chapter 39 of the AP1000 Probabilistic Risk Assessment (PRA). This revision of the report incorporates minor editorial changes. The reference in Chapter 39 of the AP1000 PRA will be updated to reflect this revision of the report.

Please contact me if you have further questions on this issue.

Very truly yours,

M. M. Corletti
Passive Plant Projects & Development
AP600 & AP1000 Projects

/Attachment
1.) Quantification of Limits to Coolability in ULPU-2000 Configuration IV

D063

CRSS-02.05.3
May 23, 2002

QUANTIFICATION OF LIMITS TO COOLABILITY IN ULPU-2000 CONFIGURATION IV

T. G. Theofanous, J.P. Tu, T. Salmassi, T.N. Dinh

Center for Risk Studies and Safety
University of California, Santa Barbara

QUANTIFICATION OF LIMITS TO COOLABILITY IN ULPU-2000 CONFIGURATION IV

T.G. Theofanous, J.P. Tu, T. Salmassi and T.N. Dinh

Center for Risk Studies and Safety
Department of Chemical Engineering
University of California, Santa Barbara
Santa Barbara, CA 93106

ABSTRACT

This report provides experimental quantification of limits to coolability in ULPU-2000 test facility. The ULPU facility was designed to study critical heat flux from a full-scale slice of a hemispherical reactor pressure vessel under externally flooding conditions. While in ULPU Configuration III we simulated the reactor vessel reflecting thermal insulation as normally is (for the AP600 design, for example) the purpose of the Configuration IV experimental campaign is to optimize (coolability) performance by streamlining the flow path between the reactor vessel and reflecting insulation. The specific idea came from scoping tests conducted in preparation for this work. In the present test program the flow path was created by a curved baffle (same curvature as the vessel) that was hinged at the upper end ($\theta \sim 90^{o}$), while its lower end ($\theta \sim 0^{o}$) was allowed to take various positions at distances of 2½, 5, 7 and 9 inches from the "reactor vessel". The experiments performed in ULPU-2000 Configuration IV show a significant enhancement of coolability. In the lowermost region ($\theta = 0\text{-}10^{o}$), an enhancement of ~60% was found. In an upper region ($\theta \sim 80^{o}$), the present experiments show an improvement of ~40%. The report also discusses potentials for further improvement and the facility modifications needed to attain and demonstrate this improvement.

TABLE OF CONTENTS

NOMENCLATURE

q	heat flux, kW/m^2
T	temperature, ^oC
θ	angular position from the lower pole, degree (^{o})

ACRONYMS

ACOPO	a IVR-related 1/2 -scale natural convection facility at UCSB
CHF	critical heat flux
CRSS	Center for Risk Studies and Safety at UCSB
IVR	in-vessel retention
UCSB	University of California, Santa Barbara
ULPU	a IVR-related full-scale boiling heat transfer facility at UCSB

1. INTRODUCTION

In-Vessel Retention (IVR) of molten core debris by means of external reactor vessel flooding as a keystone of severe accident management was introduced a little over a decade ago (Theofanous, 1989) during the PI's work for the Loviisa nuclear power plant in Finland—a Soviet VVER-440 in a Westinghouse ice-condenser containment. The whole aproach has been accepted by the Finnish regulatory authority (STUK), and it is now fully implemented, including extensive plant modifications (Tuomisto and Theofanous, 1994). At about the same time, and independently, the idea was also introduced for managing severe accidents in the AP600 (Henry and Fauske, 1993). The complete case in support of Westinghouse's AP600 (advanced passive light water reactor) licensing certification was finally made by the PI and his coworkers at UCSB's Center for Risk Studies and Safety (CRSS), and certification by the US Nuclear Regulatory Commission was received in 1998 (NUREG-1512). A successful IVR would terminate a severe accident, passively, with the core in a stable, coolable configuration (within the lower head), thus avoiding the largely uncertain accident evolution with the molten debris on the containment floor. This passive plant design is being upgraded by Westinghouse to the AP1000, a 1000 MWe plant very similar to the AP600. The severe accident management approach is very similar too, including In-Vessel Retention as the keystone feature, and initial evaluations indicate that this would be feasible at this higher power as well.

The critical elements for both the Loviisa and AP600 work were the definition of natural-convection-induced thermal loads on the inside, and the coolability limits on the outside. The technology base in both respects was established by the ACOPO and ULPU-2000 experiments, respectively (and their predecessors COPO and ULPU for the Loviisa case). In-Vessel Retention has received a great deal of attention internationally in the meanwhile, with two dedicated specialists (international) meetings (Grenoble, 1994; Garshing, 1998), and an internationally-funded program at Kurchatov (the RASPLAV program) for special-effects prototypic materials tests (Asmolov, 1998). For example, on critical heat flux, we now have also the SULTAN experiment at Grenoble, a long, straight tiltable channel with a heating strip (Rouge, 1997), and a small scale ($\cong$1/15) replica of a lower head at Penn State (Cheung and Liu, 1999). For natural convection, we also now have the BALI experiment at Grenoble (Bonnet and Seiler, 1999), a full-size two-dimensional slice of a lower head, and the COPO-II experiment at Fortrum (Finland), a 1/2-scale two-dimensional slice of the torospherical shape of the Loviisa lower head (Helle,1999). All this additional work has shown that the ACOPO and ULPU-2000 continue to define the state of the art in their respective critical roles in support of In-Vessel Retention.

The basic result from the ULPU-2000 tests that included a baffle to simulate the thermal insulation geometry in the AP600 is the critical heat flux as a function of angular position – it is given by Eq. (1) and illustrated in Figure 1.

$$q_{cr} = 490 + 30.2\theta - 0.888\theta^2 + 0.0135\theta^3 - 6.65\cdot 10^{-5}\,\theta^4 \ \ \mathrm{kW/m^2} \qquad (1)$$

where θ is the angular position expressed in degrees starting from the lower pole (0°).

In-Vessel Retention is assured if the thermal loading from the melt is exceeded by the coolability limit (the critical heat flux—CHF) on the outside, everywhere on the lower head of the reactor pressure vessel. They both depend strongly on the angular position around the lower head, so the "everywhere" refers to all angular positions, from the very bottom (position 0°) to the very edge (position 90°). From experience with the AP600 design, we know that this thermal-load-to-coolability margin is most comfortable in the lower portions, and that it reaches a minimum value at the position that corresponds to the top of the molten fuel pool (typically around 80 °). Also, we know that this margin decreases as reactor power (decay heat) increases. It is quite comfortable at 1933 MWt (AP600), but at 3400 MWt (AP1000) it drops already to under 10%, so on the basis of existing technology, it may be hard to justify an IVR-based severe accident management approach. Notably, from the AP600 study and a preliminary study for AP1000, it become evident that an important element relative to the IVR margin is the peaking of thermal load observed in the upper positions, including the metal layer. There is not much one can do here about the process itself to reduce these thermal loads. However, if IVR is to be successful in AP1000, this margin must be significantly improved, and so must, in fact, be its definition. The improvement can only come from the outside; that is, by improving the coolability limit. This places the focus on ULPU, and the need to revisit its performance in more detail as we examine potentials for improving coolability.

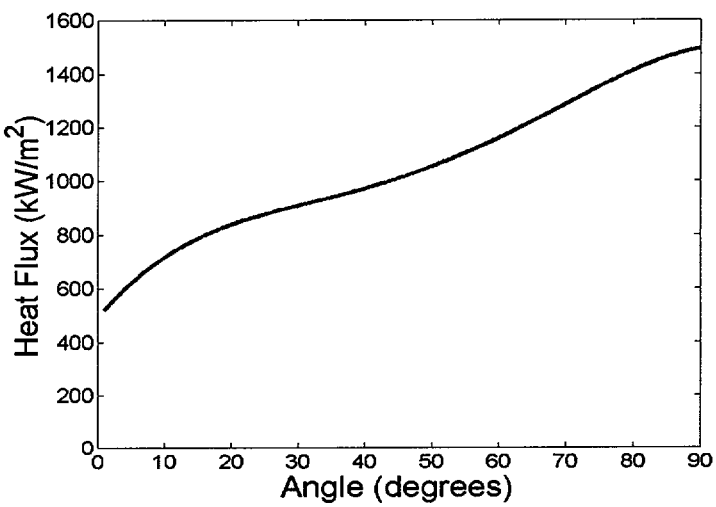

Figure 1. Critical heat flux as a function of angular position on a large scale hemispherical surface, as determined by tests in ULPU-2000 (Theofanous et al., 1996).

2. THE ULPU-2000 TEST FACILITY

The ULPU-2000 facility is illustrated in Figure 2, and an overall view of it is shown in Figure 3. It is a full-length representation of a reactor lower head as well as of the whole flow path between the reactor vessel and reflecting thermal insulation, all the way to the top venting openings. The width of the slice defined by the "Heater Blocks" is 15cm, and the blocks are thick enough (7 cm) to simulate the large thermal inertia of the lower head. These copper blocks are heated by imbedded cartridge heaters that are individually controlled to create any

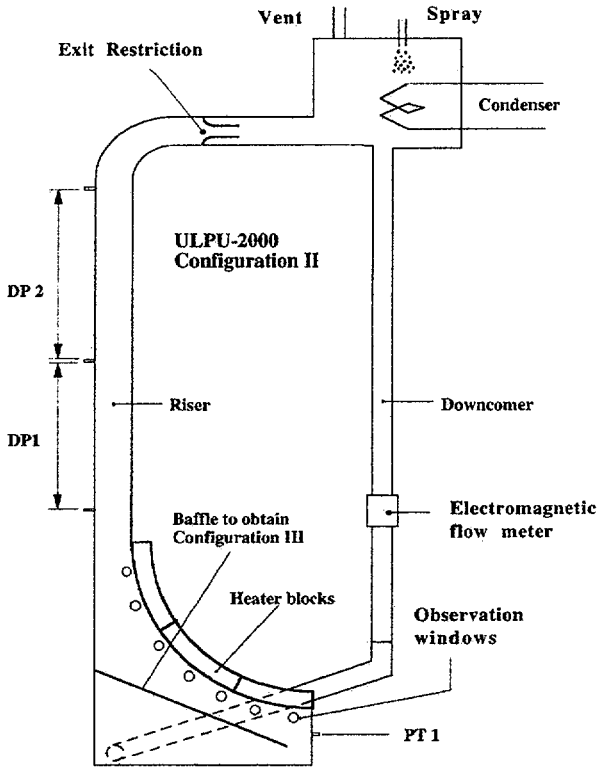

Figure 2. A schematic of the ULPU-2000 facility. The exit restriction is 4" in diameter.

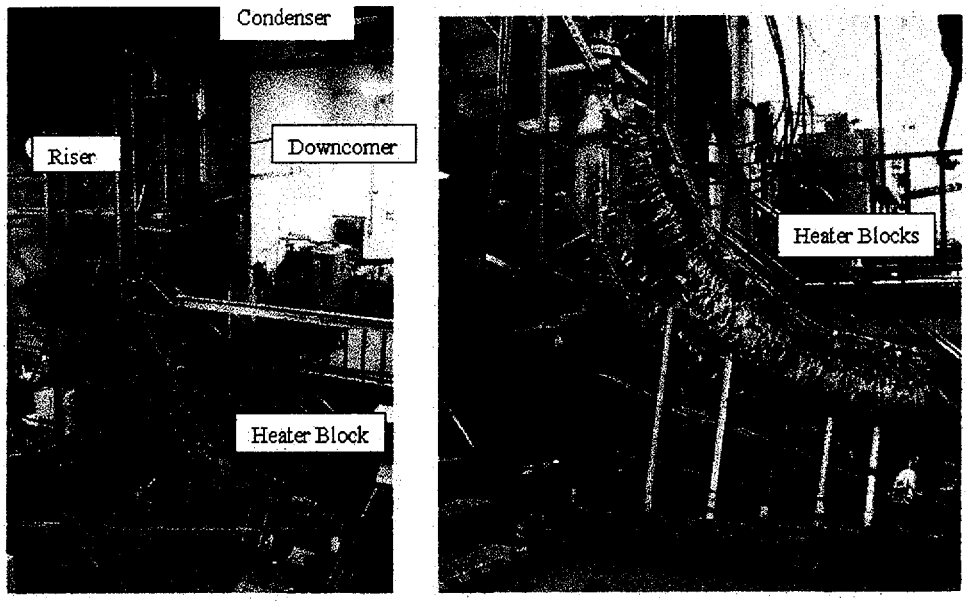

Figure 3. An overall view of the ULPU facility as it exists today.

heat flux shape at will, with a maximum local flux capability of ~2 MW/m^2 and a maximum total power of 500 kW. We use a similarity rule that matches the local quality (that is, the integral of upstream power) to map any reactor power shape to an ULPU power shape for testing the critical heat flux—this mapping changes with the position being tested (Theofanous and Syri, 1997). Detailed description about the power shaping principle is given in Appendix A of this report.

This approach allows us to achieve an effective full-scale simulation of the reactor axisymmetric geometry, by the ULPU slice geometry. The "riser" simulates the full length of the reactor vessel to the top flange (~6 m), and is made with 15.2 cm in diameter pyrex glass that allows visualization. The glass is industrial strength, rated at 60 psig, so that operating at some moderately increased pressure level is feasible. The Configuration III baffle shown in Figure 2 was to simulate the AP600 thermal insulation configuration, which constitutes the starting, reference point of the present research.

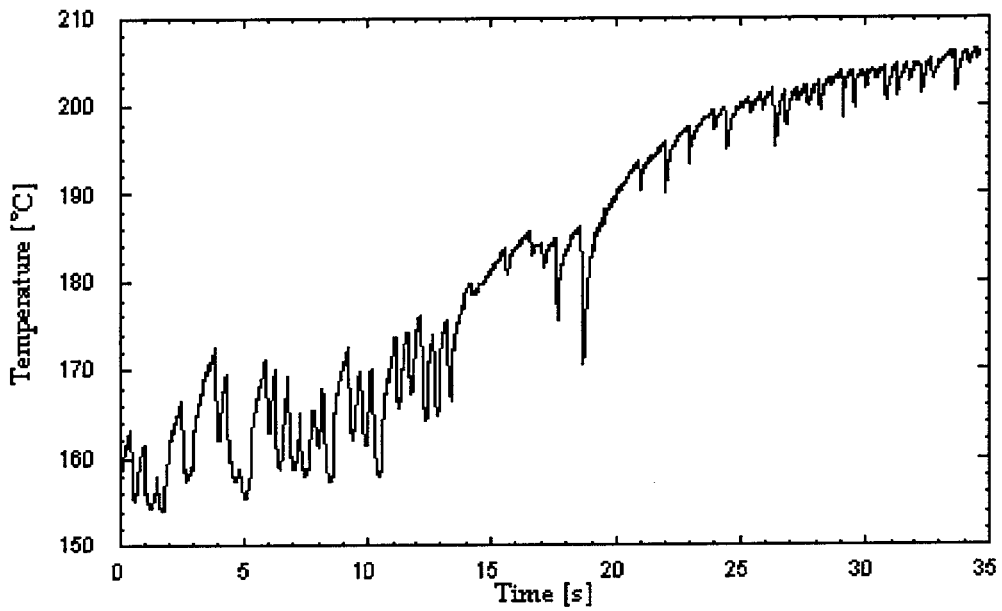

Figure 4. Illustration of the temperature transient (local microthermocouple response) associated with boiling crisis.

It is important to note that the boiling/condensation phenomena that define the coolability limits under IVR, are affected by local subcooling, so representing the full length of the flow path (gravity head) is quite essential for proper simulation. Also, it is probably worth noting that with the large heater thermal inertia, it is very easy to recover from the temperature excursion that marks the boiling crisis, and be ready for another run within minutes. This allows for a very fine resolution of the coolability limits and more thorough testing of experimental parameters. The little circles along the heater boundary shown in Figure 2 represent the windows available for visualization. Similar windows are available at the other two ends of the cavity-simulator region. Extensive thermocouple instrumentation throughout the heater blocks is used to monitor heat transfer, and to detect boiling crisis (i.e., Figure 4)

when it occurs. In addition, we have instrumentation to monitor the instantaneous flow rate in the natural circulation path, the void fractions in the riser, and the dynamic pressures at the position marked PT1 in Figure 2. Finally, the heater blocks in selected locations are equipped with flush-mounted microthermocouples that allow instantaneous reading of the heater surface temperatures—such readings are important in providing insight on the mechanisms involved.

In search for improving the technology, we looked into the effect of the flow path that allows water to circulate around the lower head and up towards the top of the reactor vessel. From previous visualizations in ULPU-2000 Configuration III, we noticed that near the edge of the lower head the two-phase boundary layer exhibited a violently pulsatile behavior with some tendency to "shoot out" the flow, in a centrifugal-like fashion, and we thought that a streamlining of the flow path might improve performance. The ULPU test facility was modified to include a curved baffle, as illustrated in Figure 5. The upper end of this baffle is hinged at a fixed point that allows a smooth transition into the riser. The lower end, on the other hand, is attached to a positioning mechanism that allows vertical placement in 1/2-inch intervals from a minimum of 2 inches, to a maximum of 9 inches. As shown, the radius of curvature of the baffle is the same as that of the vessel. The distance of the lower tip of the baffle (point A in Figure 5) from the vertical boundary just across it is 9 inches.

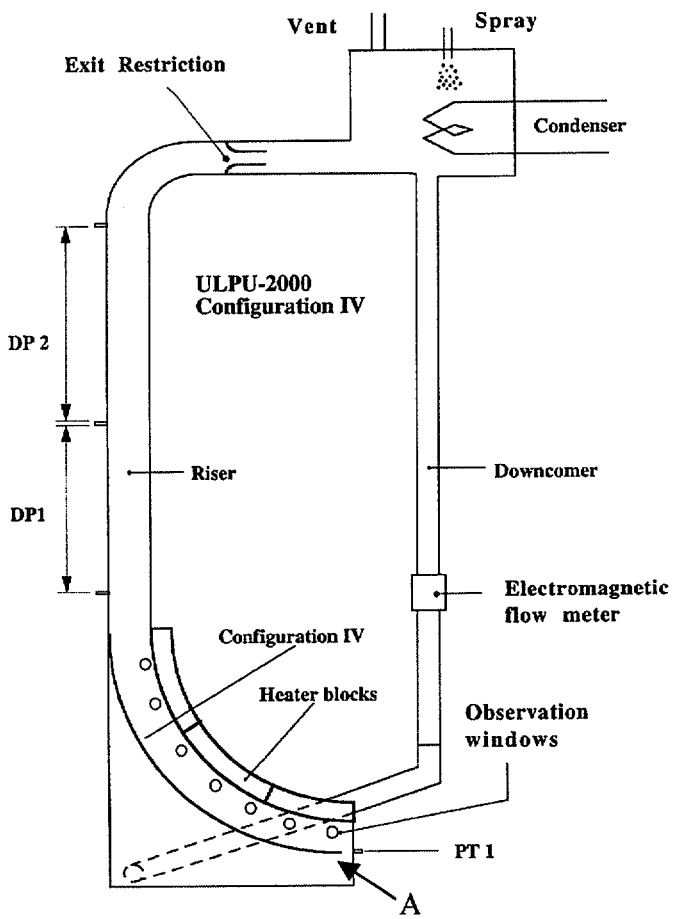

Figure 5. Schematic of the ULPU-2000 Configuration IV.

Scoping experiments were conducted in this Configuration IV in October 2000. The preliminary results showed a consistent improvement over the whole arc, with potential gains of over 25%, and this led to the present work.

3. EXPERIMENTAL PROGRAM

The objective of the present work was to obtain experimental results on critical heat flux in the ULPU-2000 facility with the flow channel made up by the presently installed curved baffle (Configuration IV; Figure 5). The principal parameter studied was the baffle position as defined by the distance of its lower end from the lower head simulating block. Four distances – $2\frac{1}{2}$, 5, 7, and 9 inches – were selected to discretize the available domain of this parameter. In addition, we considered the effect of low-enough fill level to interrupt natural circulation around the riser-downcomer loop. Our original plan was to also consider the effect of exit restriction by removing the exit nozzle; however, the improvement obtained with the nozzle in place brought us already to the flux levels above which the facility could not be run safely, so these tests were postponed for the next phase of the program, after certain upgrades to be carried out under our K-INERI program that is about to start.

In each experimental run, power shape, power history, thermocouple data were recorded. Before and after each ULPU run we check the heaters to ensure that the heaters were intact and able to deliver the power designed. The power shaping is based on the same principle established in the ULPU technology and described in details by Theofanous et al. (1996); Theofanous and Syri (1997). In Appendix A, we provide the 7 power shapes employed in the present series of ULPU runs, namely U0A, U8A, U14A, U24A, U30A, U40A, and U48A, investigate CHF positions 5°, 14°, 25°, 44°, 55°, 74°, and 90° respectively. During the run, heater temperature is closely monitored by embedded and surface thermocouples positioned in the heater blocks, as shown in Appendix B.

For each CHF determination (a fixed power shape) the power level was first increased in steps until a temperature excursion was observed After recovery of nucleate boiling we brought up the power to a level at which the power could be dissipated stably for at least 10 minutes. This was done in 5% intervals, so eventually we had the flux that yielded burnout (this is the CHFs reported) and a flux lower by 5%, which could sustain nucleate boiling for ~10 minutes. Since reproducibility is excellent and measurement error less than 1%, this 5% interval defines the uncertainty in ULPU-2000 CHF results.

Temperature and flow measurements were conducted using K-type thermocouples (± 1K) and electromagnetic *625-Tigermag* flowmeter (±0.36% in the range 0-200 gpm). The instruments were manufacturer-calibrated, on-site tested, and found to perform excellently.

In total, 28 experiments were conducted, including 18 runs with recirculating flow and 10 runs, in which water level in the riser is lowered to prevent recirculating flow. A listing of the 28 ULPU-2000 runs performed is given in Table 1.

4. EXPERIMENTAL RESULTS

The results of this set of tests are summarized in Table 1 and in graphical form in Figures 6 and 7. Detailed data, covering the whole history of each run, are collected in Appendix C.

Table 1. Summary of ULPU-2000 runs (Configuration IV)

Run #	Power Name	Peak-Flux Angular Position °	CHF with Natural Convection (kW/m^2)	CHF with Open Loop CHF (kW/m^2)	Burnout Inception Position °	Baffle Position (Inch)
1	U0A	0~13	855		10~16	9
2	U8A	11~15	940		10~16	9
3				695	10~16	9
4			940/Null			$2\frac{1}{2}$
5			940/Null			5
6			940		10~16	7
7	U14A	23~27	940		22~30	9
8				789	19~26	9
9			940/Null			$2\frac{1}{2}$
10				940/Null		$2\frac{1}{2}$
11				705	19~26	5
12	U24A	42~46	1198		43~50	9
13				902	40~46	9
14			1410/Null			$2\frac{1}{2}$
15			1128		40~46	5
16			1198		40~46	7
17	U30A	53~57	1269		50~56	9
18				1057	50~56	9
19			1410/Null			$2\frac{1}{2}$
20	U40B	72~76	1786		67~73	9
21				1316/Null	80~83	9
22				1316/Null	83~86	$2\frac{1}{2}$
23			1786/Null		80	$2\frac{1}{2}$
24			1880/Null			5
25				1222	86~90	5
26	U48A	88~90	1598		83~90	9
27				1052	83~90	9
28		83~90	1598		83~90	9

/Null: means no CHF happen. The number is maximum power level reached at this position

Note that in ten cases CHF could not be reached with the power capability of the facility — these not-yet-at-burnout fluxes are marked as "null" in Table 1, and with arrows in Figures 6 and 7. The enhancement relative to the Configuration III performance, expressed as the ratio of CHF values at each position, is shown in Figure 8 – circulations flow only. These data reveal some interesting trends, which we believe will be very helpful in judging our next moves as we seek to further optimize performance through modifications of the flow path. The no-circulation data, on the other hand, are found to be generally comparable to the Configuration III results — the CHF values are probably too low to be of interest to AP1000, and will not be pursued further here. In the discussion that follows it is convenient to take up in turn the lower (0-30°), middle (30-60°), and upper (60-90°) regions of the lower head.

Lower Region. Over this whole region the effect of increased convection in Configuration IV was to bring CHF up to the power capability limit of the lower block – 940 kW/m^2 to ~850 kW/m^2, almost linearly, as we move from position 0° to 30°, which is gradually reduced to just a few percent at 30° for the large gap (9"). The smaller gaps, $2\frac{1}{2}$" and 5" would be expected to show continuing enhancement, along the flow path, but the 940 kW/m^2 limit of the facility did not allow us at this time to distinguish trends. Nevertheless, based on these data we can put a clear lower bound of 900 kW/m^2 over this whole lower region, and this is very comfortable for the kinds of thermal loads expected in AP1000.

Middle Region. Here, we see a very significant increase of CHF due to the presence of the Configuration IV baffle as well. In this heat block (30° to 60°), the heat flux limit is 1410 kW/m^2, and this was reached under the 2½"-gap configuration. We can also see that all other gap dimensions (5", 7", 9") produced essentially the same CHF of ~1200 kW/m^2. Note that in Configuration III the CHF in this region varies from ~900 to ~1100 kW/m^2, so enhancement is relatively small. This is because convection in this region, in Configuration III, is already quite strong, so rather small gaps are required to significantly improve upon it.

Upper Region. The behavior in the upper region is characterized well by performance at two positions — 75° to 80° and ~90°. In the 75° to 80° region, we reached the facility heat flux limit (third block) of 1880 kW/m^2, and the data show an optimal gap of 5", for which the limit was reached without observing burnout. Both a larger and a smaller gap produced burnouts at somewhat smaller fluxes — 1786 kW/m^2 for 9", while with 2½ " we could only reach 1786 kW/m^2 because the run was interrupted with a burnout occurring in the downstream position. Clearly with a very small gap, in the upper positions we may be starving the liquid flow, and this suggests a design where side slots on the insulation (baffle) would allow water to enter along the path as needed by the pressure differential. In the 90° position, on the other hand, we observe a decrease of CHF to ~1600 kW/m^2, which is essentially the Configuration III value. We suspect that this is due to an "exit" phenomenon, whereby local convection is affected by the absence of vapor generation beyond the 90° position. If so, it also would be very relevant to the reactor, as this is exactly the situation at the top of the metal layer. We believe we can overcome this by locally tailoring the flow path, which we could not do in the present series of tests with the baffle hinged at the top, at a fixed distance of 9". With this local problem alleviated, we can look at this upper region as easily accommodating fluxes of ~2 MW/m^2, which should provide a comfortable margin to the need of AP1000.

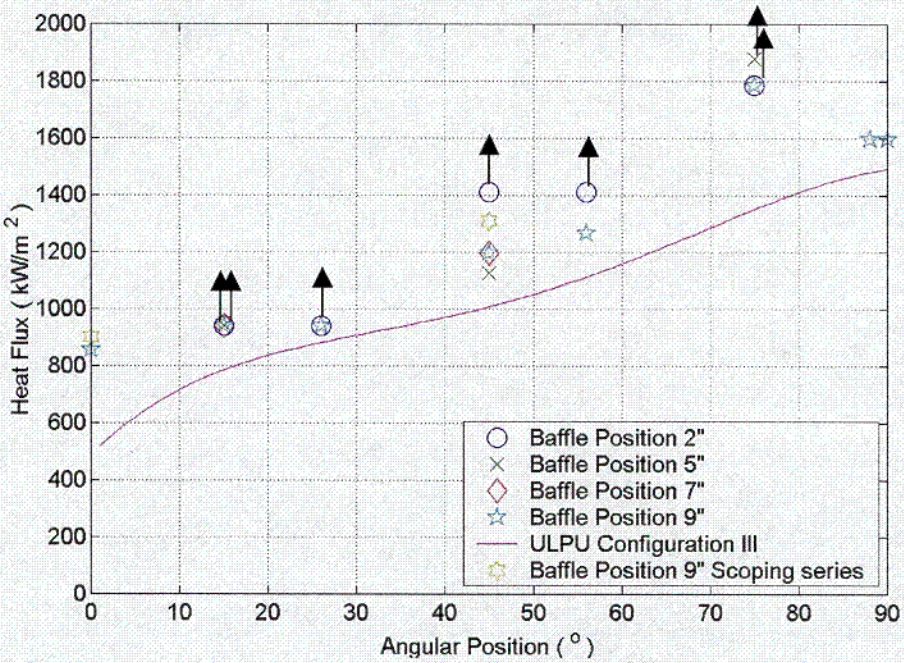

Figure 6. Maximum heat flux measured in the ULPU-2000 Configuration IV runs in the presence of natural circulation flow.

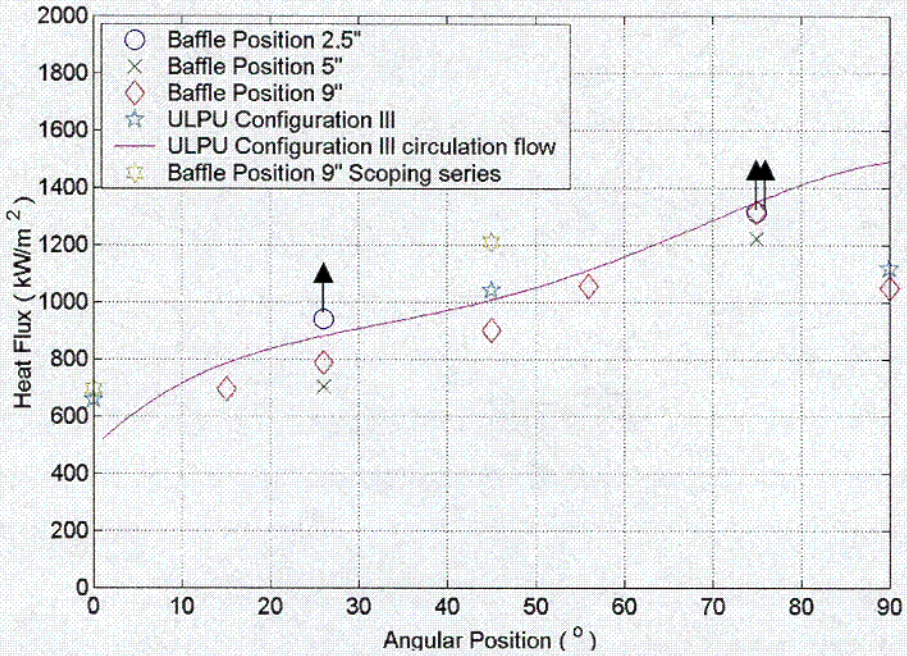

Figure 7. Maximum heat flux measured in the ULPU-2000 Configuration IV runs with an open loop (half water level in riser)

C-01

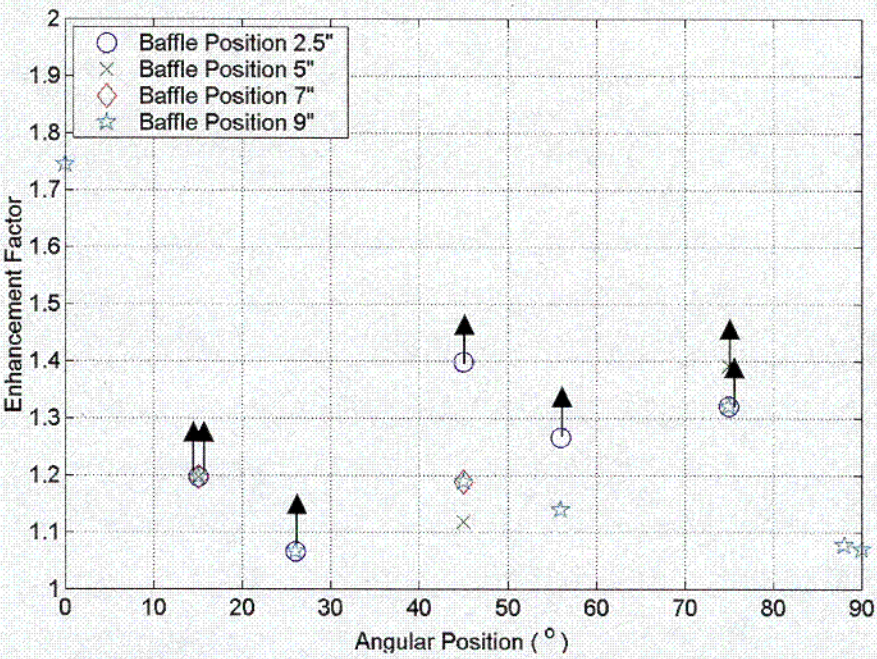

Figure 8. Enhancement factor in the ULPU-2000 Configuration IV runs (compared to AP-600 Configuration III). Recirculating flow.

5. CONCLUSIONS AND FUTURE PLANS

We have completed a series of 28 determinations of simulated burnout heat fluxes in the ULPU-2000 Configuration IV facility. The results confirm preliminary indications taken prior to commencing this work that streamlining the flow path around the lower head, and enhancing convection is beneficial to performance. In fact, the improvement was so great that in many locations we reached the power capability of the facility without observing burnout. Still, we have sufficient data to observe key trends, and proceed intelligently towards further optimizing the design. As part of this work, we have also made the necessary changes in facility specifications, and we are ready to proceed with modifications that will allow us to reach ~2.5 MW/m^2.

Several key conclusions made on the basis of present data can be listed as follows:

- In the upper region (~75°) we reached the limit of 1880 kW/m^2 without observing burnout. We believe there is a strong basis for expecting coolability to persist above 2 MW/m^2.
- At the very top of the heated wall (90°) we found a sudden drop of performance to ~1.6 MW/m^2, and this appears to be related to "exit" phenomena that affect (adversely) local

C-02

two-phase flow structure. This needs further study, and remedy, most likely possible with the aid of locally tailoring further the flow path.

- In the middle (30° – 60°) and lower (0° – 30°) regions we can easily exceed 1410 kW/m^2 and 940 kW/m^2 respectively; that is, CHF levels that, as in the case of AP600, make these regions totally unimportant for IVR performance.

REFERENCES

Angelini, S., J.P. Tu, Yu.A. Buyevich and T.G. Theofanous, The Mechanism and Prediction of Critical Heat Flux in Inverted Geometries, Nuclear Engineering & Design **200** (2000) 83-94.

Asmolov, V.V., The RASPLAV Project. Proc. OECD/CSNI Workshop on In-Vessel Core Debris Retention and Coolability, Garching, 1998.

Bonnet, J.M. and J.M. Seiler, Thermal hydraulic phenomena in corium pools, CD-ROM proceedings of the 7th Intern. Conf. On Nuclear Engineering, Tokyo, Japan, April 19-23, 1999, ICONE-7057.

Cheung, F.B. and Y. C. Liu, Effects of thermal insulation of reactor vessels under severe accident conditions, CD-ROM proceeding, session J-4, Ninth International Topical Meeting on Nuclear Reactor Thermal Hydraulics (NURETH-9) San Francisco, California, October 3 - 8, 1999.

Garching: OECD Workshop on In-Vessel Core Debris Retention and Coolability, Garching, Germany, March 3-6, 1998.

Grenoble: OECD/CSNI/NEA Workshop on Large Molten Pool Heat Transfer, Nuclear Research Centre, Grenoble, France, March 9-11, 1994.

Helle M, COPO II experiments with a stratified pool. IVO Group. Report, January 1999.

Henry, R.E. and H.K. Fauske, External Cooling of a Reactor Vessel Under Severe Accident Conditions, Nuclear Engineering and Design **139** (1993) 31.

NUREG-1512, Final Safety Evaluation Report Related to Certification of the AP600 Standard Design, September 1998.

Rouge, S. SULTAN test facility for large-scale vessel coolability in natural convection at low pressure. Nuclear Engineering and Design **169** (1997) 185-95.

Theofanous, T.G., Some Considerations on Severe Accidents at Loviisa, Theofanous & Co., Inc., January 1989, IVO Proprietary Report.

Theofanous, T.G. and S. Syri, The Coolability Limits of a Reactor Pressure Vessel Lower Head, Nuclear Engineering and Design **169** (1997) 59-76.

Theofanous, T.G., C. Liu, S. Additon, S. Angelini, O. Kymäläinen, and T. Salmassi, In-Vessel Coolability and Retention of a Core Melt, DOE/ID-10460, October 1996.

Tuomisto, H. and T.G. Theofanous, A Consistent Approach to Severe Accident Management, Nuclear Engineering and Design **148** (1994) 171-183.

APPENDIX A. Power shape in ULPU experiments

The main requirement for the power shaping in the full-scale slice ULPU experiment is that in the experiments, local structures and dynamics of the two-phase boundary layer to the local surface inclination match those to be found in the prototype, all along the vertical arc length from $\theta = 0^\circ$ to $\theta \sim 90^\circ$. This cannot be accomplished in sub-scale models, while a full-scale representation in an experiment with prototypic heat flux at all locations is clearly impractical, if not impossible. We use an approach that takes advantage of the axial symmetry in the prototype, in combination with a power-shaping approach in the experiment. The axial symmetry allows a "pie" segment representation of the hemisphere, but this is still, for a variety of reasons, a formidable experimental geometry to work with. By power-shaping we can effectively represent the flow behavior in such a pie segment with a uniform (in thickness) vertical slice, which is experimentally feasible.

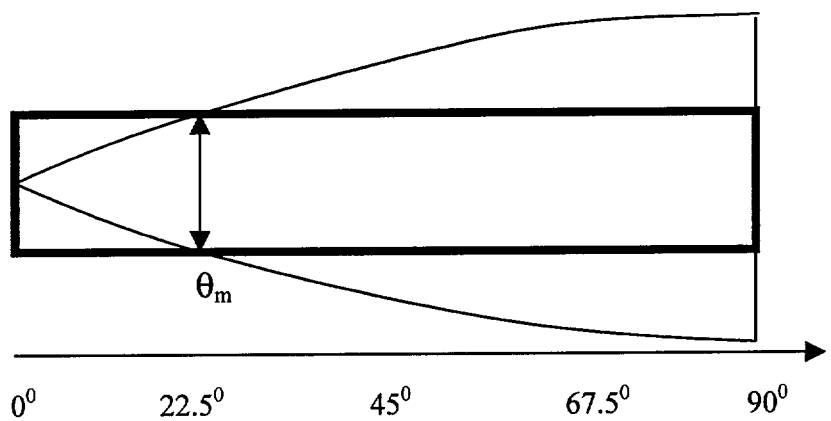

To perform simulation experiments that allow the determination of the critical heat flux, $q_{P,CR}$ in the reactor, as a function of the angular position θ under the constraint of a specified power shape, say $q_P(\theta)$, we choose to make this determination for a discrete set $\theta_{m,I}$, i = 1...n of values of the angular position, by a corresponding set of experiments, each simulating the prototype for the particular angular position considered (see sketch above). For this we require (i) that the superficial vapor velocities (expressed as volumetric flow rate per unit width) match up with those of the prototype for all $\theta > \theta_m$, and (ii) that for $\theta < \theta_m$ the vapor flow rates build up gradually, so as to smoothly approach the value required at $\theta = \theta_m$, while allowing a "natural" development of the boundary layer in all of the upstream region. By satisfying these requirements, we ensure that the two-phase boundary layer is properly driven in a broad neighborhood of the location under consideration (θ_m) as well as all of the downstream region.

The above requirements provide a basis to calculate power shapes in ULPU experiments for a given angular position θ_m (Theofanous and Syri, 1997). As a reference for prototypic reactor heat flux, we use heat flux distribution determined for a curved boundary of an internally-heated naturally-convecting hemispherical liquid pool at high Rayleigh number. The resulting power shapes used in ULPU experiments are shown In Figures A.1-A.7 below.

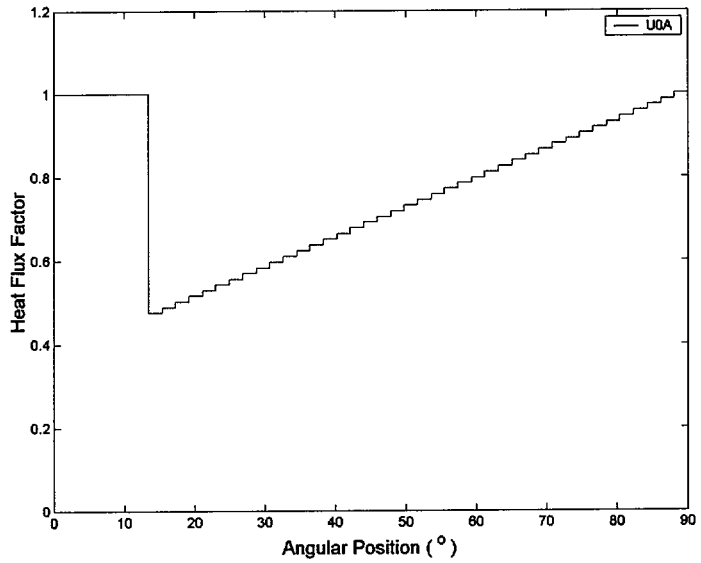

Figure A.1. The heat flux profile according to the power shaping principle for CHF at angular position 0-13°

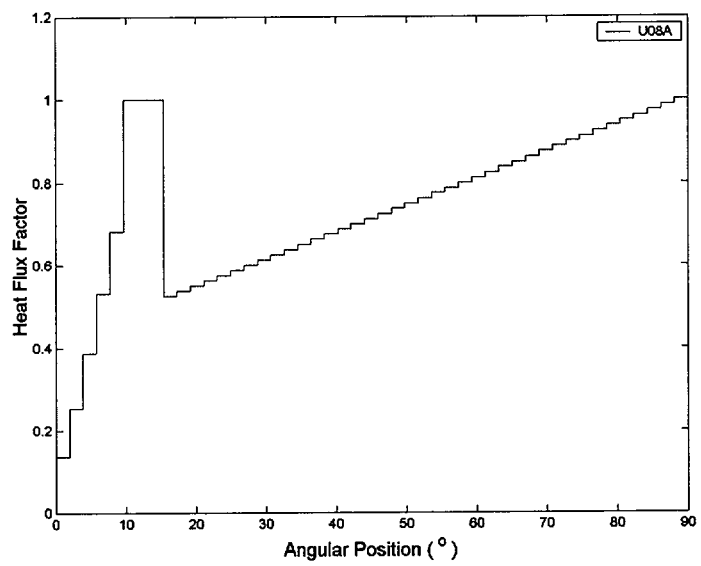

Figure A.2. The heat flux profile according to the power shaping principle for CHF at angular position 11-15°

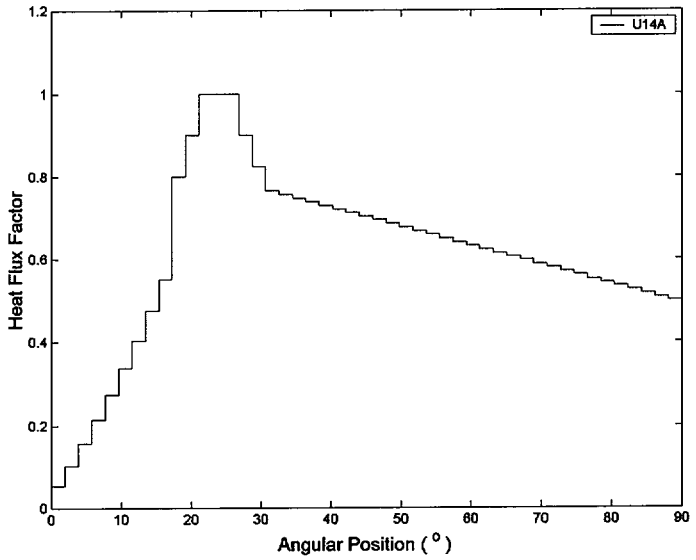

Figure A.3. The heat flux profile according to the power shaping principle for CHF at angular position 23-27°

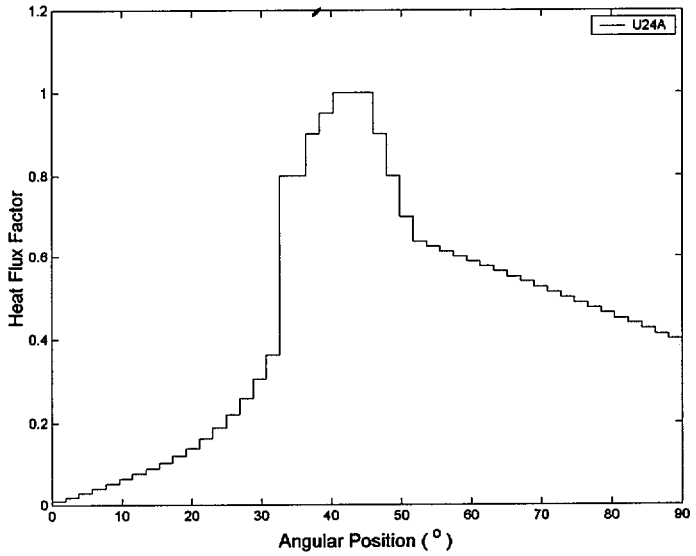

Figure A.4. The heat flux profile according to the power shaping principle for CHF at angular position 42-46°

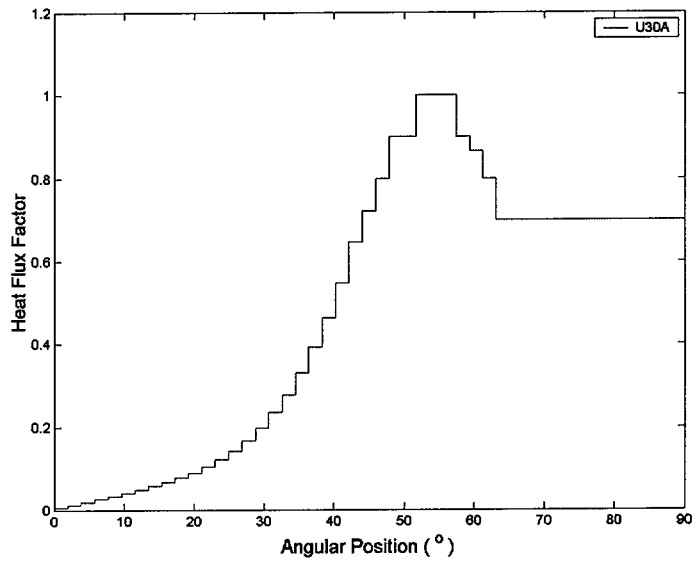

Figure A.5. The heat flux profile according to the power shaping principle for CHF at angular position 53-57°

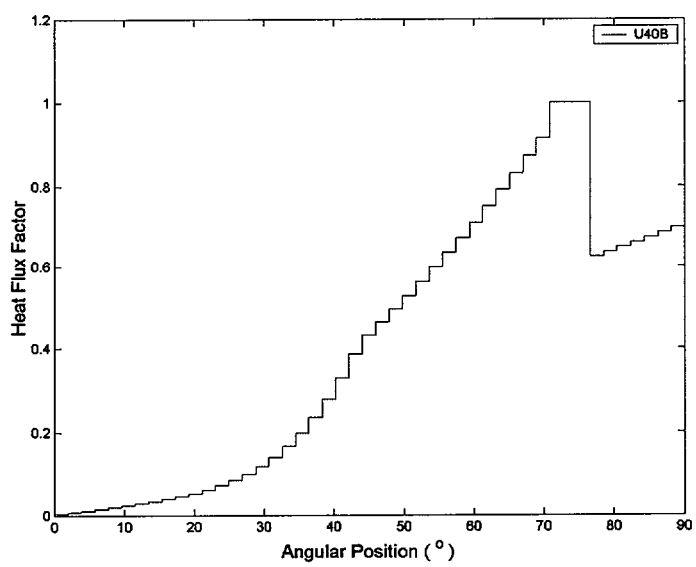

Figure A.6. The heat flux profile according to the power shaping principle for CHF at angular position 72-76°

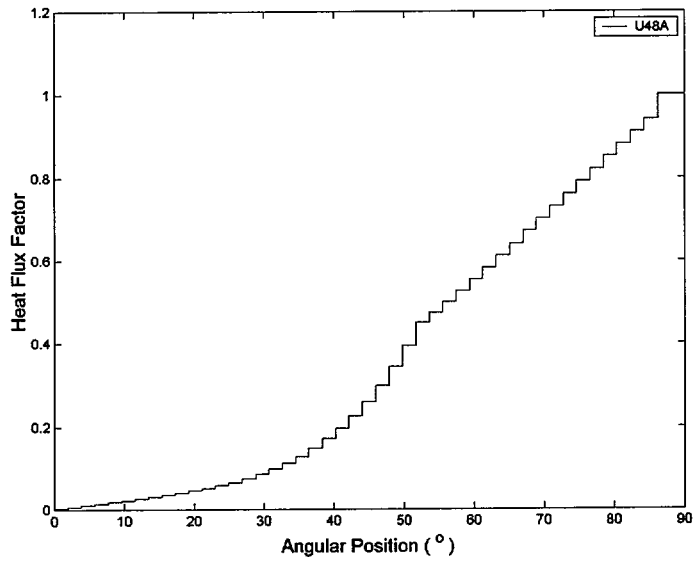

Figure A.7. The heat flux profile according to the power shaping principle for CHF at angular position 88-90°

APPENDIX B. Thermocouple locations in the ULPU-2000 experiments

Table B.1. Thermocouples name and location (blocks A, B, and C correspond to the lower, middle, and upper heaters section).

Block A	Surface TC	A1 A2 A3				A4 A5 A6				A6 A7 A8
	Left side TC	LA1	LA2	LA3	LA4		LA5	LA6	LA7	LA8
	Right side TC	RA1	RA2	RA3	RA4		RA5	RA6	RA7	RA8
	Angular position	3.75	6.96	10.17	13.38	15	16.59	19.8	23.01	26.22
Block B	Surface TC	B1 B2 B3				B4 B5 B6				B6 B7 B8
	Left side TC	LB1	LB2	LB3	LB4		LB5	LB6	LB7	LB8
	Right side TC	RB1	RB2	RB3	RB4		RB5	RB6	RB7	RB8
	Angular position	33.75	36.96	40.17	43.38	45	46.59	49.8	53.01	56.25
Block C	Surface TC	C1 C2 C3				C4 C5				
	Left side TC	LC1	LC2	LC3	LC4		LC5	LC6	LC7	LC8
	Right side TC	RC1	RC2	RC3	RC4		RC5	RC6	RC7	RC8
	Angular position	63.75	66.96	70.17	73.38	75	76.59	79.8	83.01	86.25

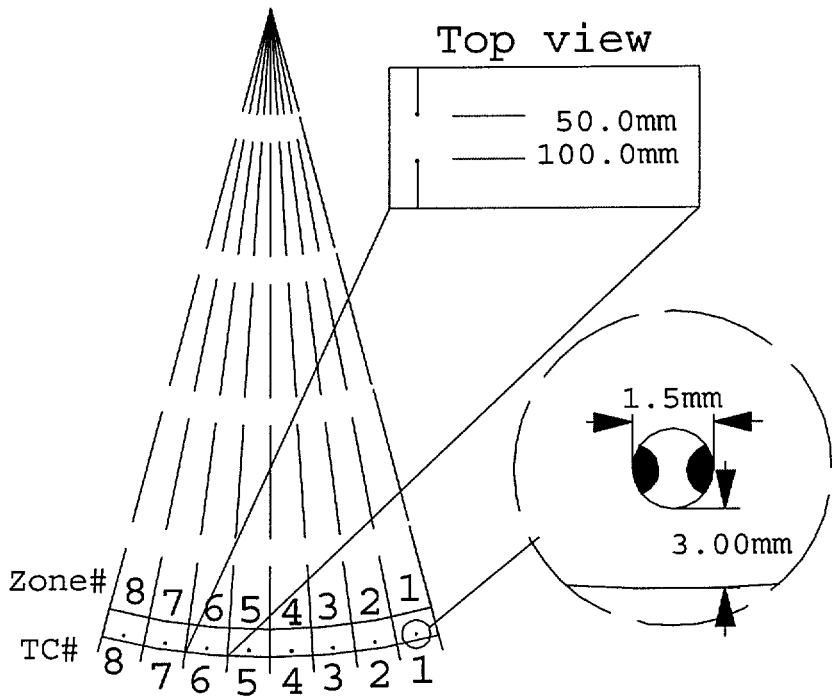

Figure B.1. Position of thermocouples (sketch)

APPENDIX C. Original experimental data

Run #1

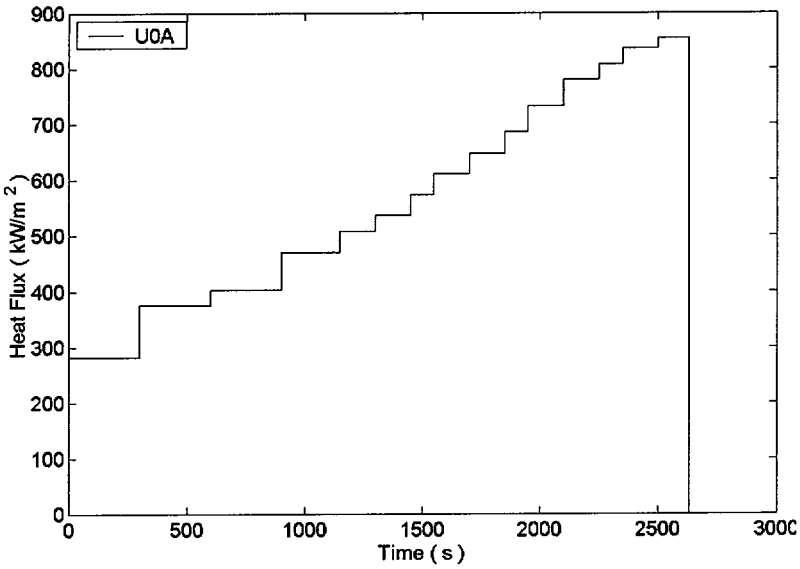

Figure C.1.1. Power history (heat flux) in the CHF-designed block A

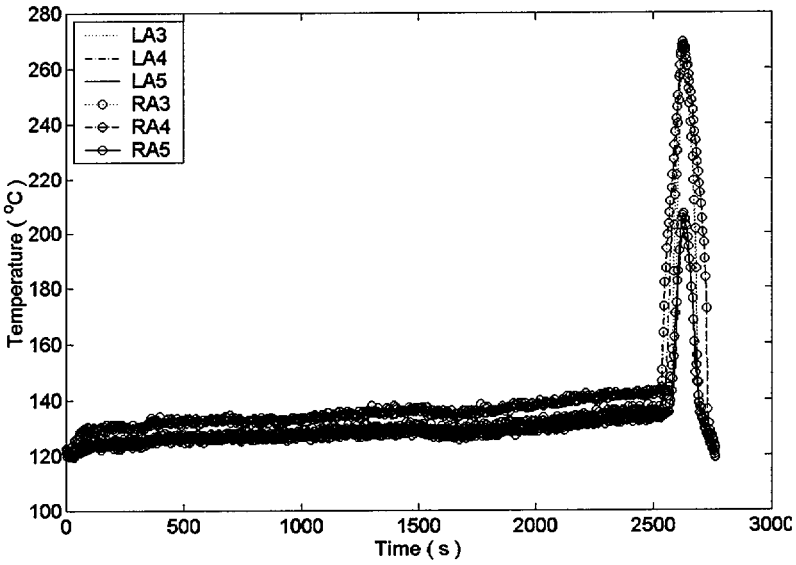

Figure C.1.2. Embedded thermocouple data in CHF-designed block (overall)

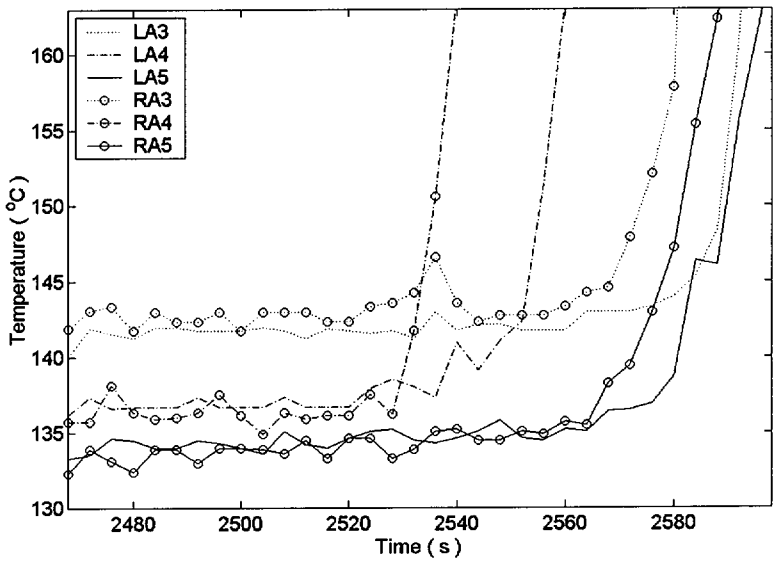

Figure C.1.3. Embedded thermocouple data in CHF-designed block (excursion)

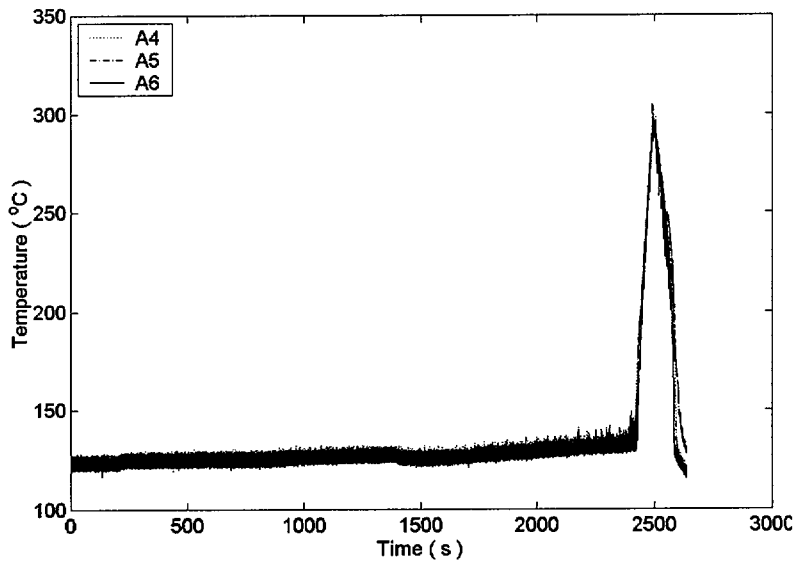

Figure C.1.4. Surface thermocouple data in CHF-designed block (overall)

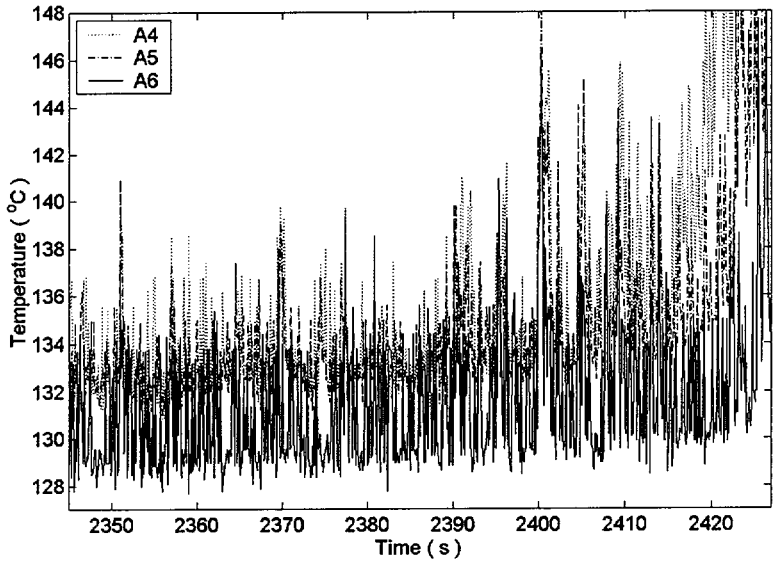

Figure C.1.5. Surface thermocouple data in CHF-designed block (excursion)

Run #2

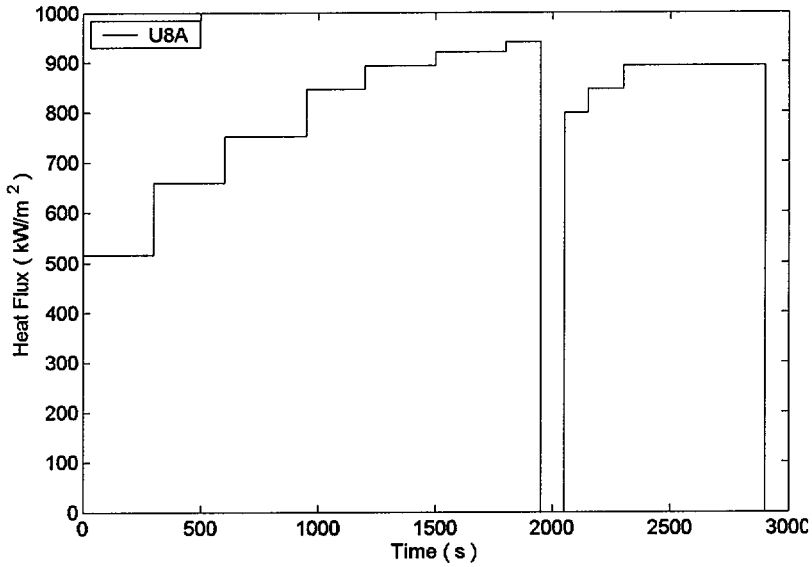

Figure C.2.1. Power history (heat flux) in the CHF-designed block A

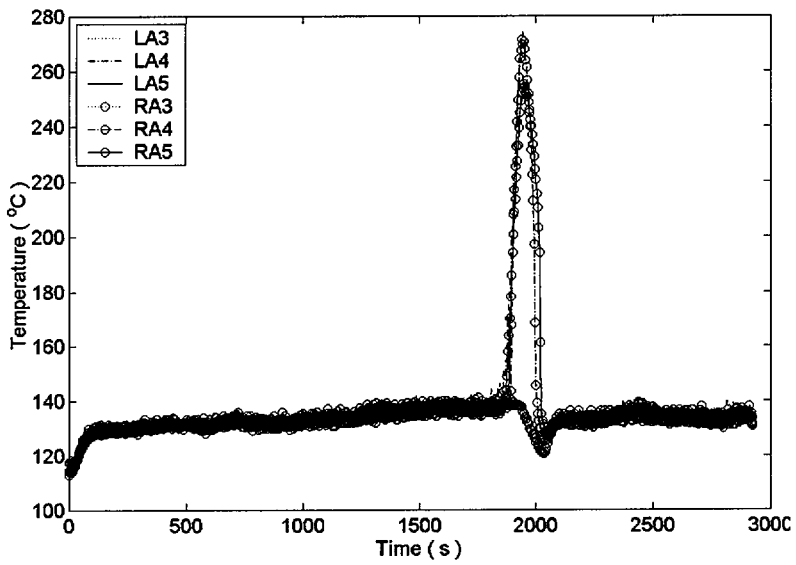

Figure C.2.2. Embedded thermocouple data in CHF-designed block (overall)

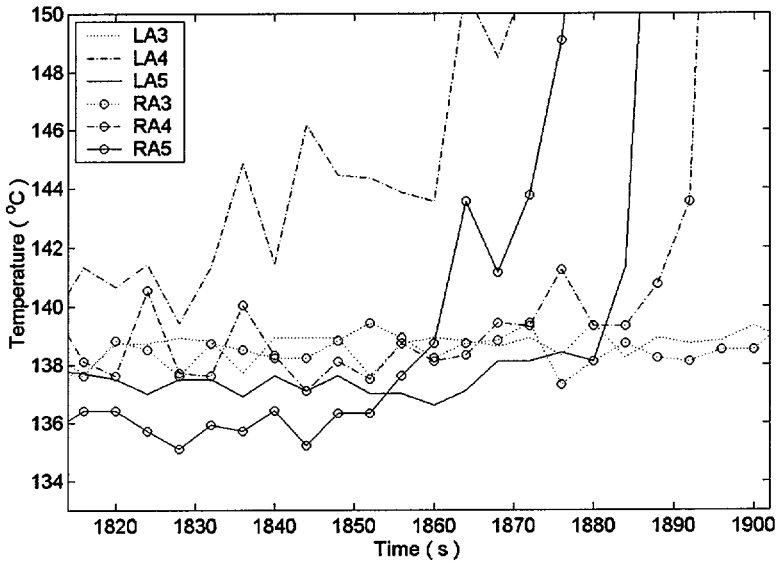

Figure C.2.3. Embedded thermocouple data in CHF-designed block (excursion)

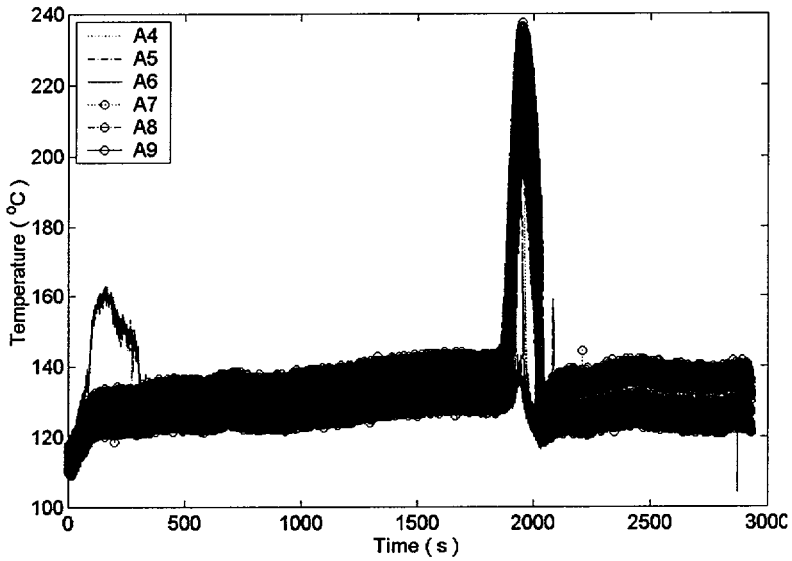

Figure C.2.4. Surface thermocouple data in CHF-designed block (overall)

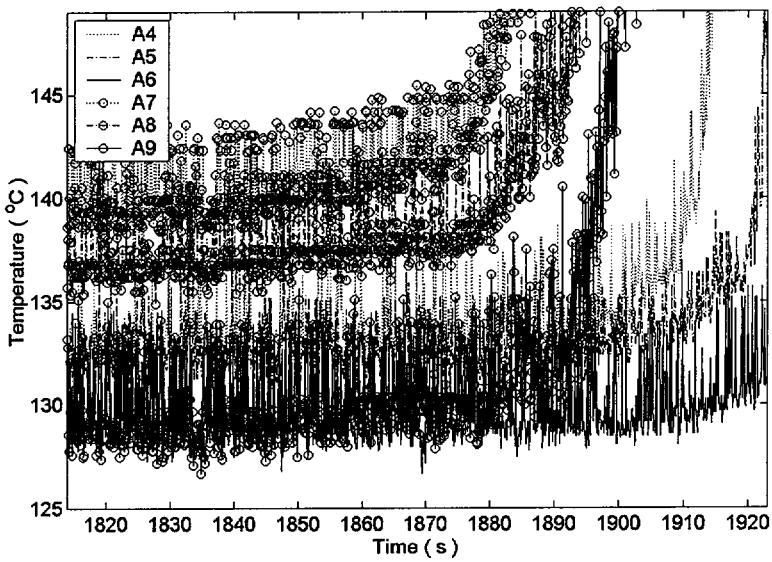

Figure C.2.5. Surface thermocouple data in CHF-designed block (excursion)

Run #3

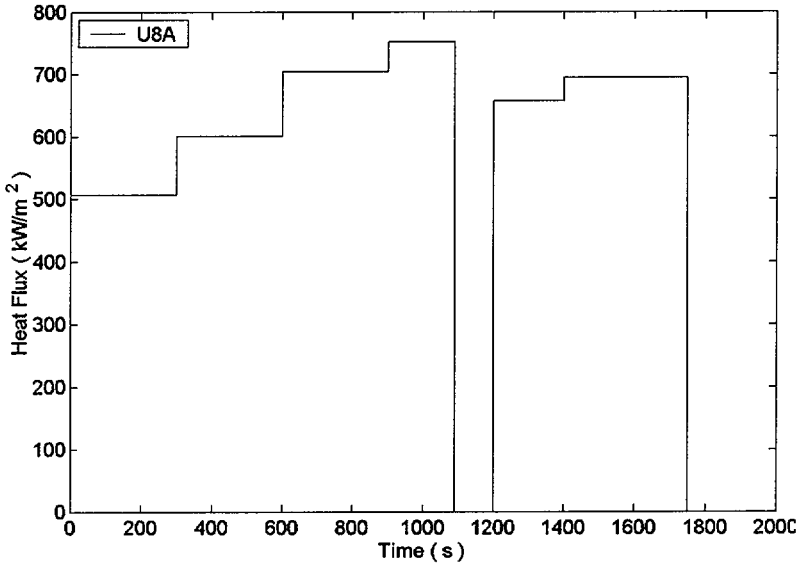

Figure C.3.1. Power history (heat flux) in the CHF-designed block A

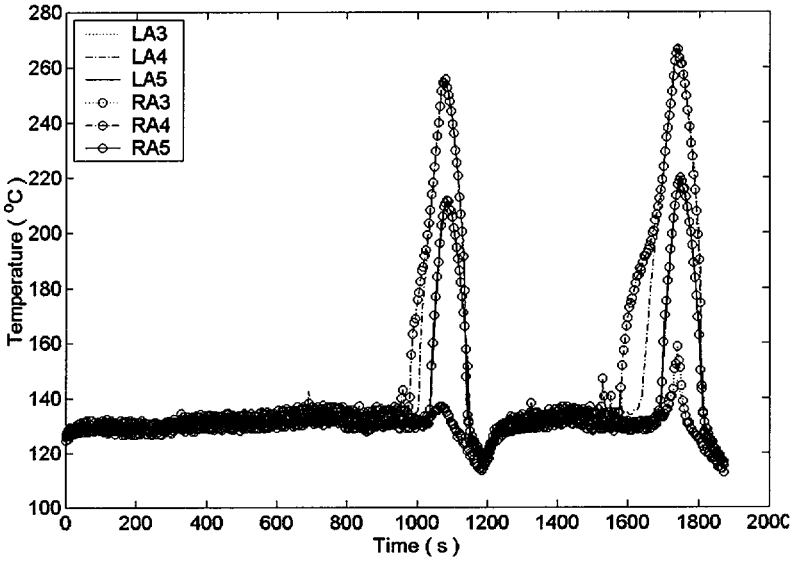

Figure C.3.2. Embedded thermocouple data in CHF-designed block (overall)

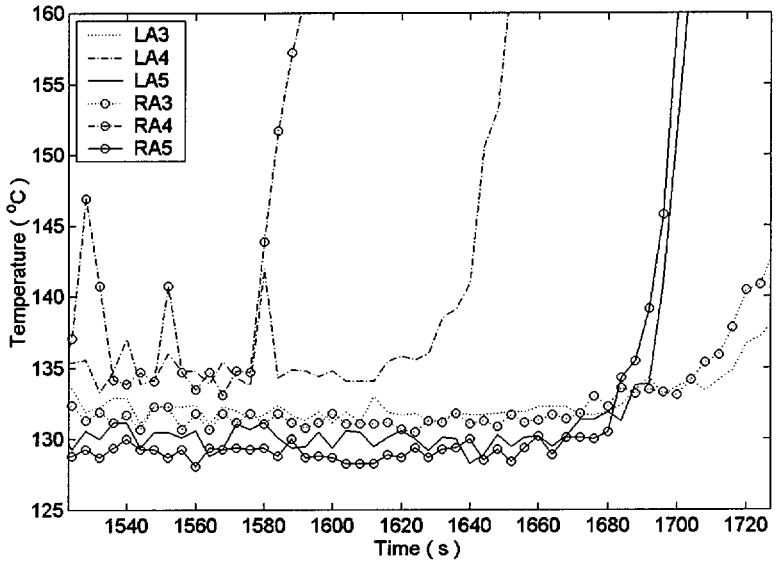

Figure C.3.3. Embedded thermocouple data in CHF-designed block (excursion)

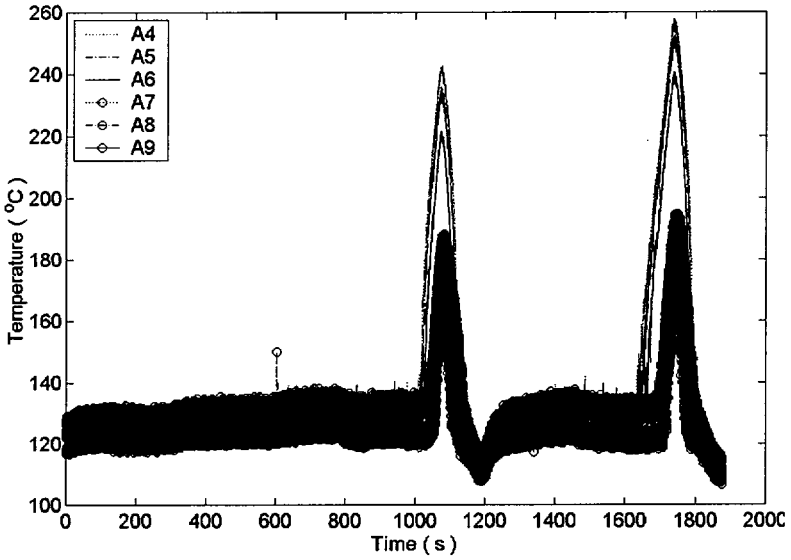

Figure C.3.4. Surface thermocouple data in CHF-designed block (overall)

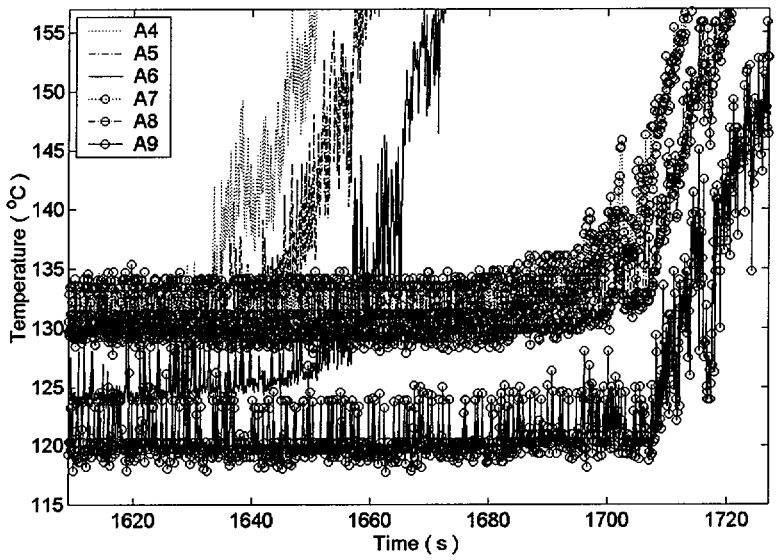

Figure C.3.5. Surface thermocouple data in CHF-designed block (excursion)

Run #4

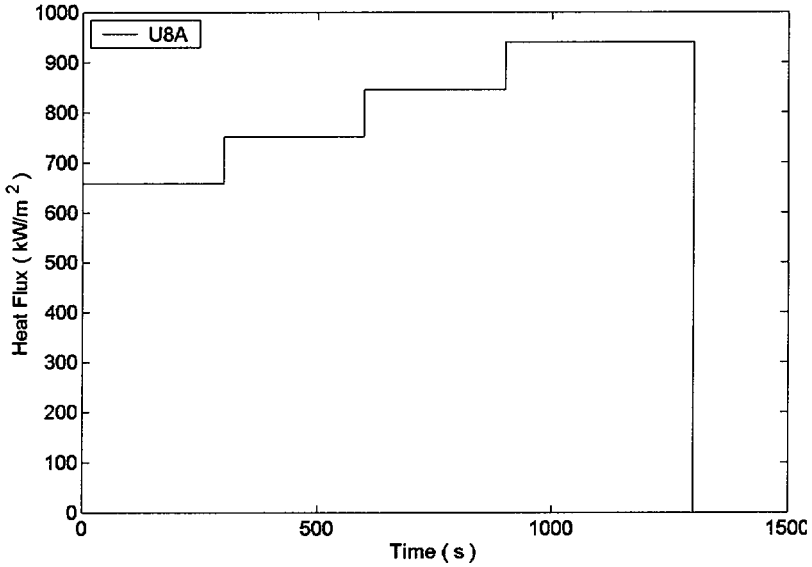

Figure C.4.1. Power history (heat flux) in the CHF-designed block A

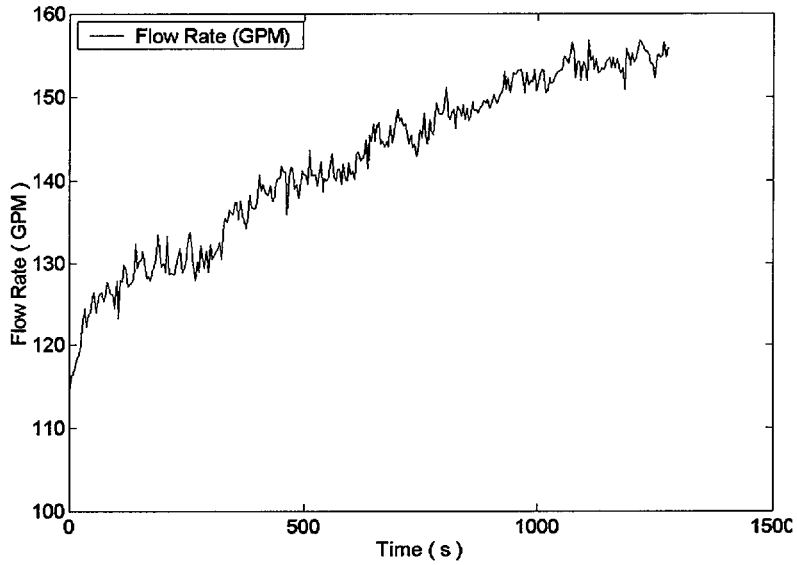

Figure C.4.2. Flow rate measurement

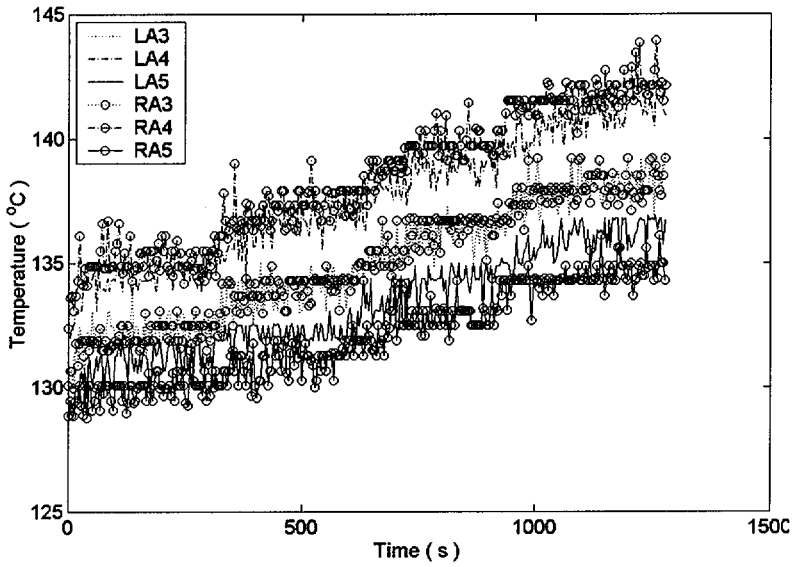

Figure C.4.3. Embedded thermocouple data in CHF-designed block (overall)

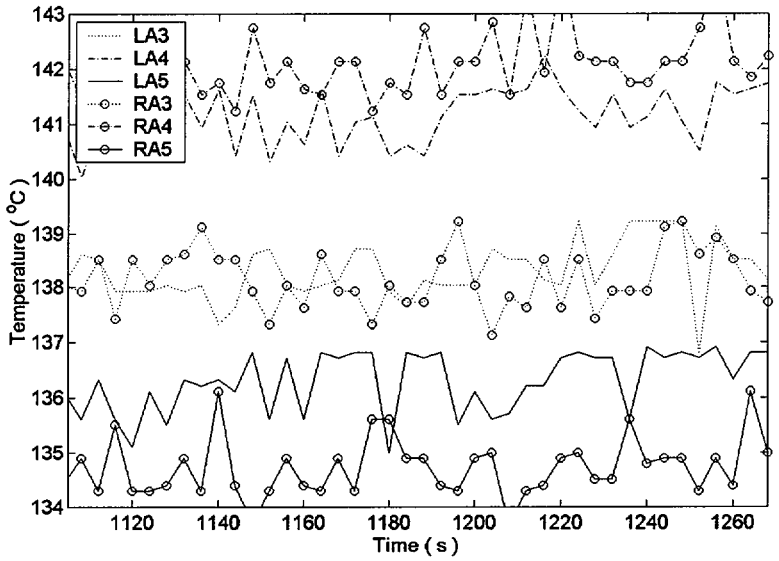

Figure C.4.4. Embedded thermocouple data in CHF-designed block (detail)

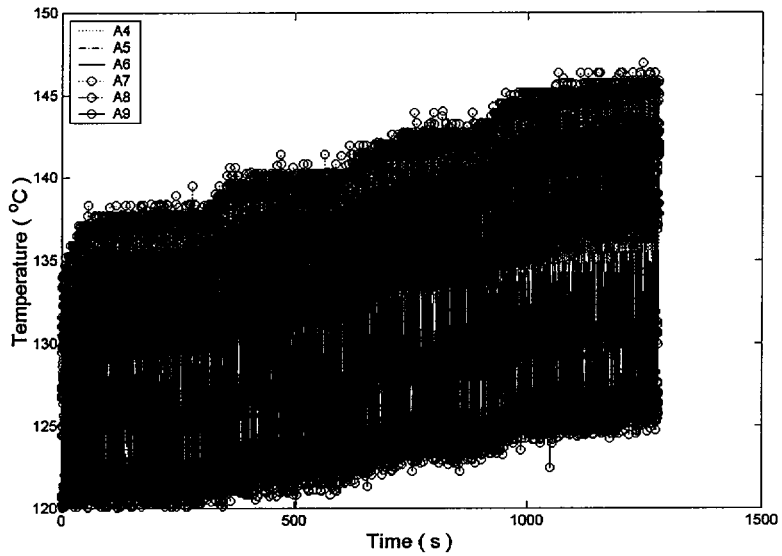

Figure C.4.5. Surface thermocouple data in CHF-designed block (overall)

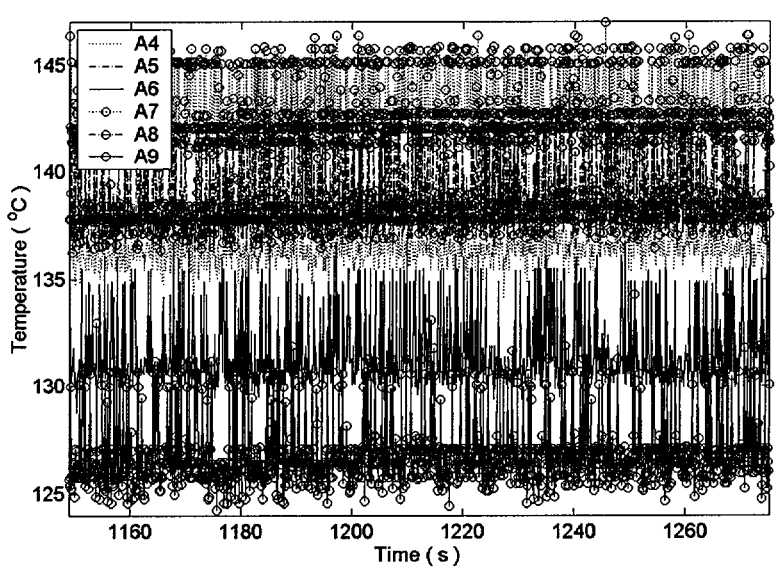

Figure C.4.6. Surface thermocouple data in CHF-designed block (detail)

Run #5

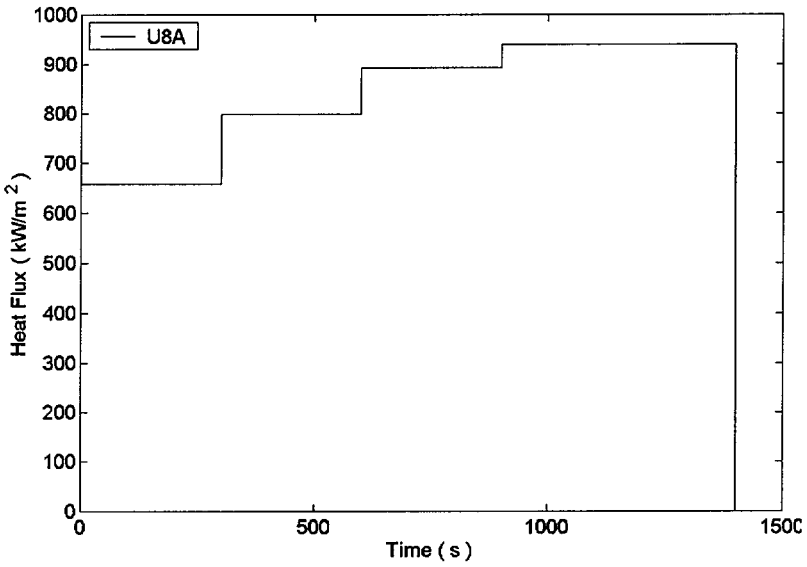

Figure C.5.1. Power history (heat flux) in the CHF-designed block A

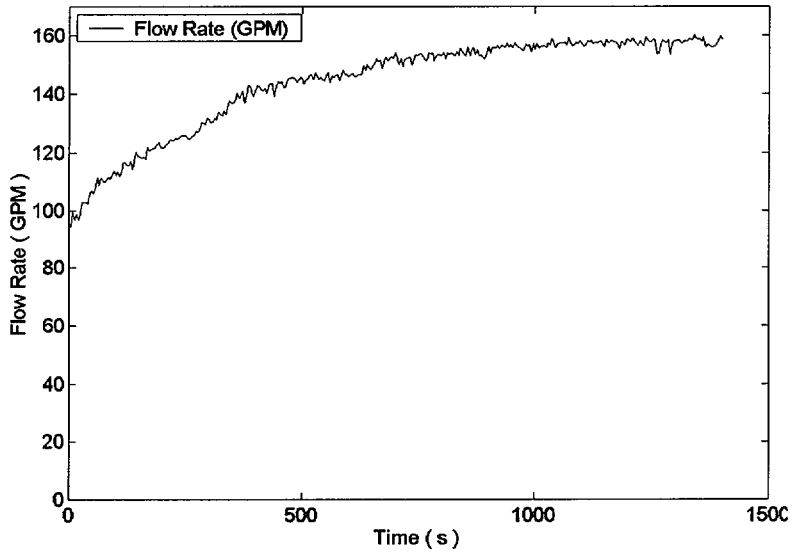

Figure C.5.2. Flow rate measurement

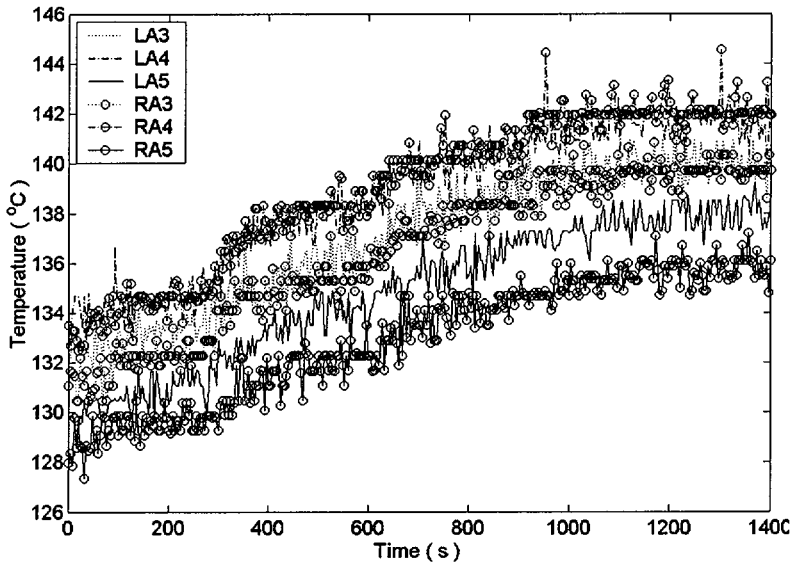

Figure C.5.3. Embedded thermocouple data in CHF-designed block (overall)

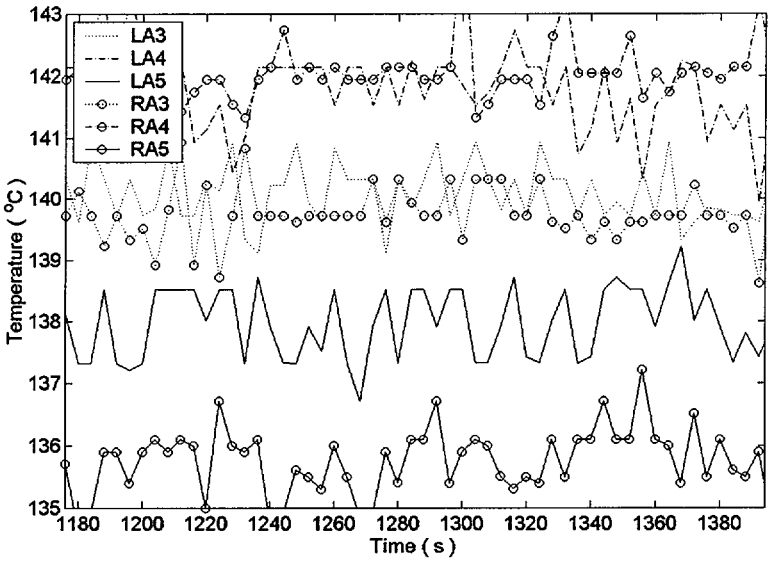

Figure C.5.4. Embedded thermocouple data in CHF-designed block (detail)

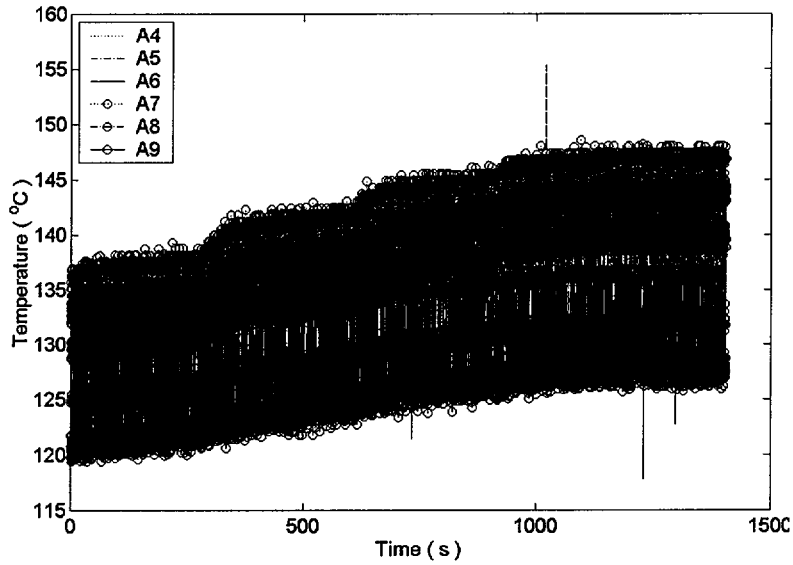

Figure C.5.5. Surface thermocouple data in CHF-designed block (overall)

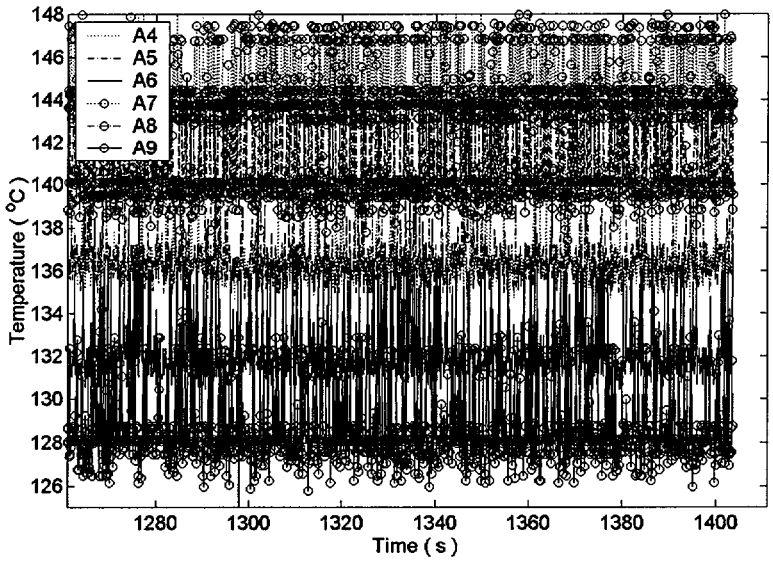

Figure C.5.6. Surface thermocouple data in CHF-designed block (detail)

Run #6

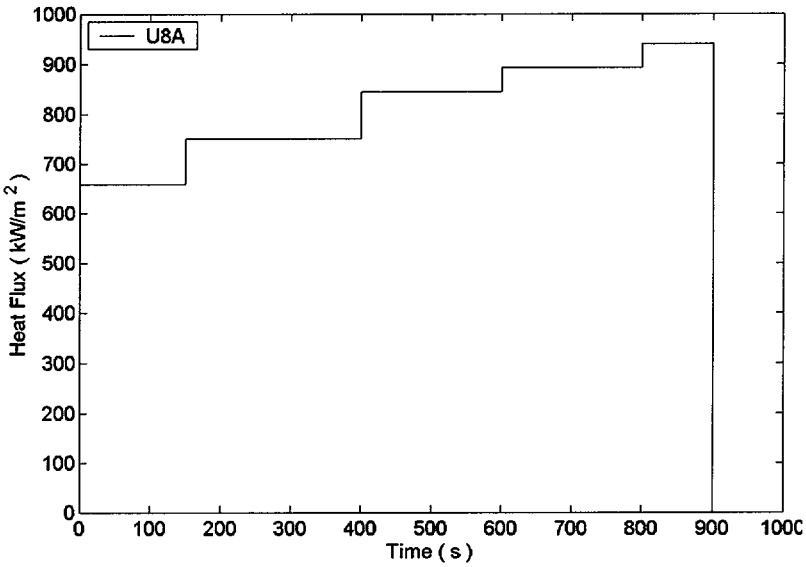

Figure C.6.1. Power history (heat flux) in the CHF-designed block A

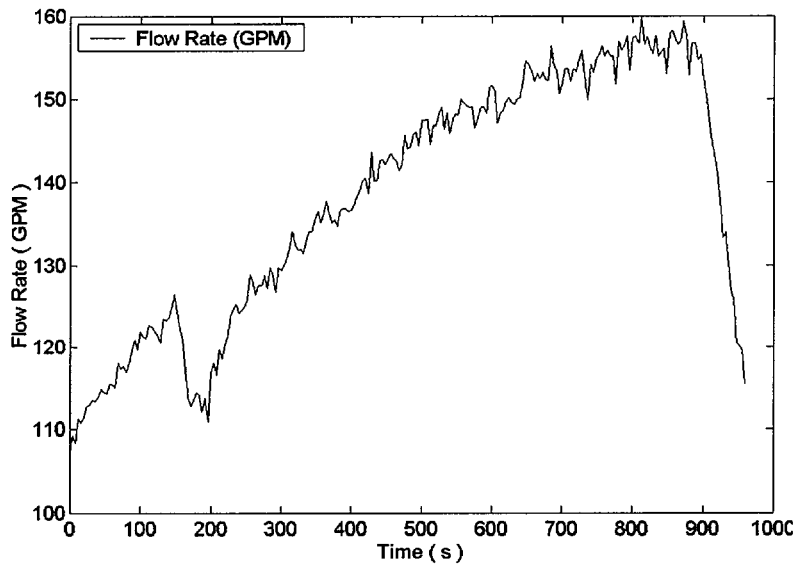

Figure C.6.2. Flow rate measurement

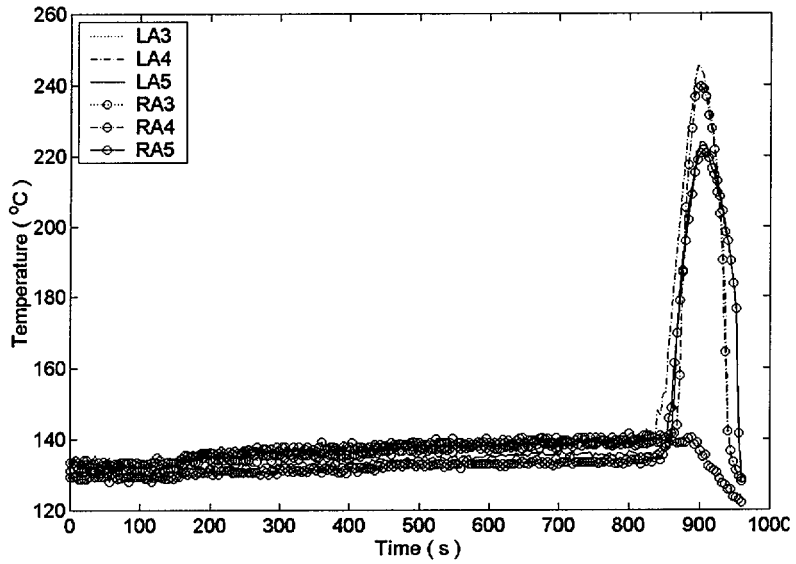

Figure C.6.3. Embedded thermocouple data in CHF-designed block (overall)

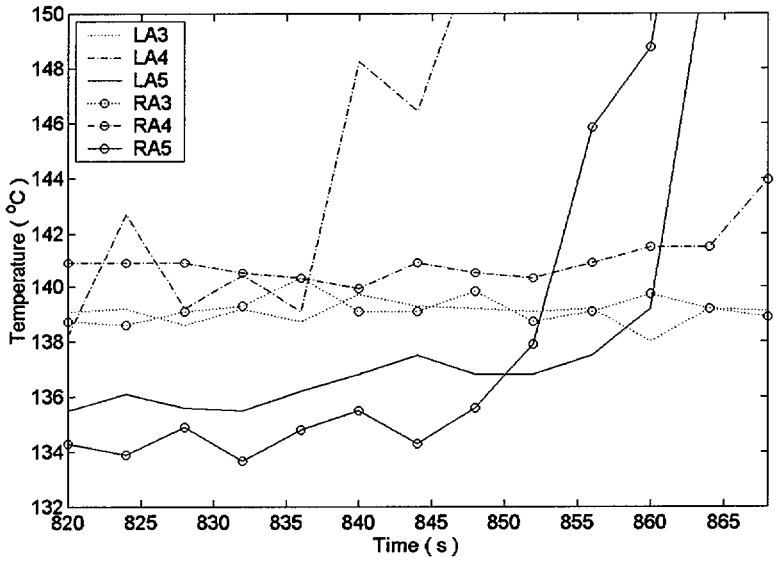

Figure C.6.4. Embedded thermocouple data in CHF-designed block (excursion)

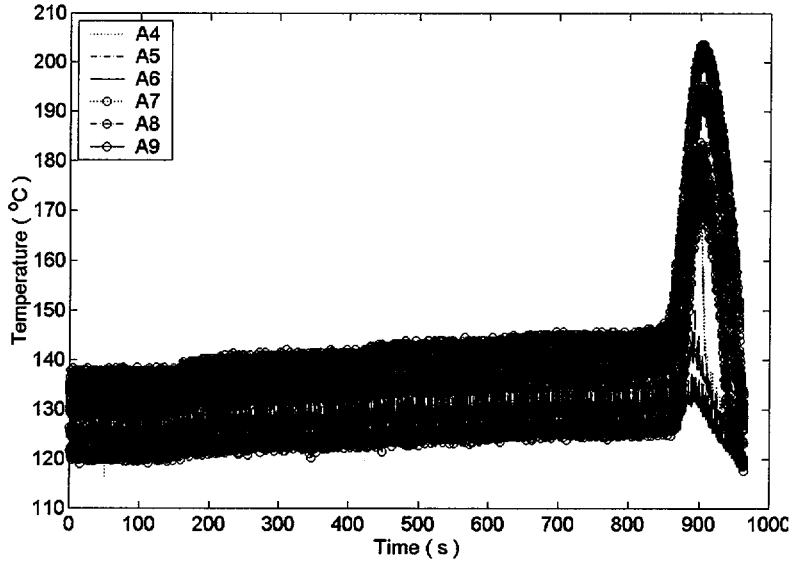

Figure C.6.5. Surface thermocouple data in CHF-designed block (overall)

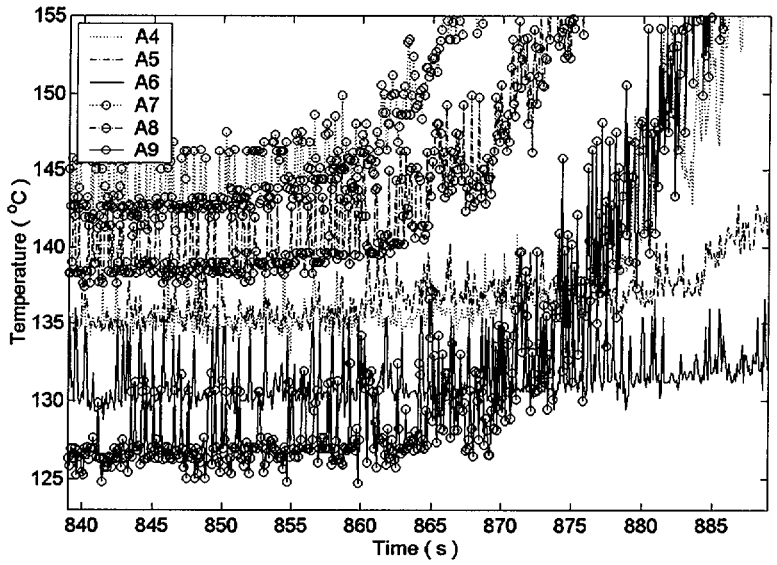

Figure C.6.6. Surface thermocouple data in CHF-designed block (excursion)

Run #7

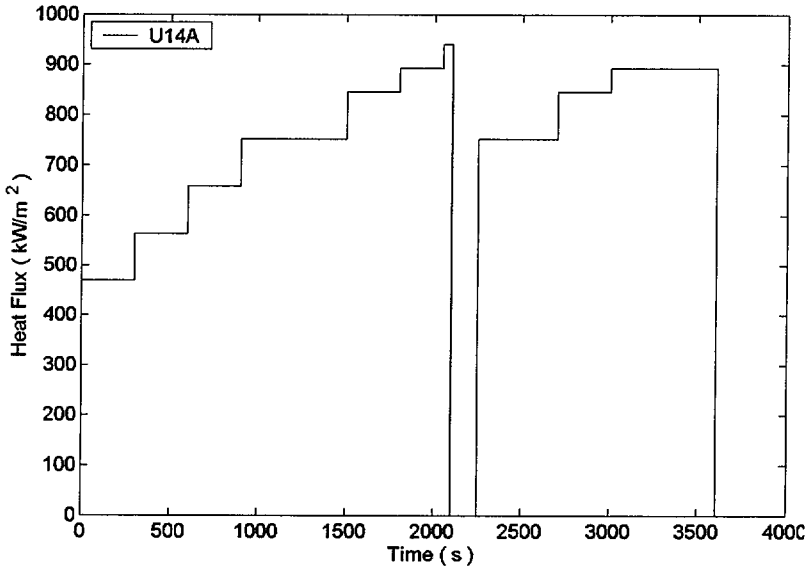

Figure C.7.1. Power history (heat flux) in the CHF-designed block A

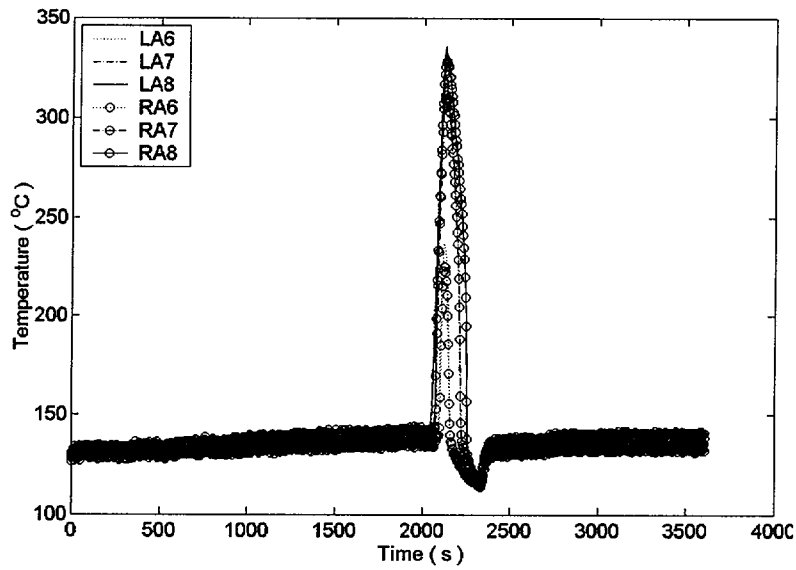

Figure C.7.2. Embedded thermocouple data in CHF-designed block (overall)

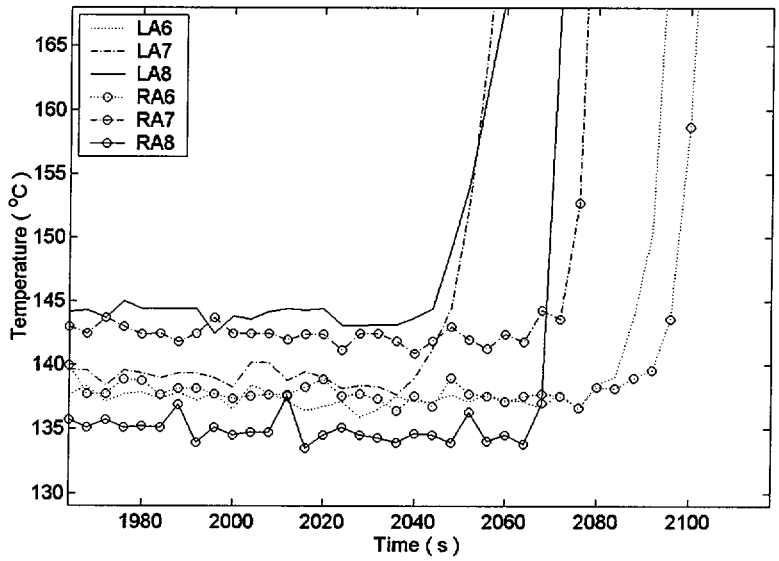

Figure C.7.3. Embedded thermocouple data in CHF-designed block (detail)

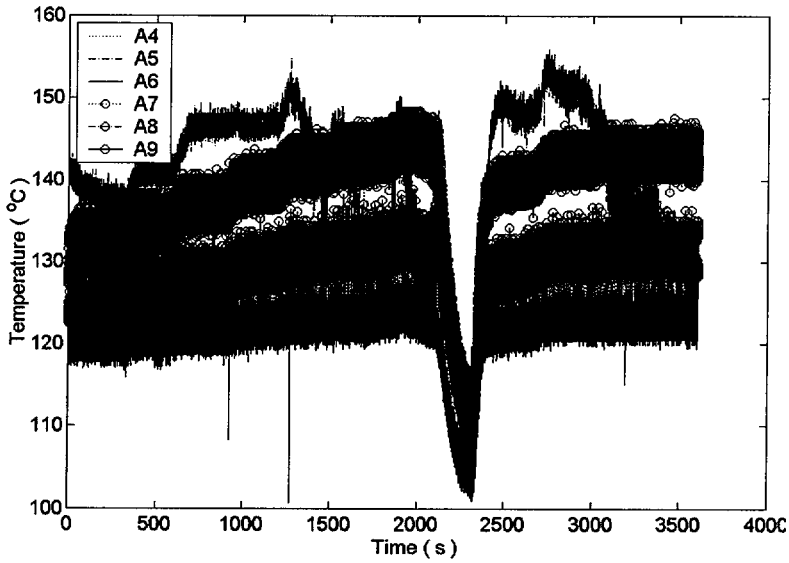

Figure C.7.4. Surface thermocouple data in CHF-designed block (overall)

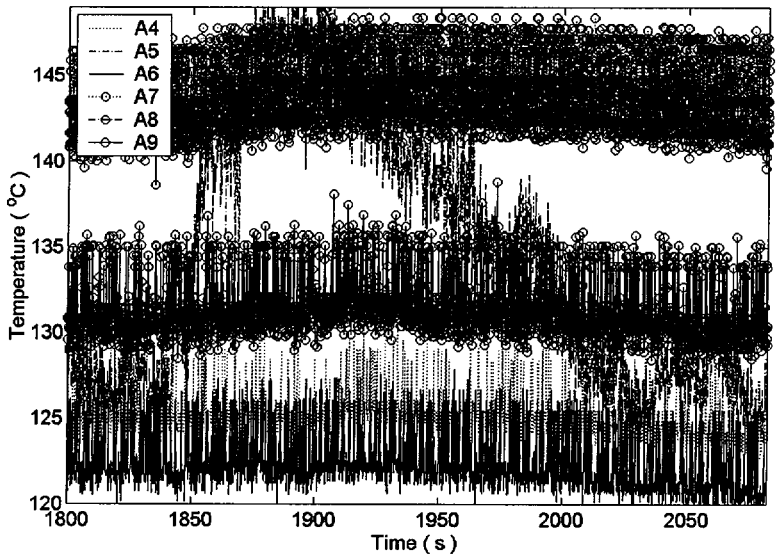

Figure C.7.5. Surface thermocouple data in CHF-designed block (detail)

Run #8

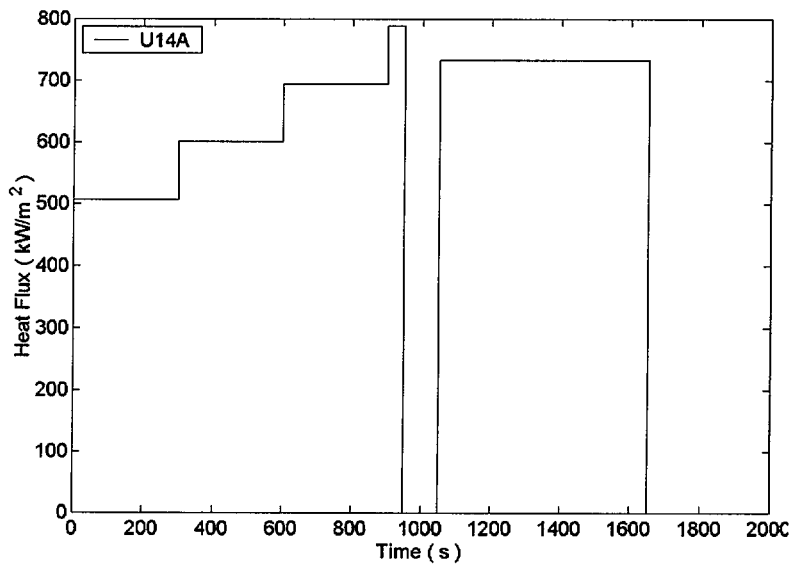

Figure C.8.1. Power history (heat flux) in the CHF-designed block A

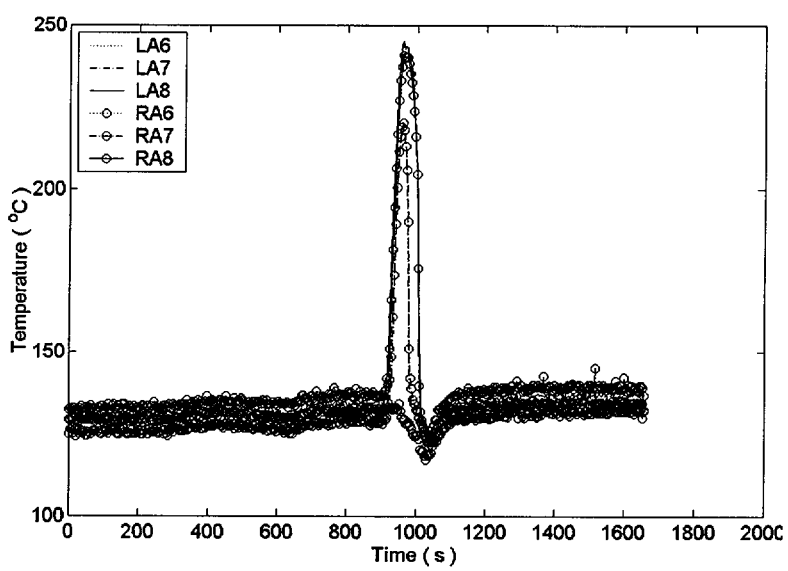

Figure C.8.2. Embedded thermocouple data in CHF-designed block (overall)

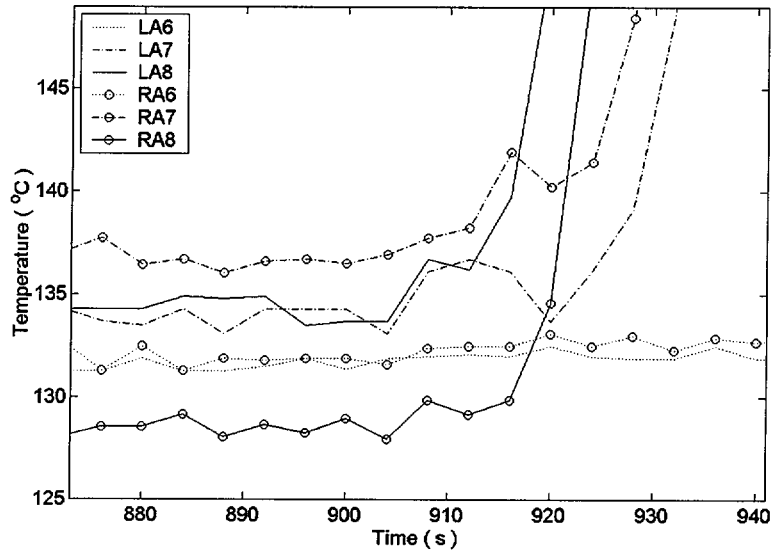

Figure C.8.3. Embedded thermocouple data in CHF-designed block (detail)

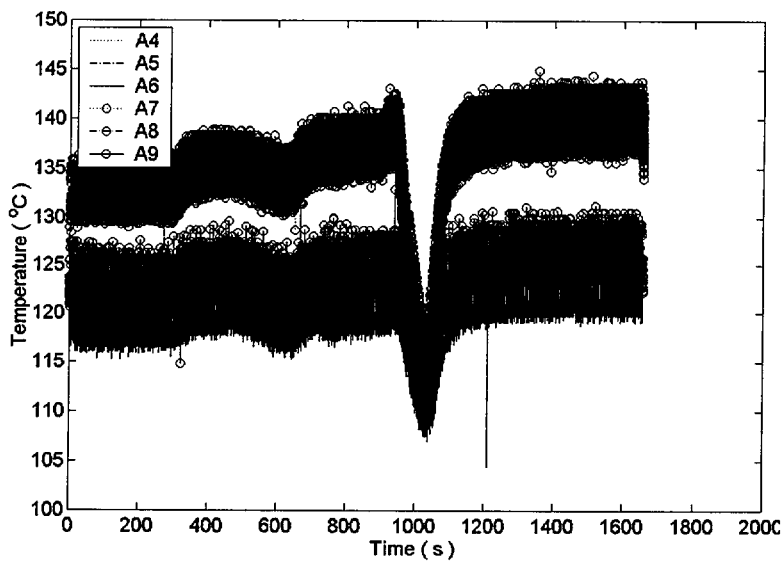

Figure C.8.4. Surface thermocouple data in CHF-designed block (overall)

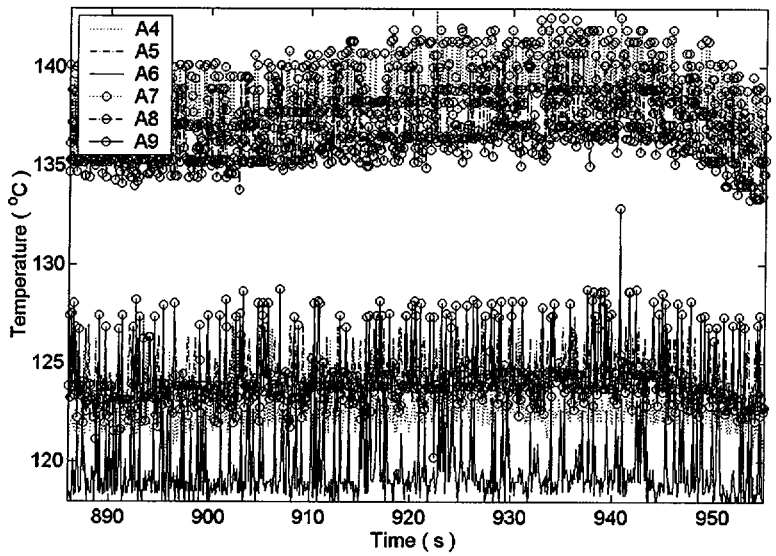

Figure C.8.5. Surface thermocouple data in CHF-designed block (detail)

Run #9

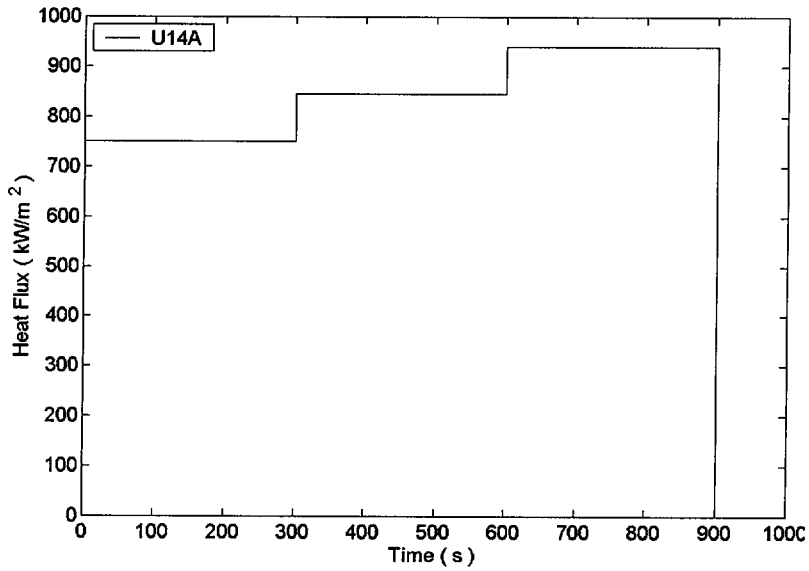

Figure C.9.1. Power history (heat flux) in the CHF-designed block A

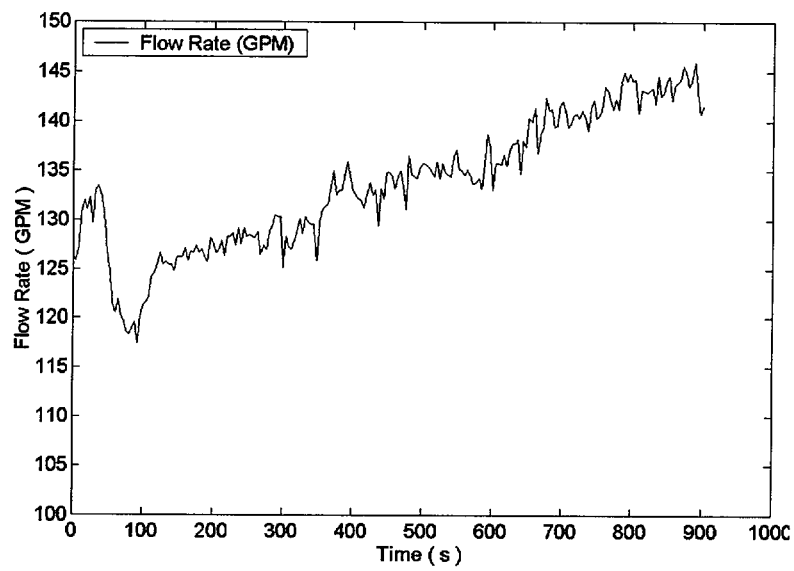

Figure C.9.2. Flow rate measurement

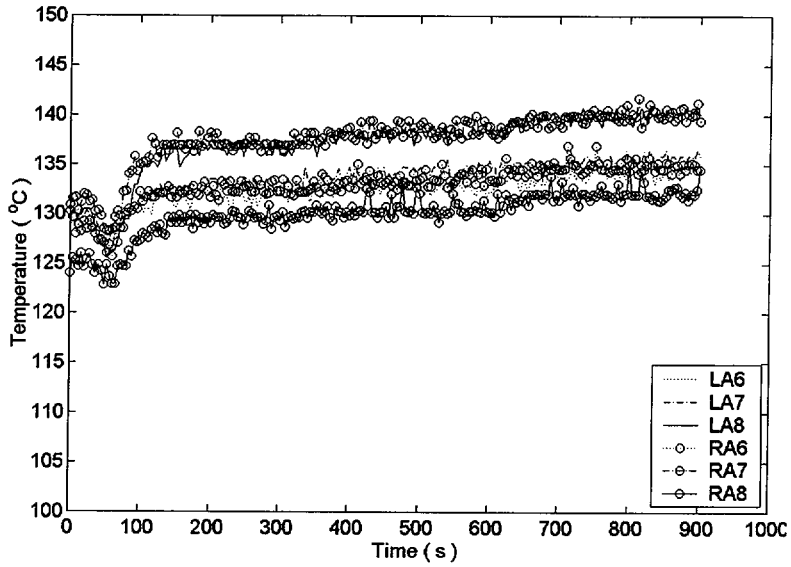

Figure C.9.3. Embedded thermocouple data in CHF-designed block (overall)

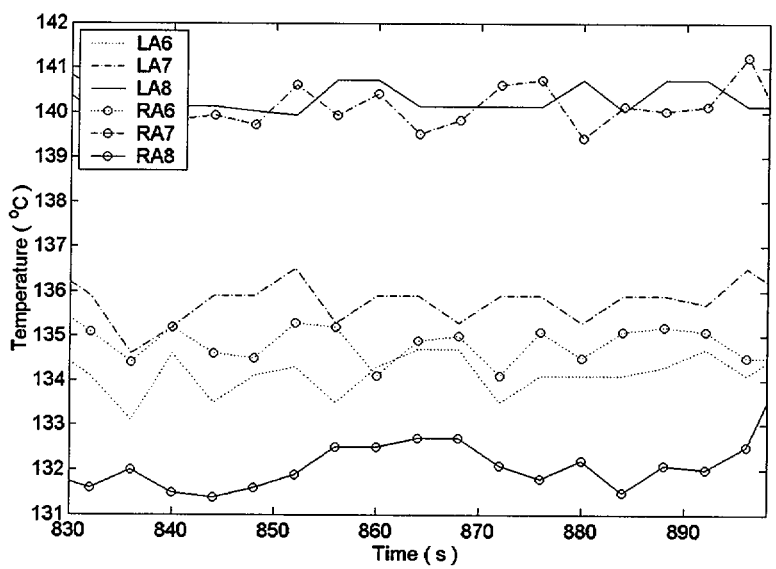

Figure C.9.4. Embedded thermocouple data in CHF-designed block (detail)

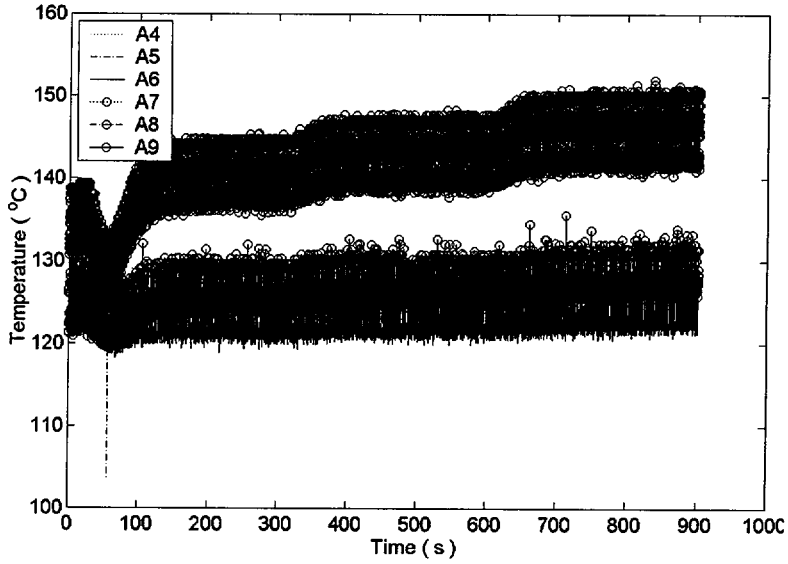

Figure C.9.5. Surface thermocouple data in CHF-designed block (overall)

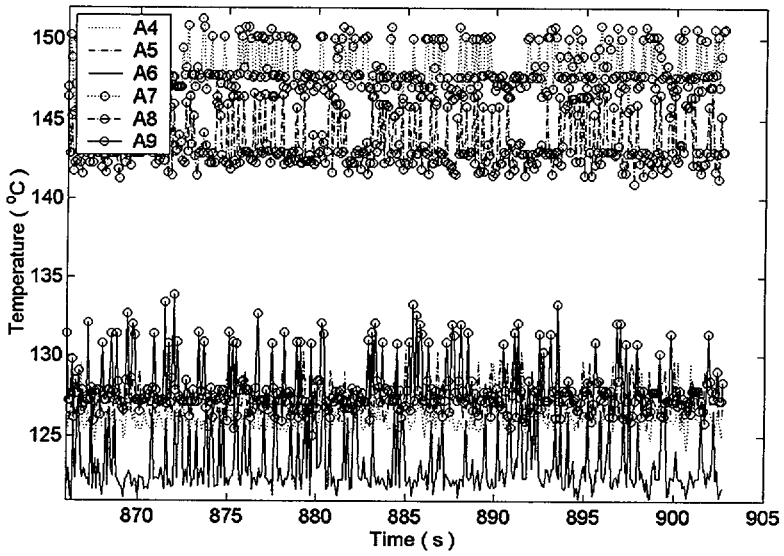

Figure C.9.6. Surface thermocouple data in CHF-designed block (detail)

Run #10

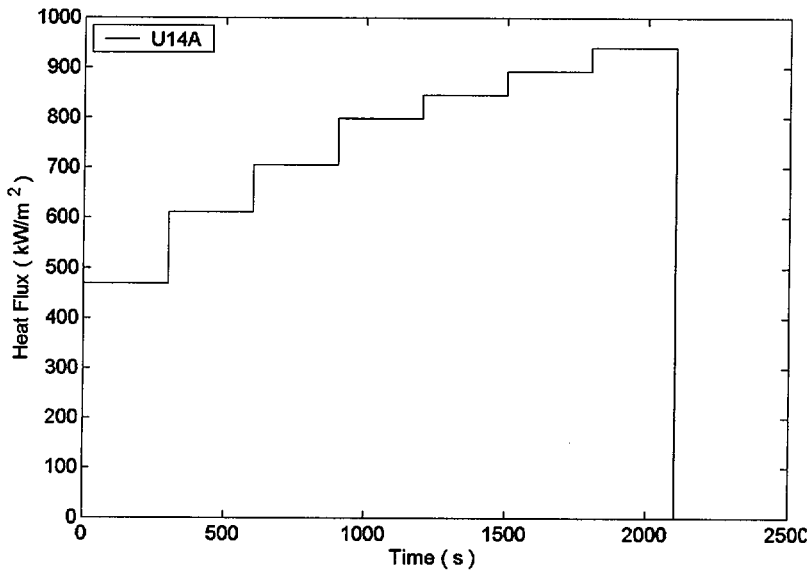

Figure C.10.1. Power history (heat flux) in the CHF-designed block A

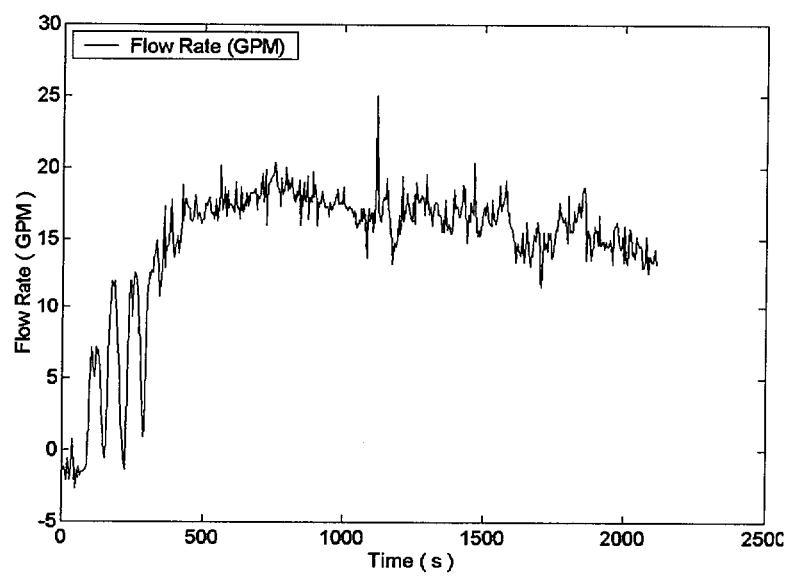

Figure C.10.2. Flow rate measurement

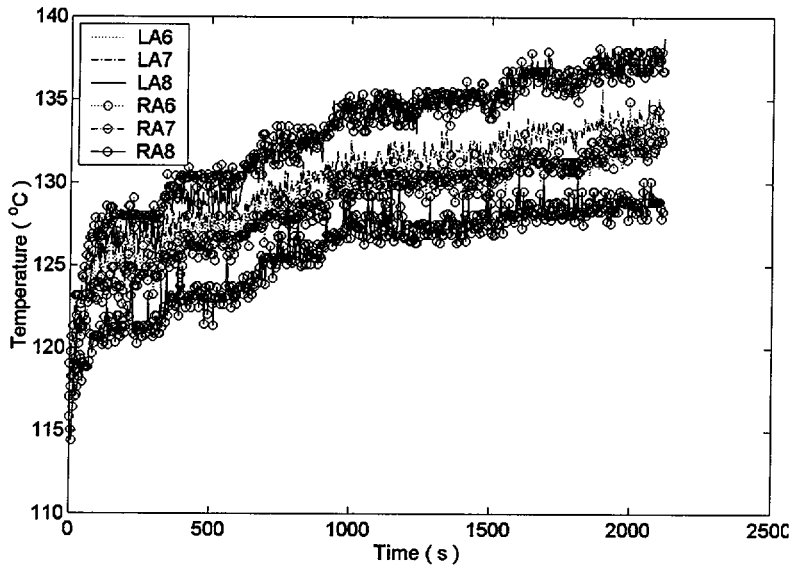

Figure C.10.3. Embedded thermocouple data in CHF-designed block (overall)

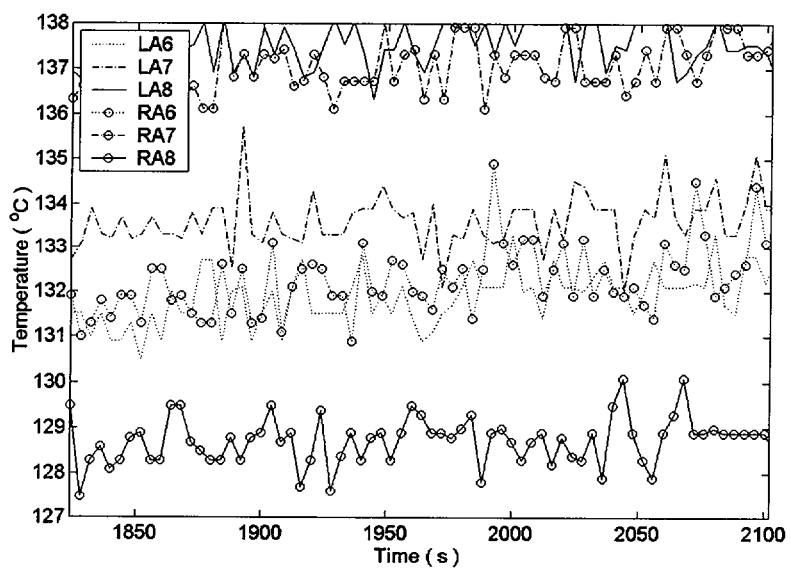

Figure C.10.4. Embedded thermocouple data in CHF-designed block (detail)

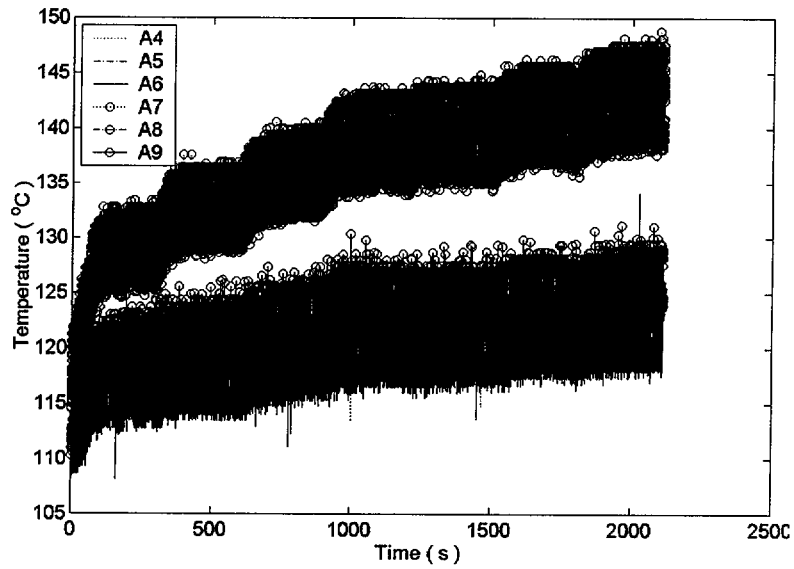

Figure C.10.5. Surface thermocouple data in CHF-designed block (overall)

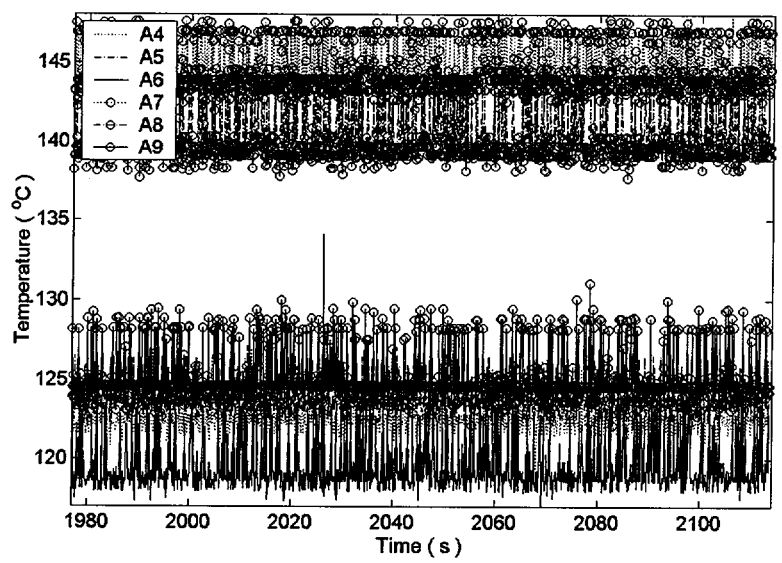

Figure C.10.6. Surface thermocouple data in CHF-designed block (detail)

Run #11

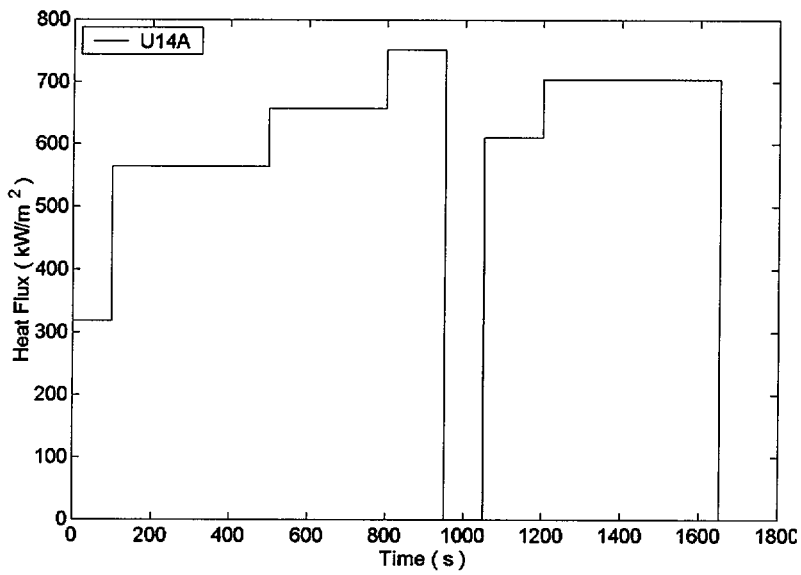

Figure C.11.1. Power history (heat flux) in the CHF-designed block A

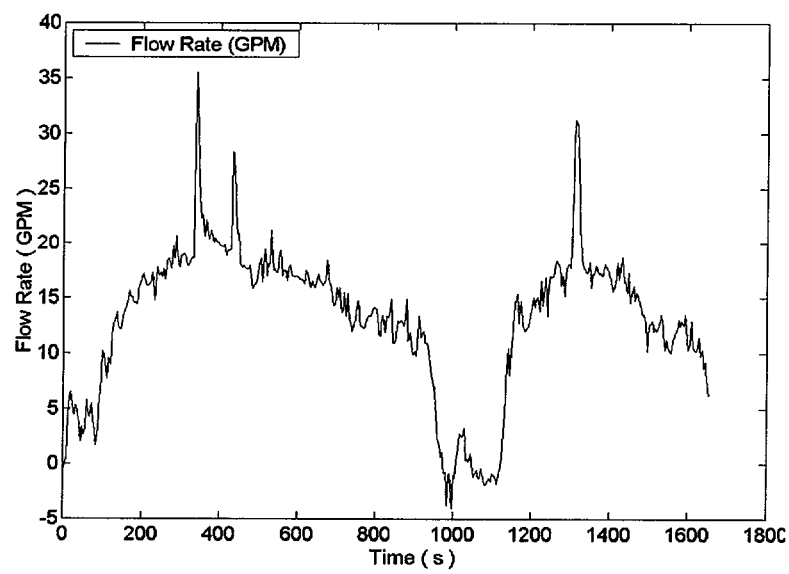

Figure C.11.2. Flow rate measurement

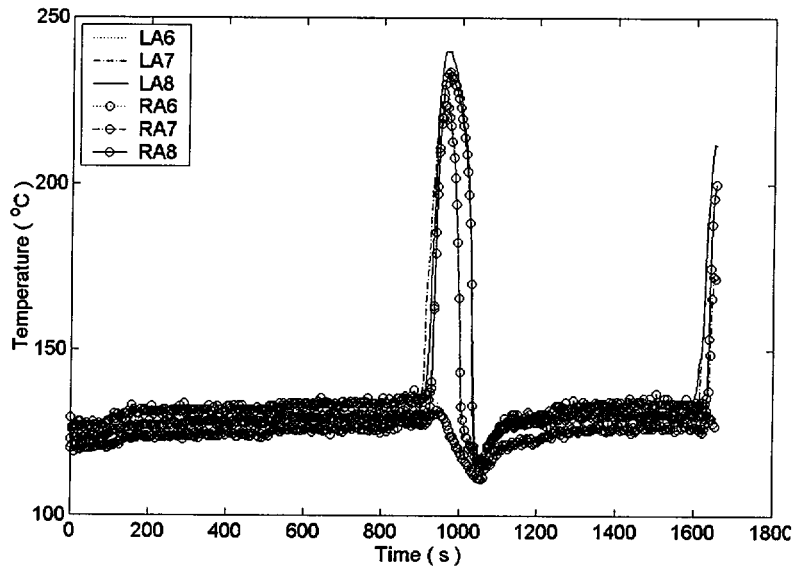

Figure C.11.3. Embedded thermocouple data in CHF-designed block (overall)

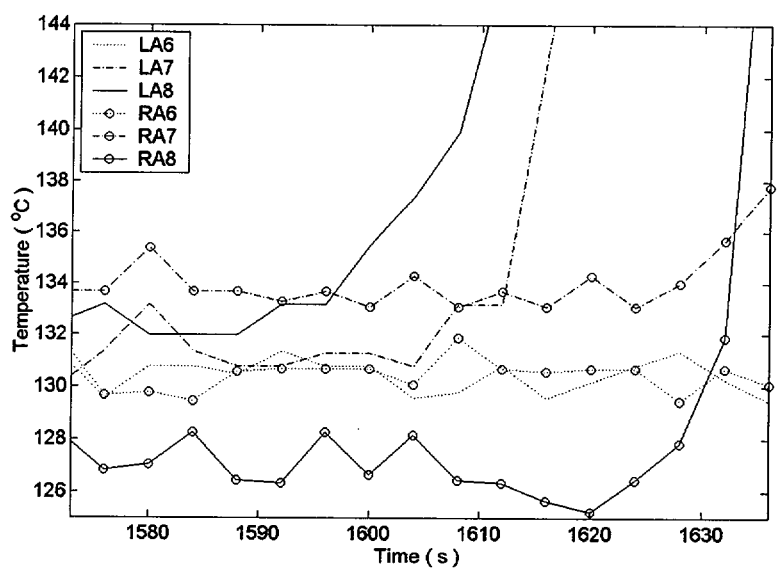

Figure C.11.4. Embedded thermocouple data in CHF-designed block (excursion)

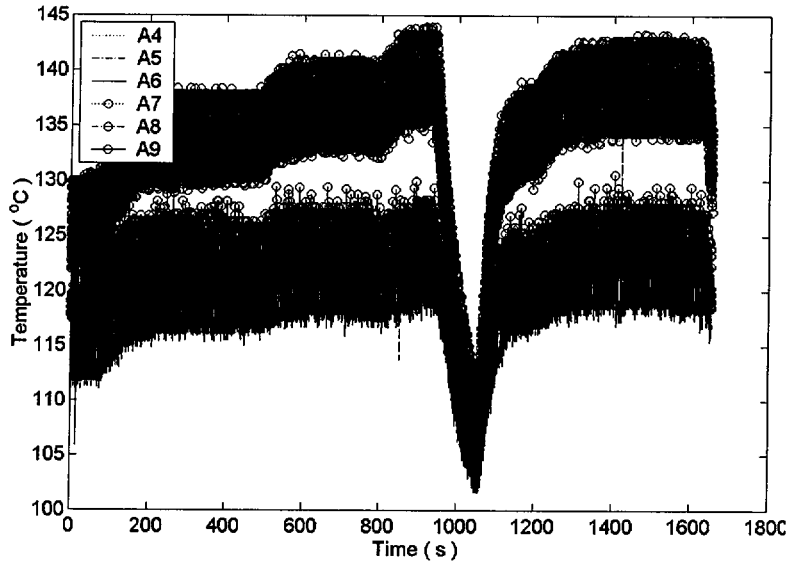

Figure C.11.5. Surface thermocouple data in CHF-designed block (overall)

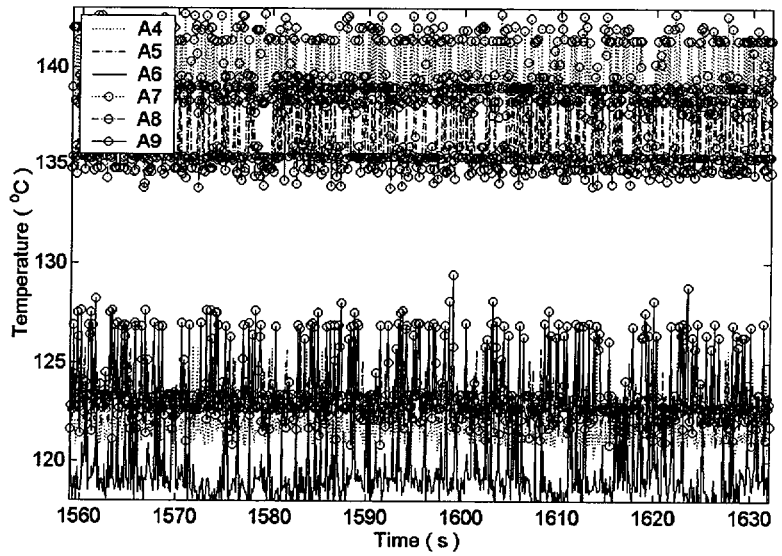

Figure C.11.6. Surface thermocouple data in CHF-designed block (detail)

Run #12

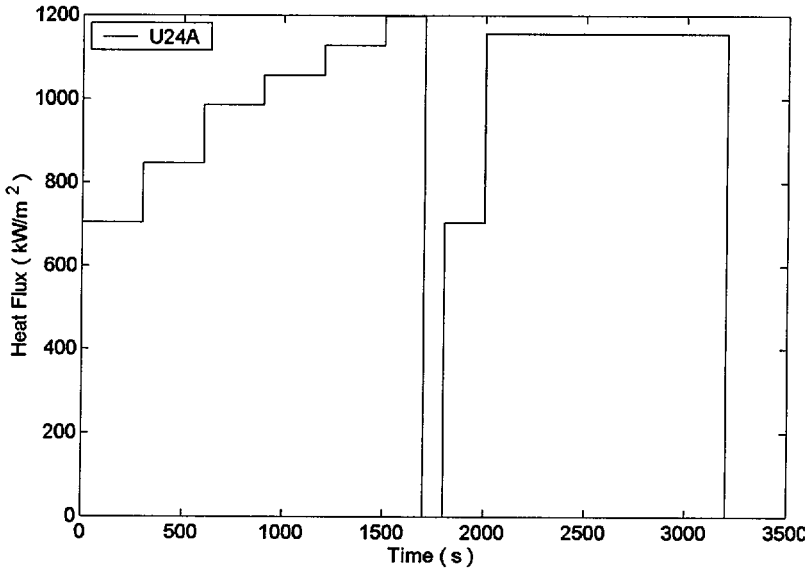

Figure C.12.1. Power history (heat flux) in the CHF-designed block B

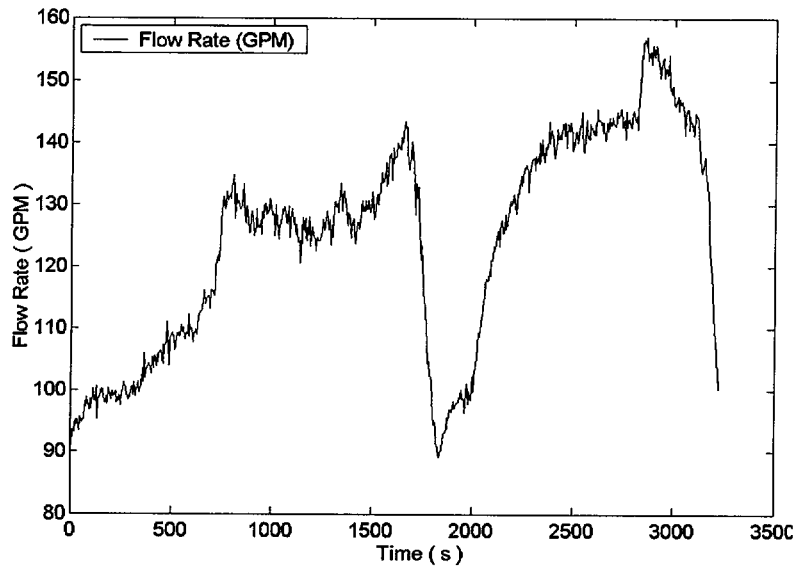

Figure C.12.2. Flow rate measurement

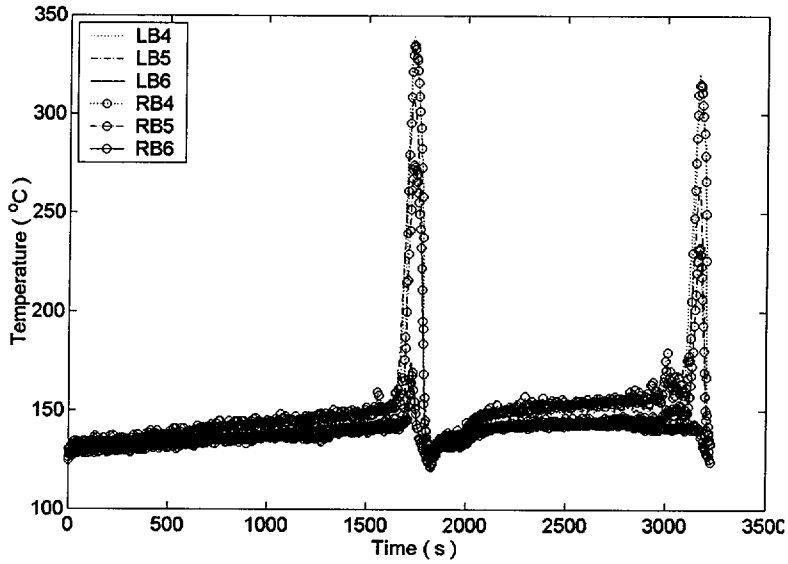

Figure C.12.3. Embedded thermocouple data in CHF-designed block (overall)

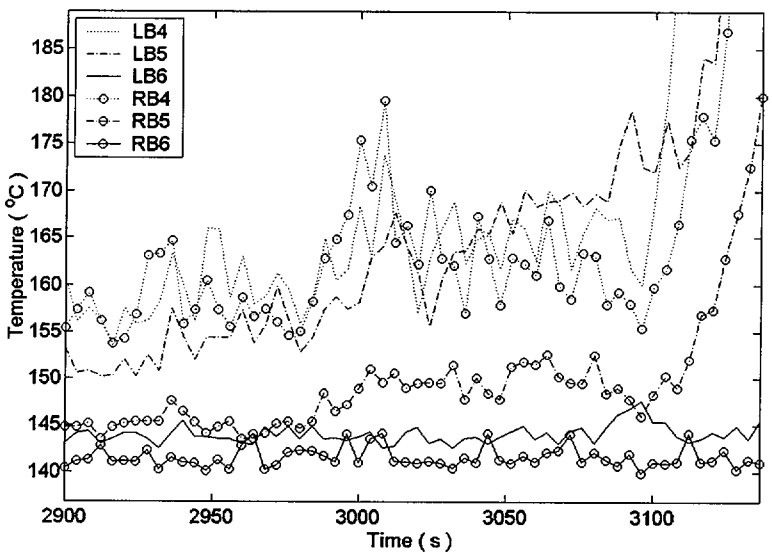

Figure C.12.4. Embedded thermocouple data in CHF-designed block (excursion)

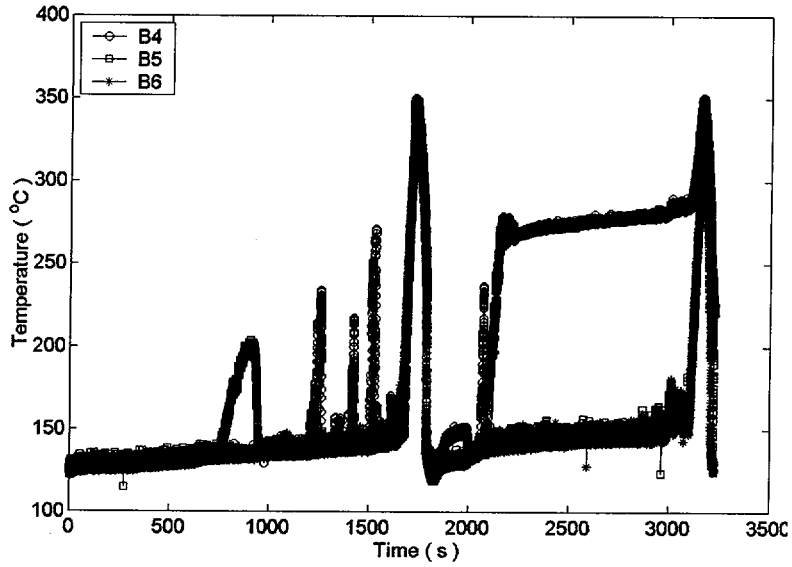

Figure C.12.5. Surface thermocouple data in CHF-designed block (overall)

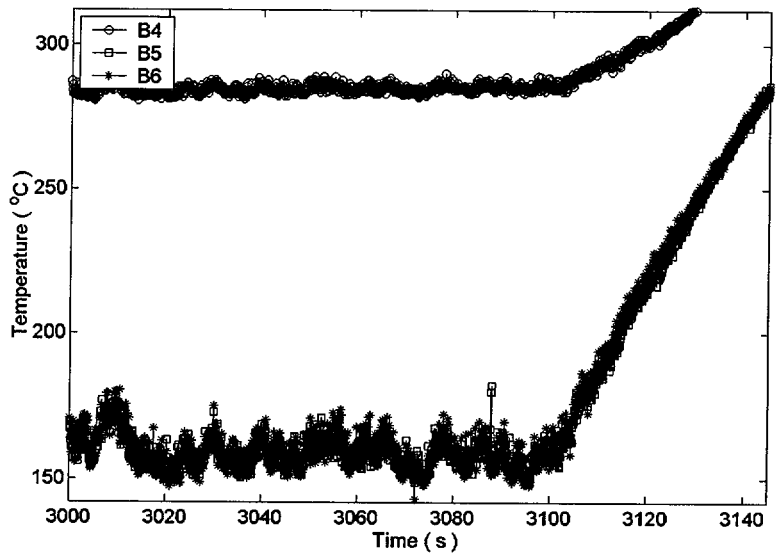

Figure C.12.6. Surface thermocouple data in CHF-designed block (excursion)

Run #13

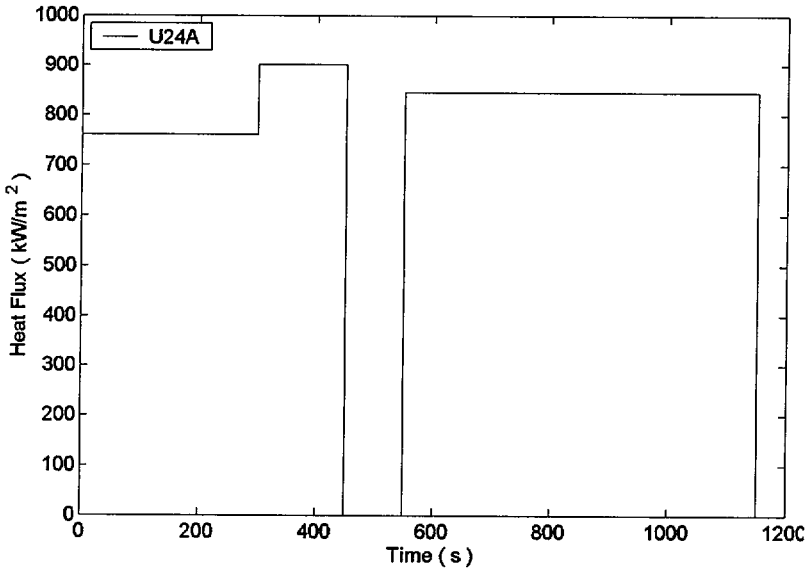

Figure C.13.1. Power history (heat flux) in the CHF-designed block B

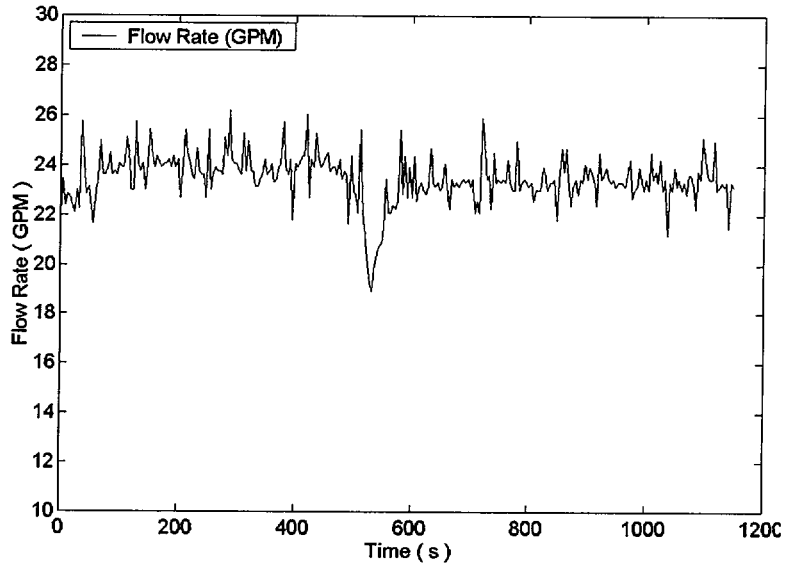

Figure C.13.2. Flow rate measurement

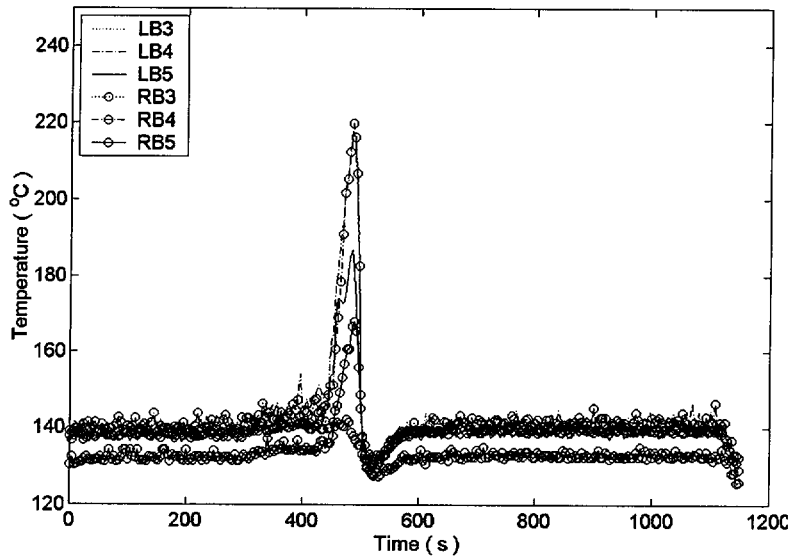

Figure C.13.3. Embedded thermocouple data in CHF-designed block (overall)

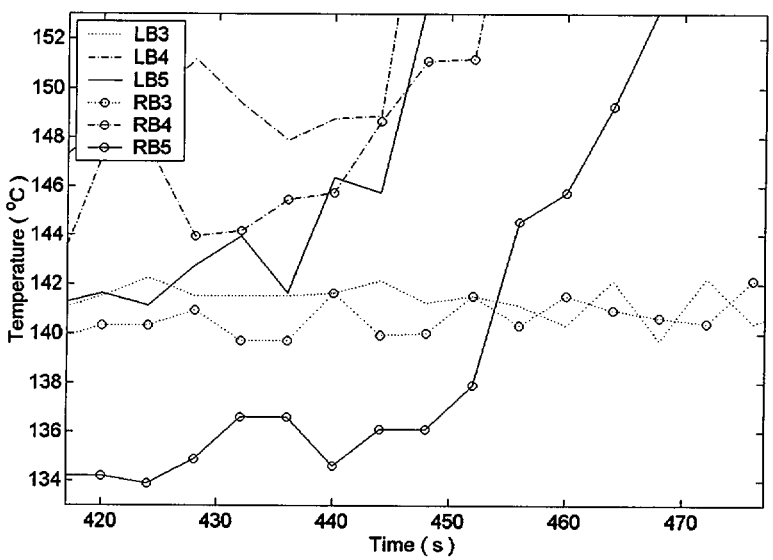

Figure C.13.4. Embedded thermocouple data in CHF-designed block (excursion)

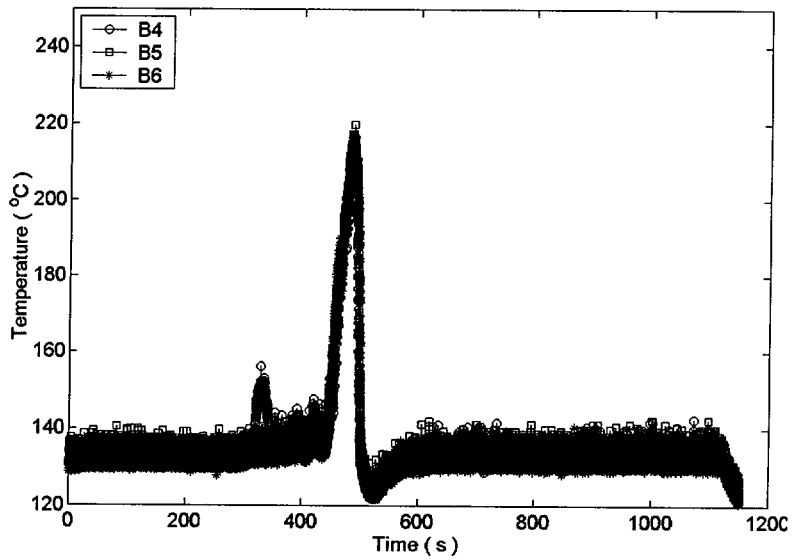

Figure C.13.5. Surface thermocouple data in CHF-designed block (overall)

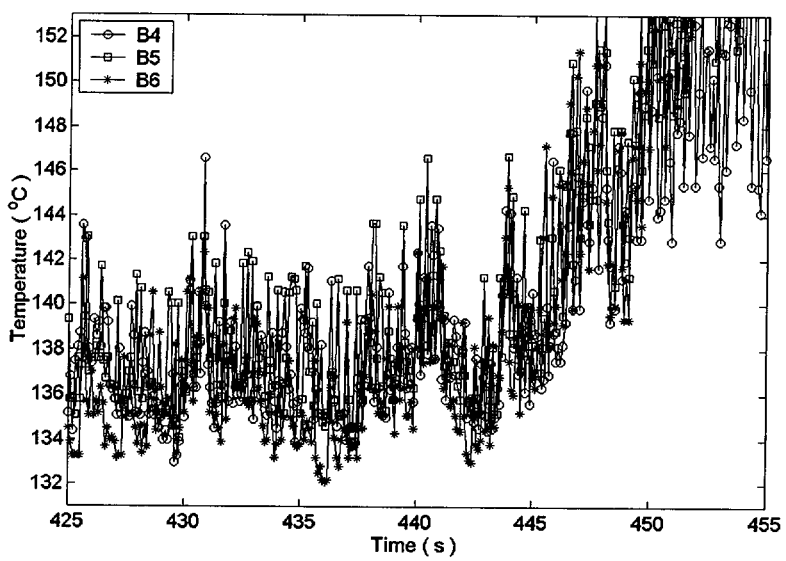

Figure C.13.6. Surface thermocouple data in CHF-designed block (excursion)

Run #14

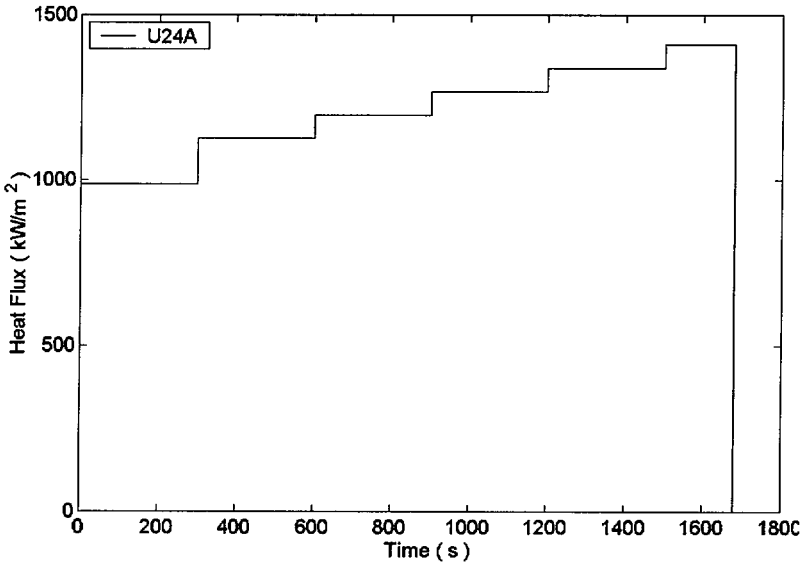

Figure C.14.1. Power history (heat flux) in the CHF-designed block B

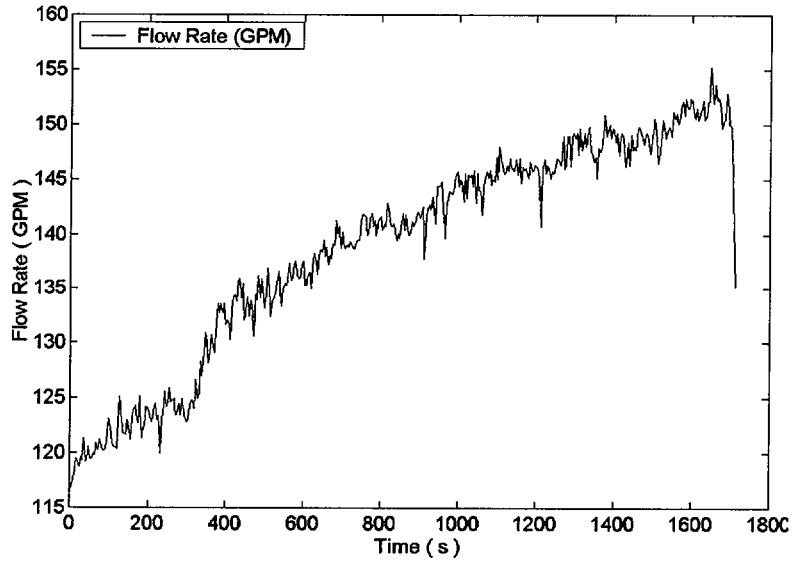

Figure C.14.2. Flow rate measurement

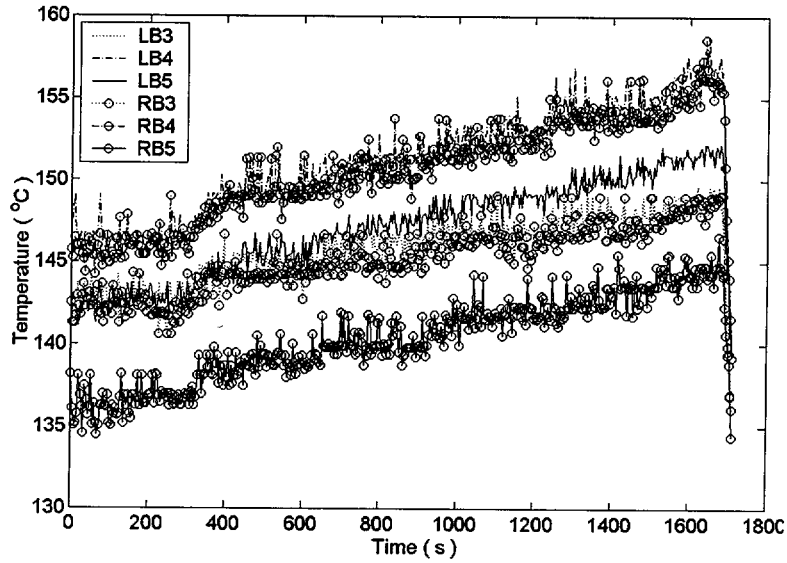

Figure C.14.3. Embedded thermocouple data in CHF-designed block (overall)

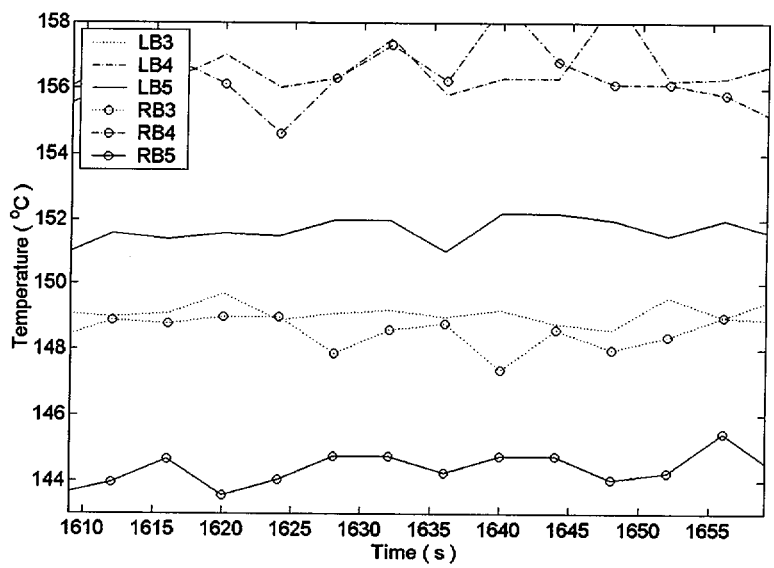

Figure C.14.4. Embedded thermocouple data in CHF-designed block (detail)

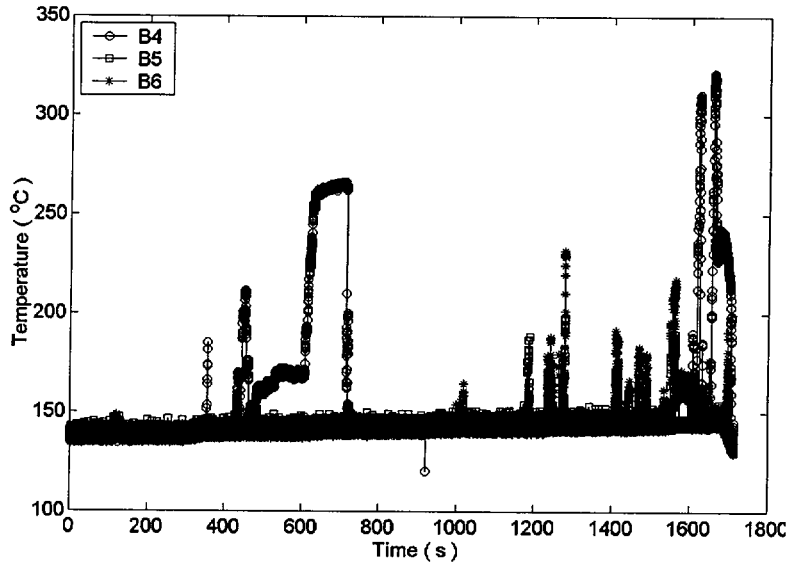

Figure C.14.5. Surface thermocouple data in CHF-designed block (overall)

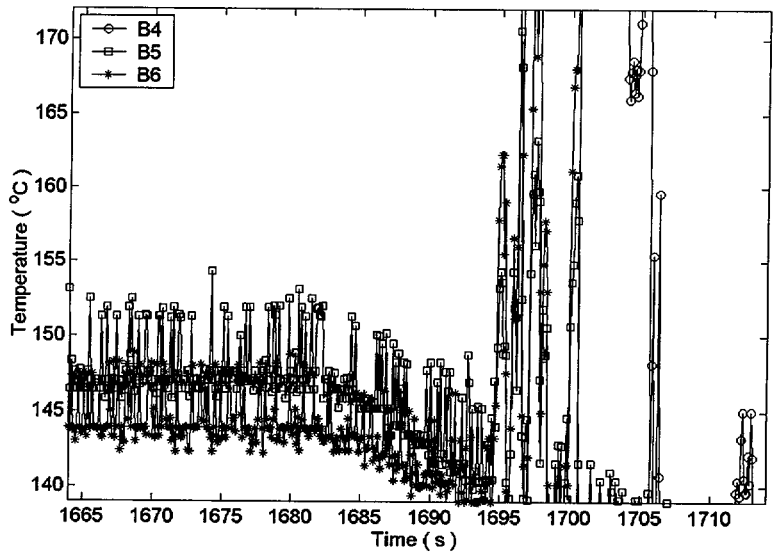

Figure C.14.6. Surface thermocouple data in CHF-designed block (detail)

Run #15

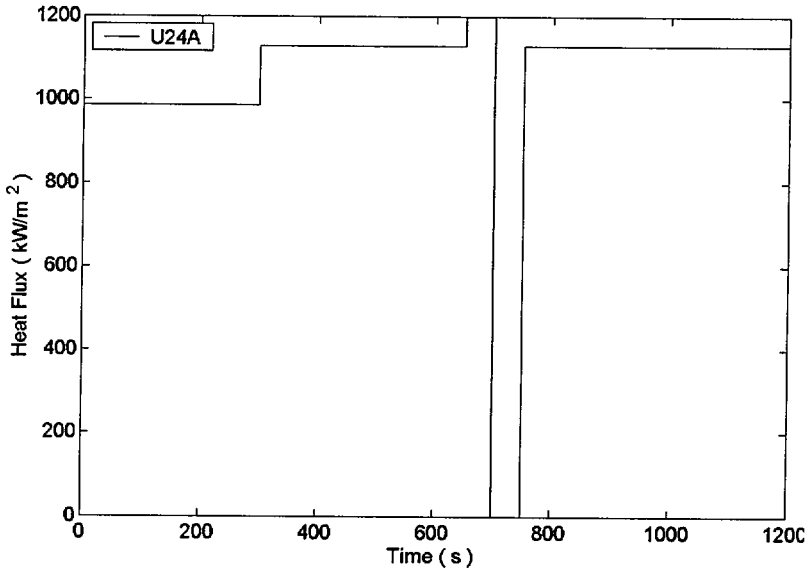

Figure C.15.1. Power history (heat flux) in the CHF-designed block B

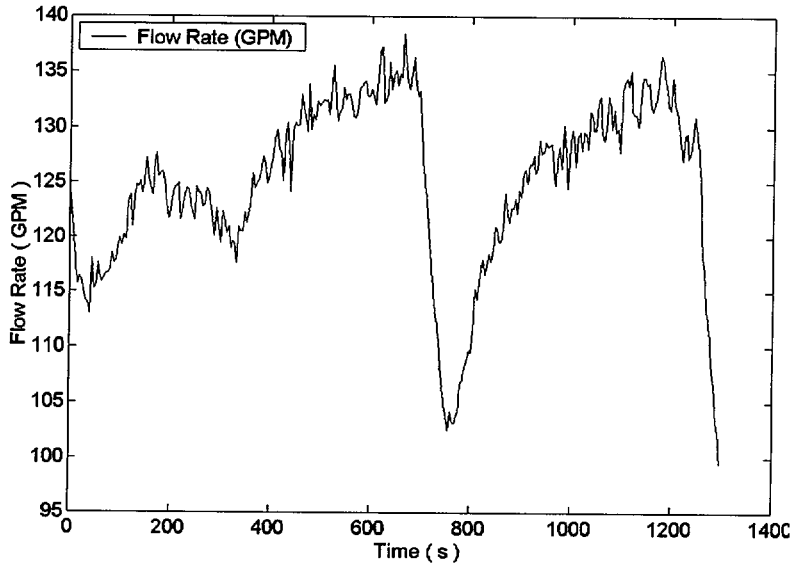

Figure C.15.2. Flow rate measurement

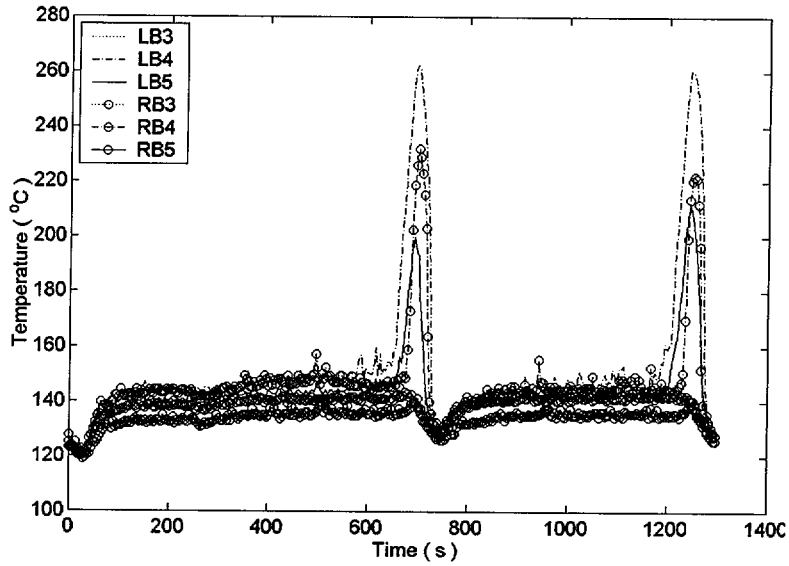

Figure C.15.3. Embedded thermocouple data in CHF-designed block (overall)

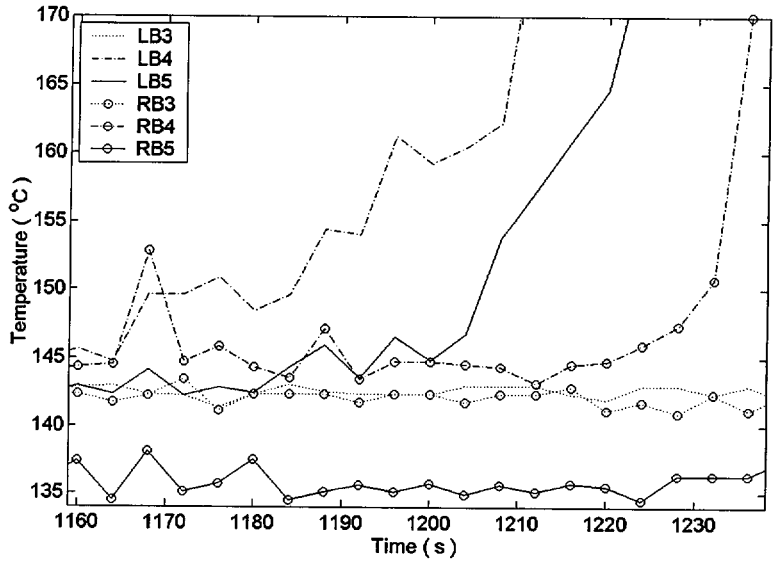

Figure C.15.4. Embedded thermocouple data in CHF-designed block (excursion)

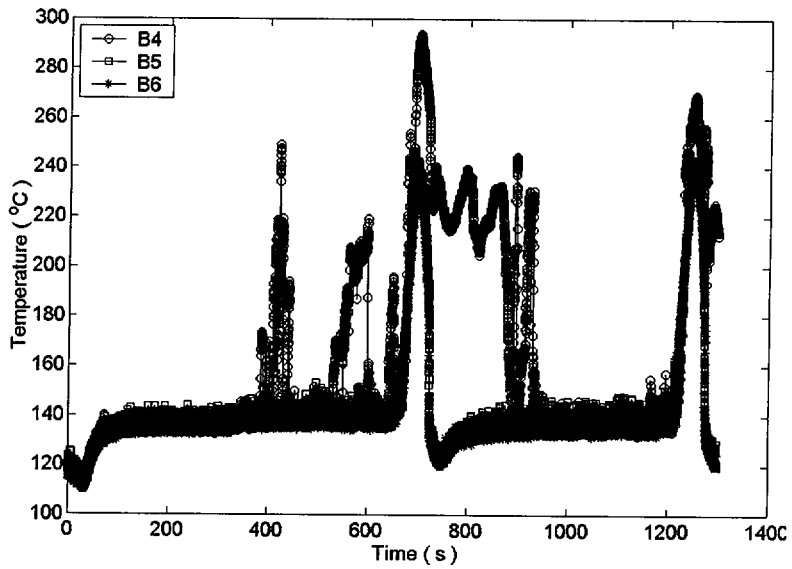

Figure C.15.5. Surface thermocouple data in CHF-designed block (overall)

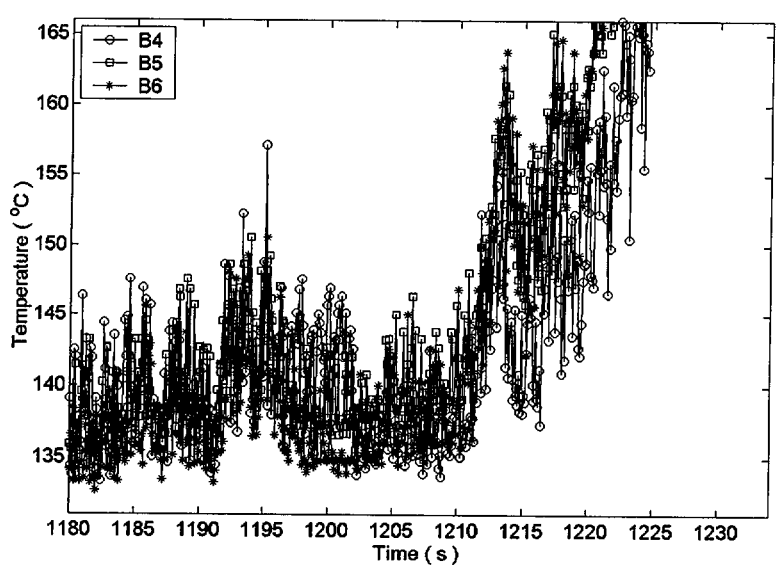

Figure C.15.6. Surface thermocouple data in CHF-designed block (excursion)

Run #16

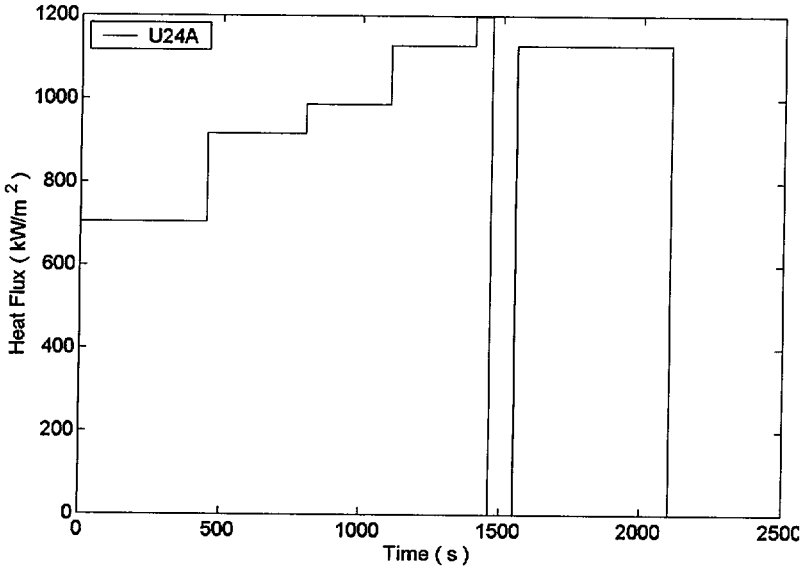

Figure C.16.1. Power history (heat flux) in the CHF-designed block B

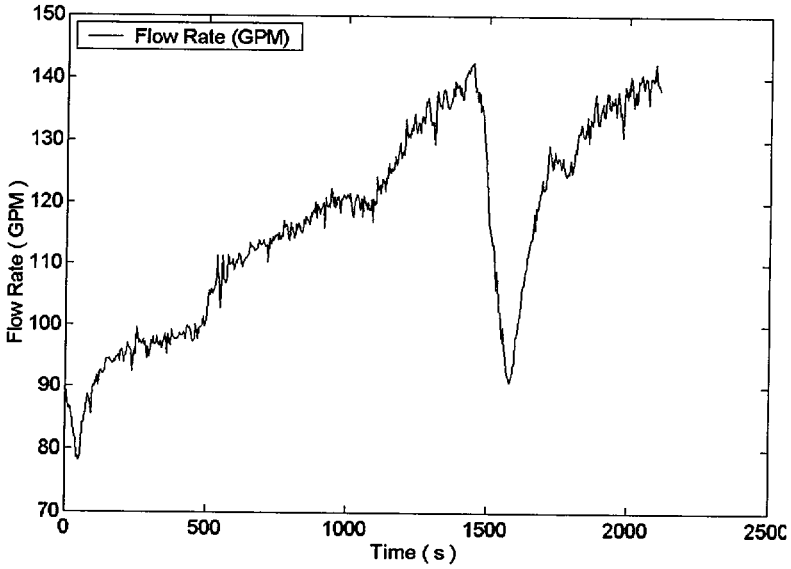

Figure C.16.2. Flow rate measurement

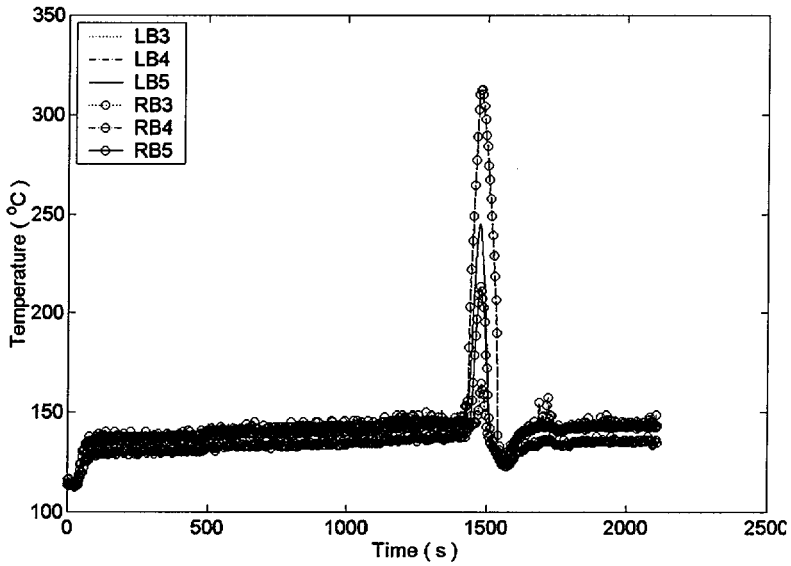

Figure C.16.3. Embedded thermocouple data in CHF-designed block (overall)

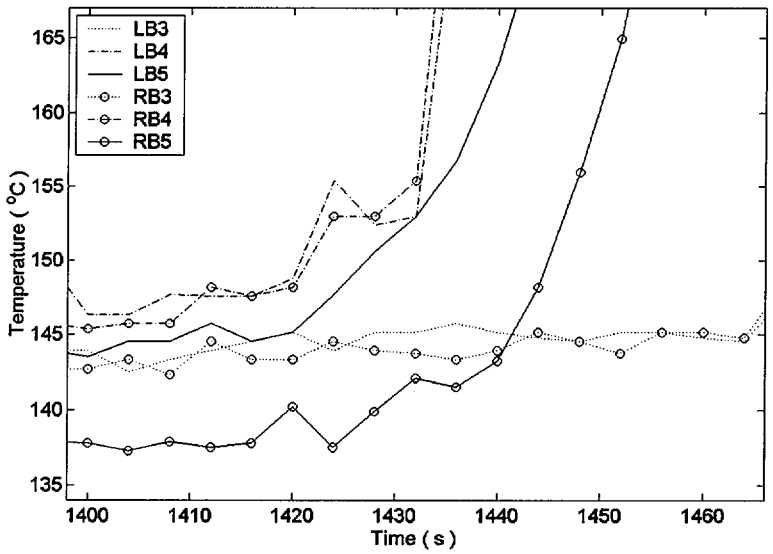

Figure C.16.4. Embedded thermocouple data in CHF-designed block (excursion)

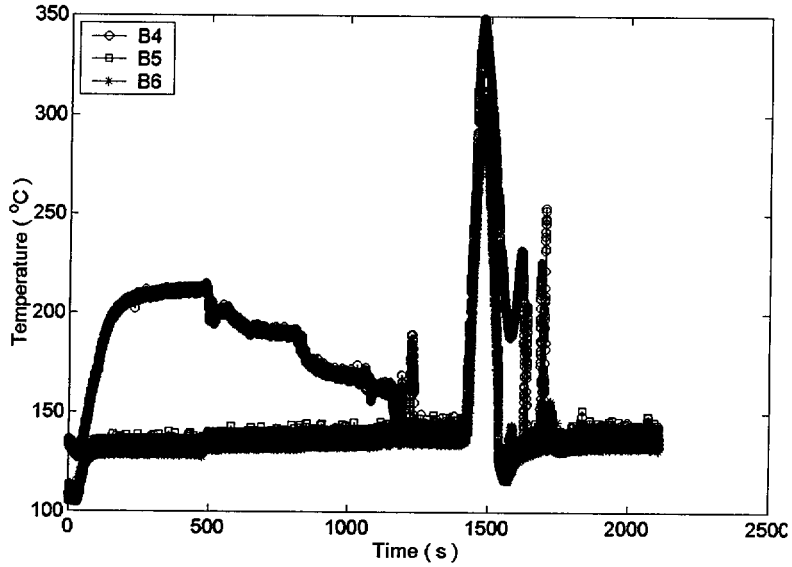

Figure C.16.5. Surface thermocouple data in CHF-designed block (overall)

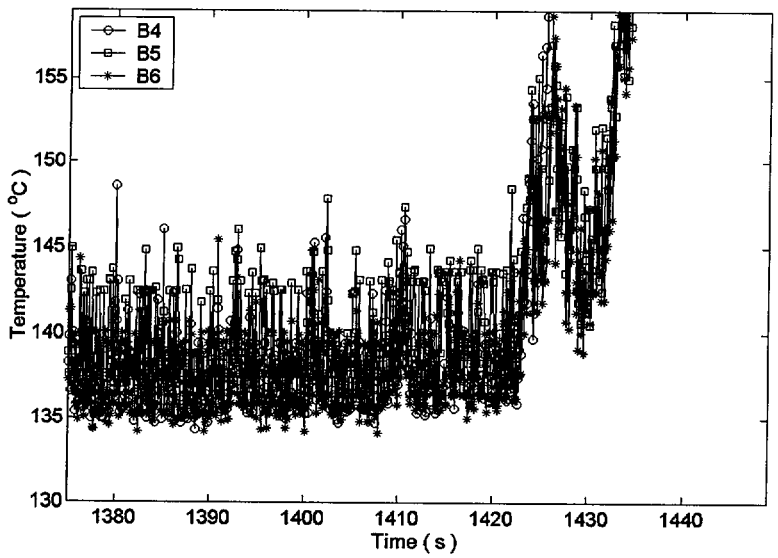

Figure C.16.6. Surface thermocouple data in CHF-designed block (excursion)

Run #17

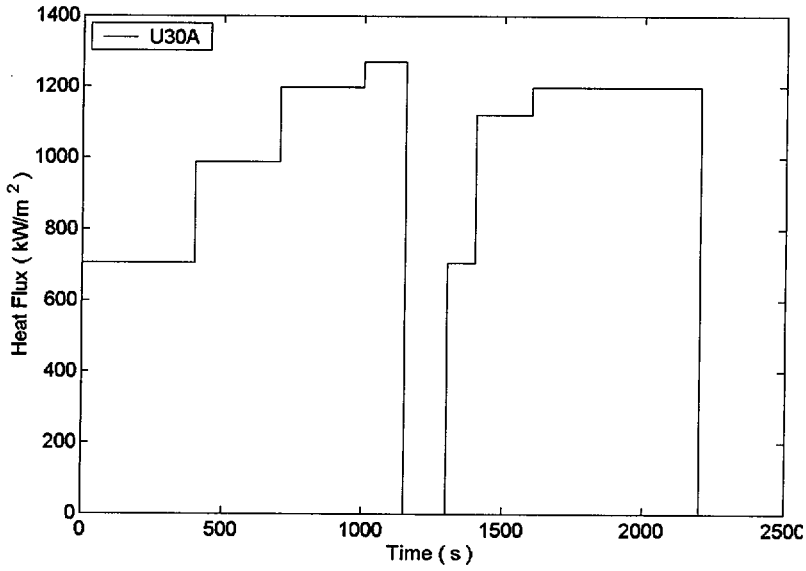

Figure C.17.1. Power history (heat flux) in the CHF-designed block B

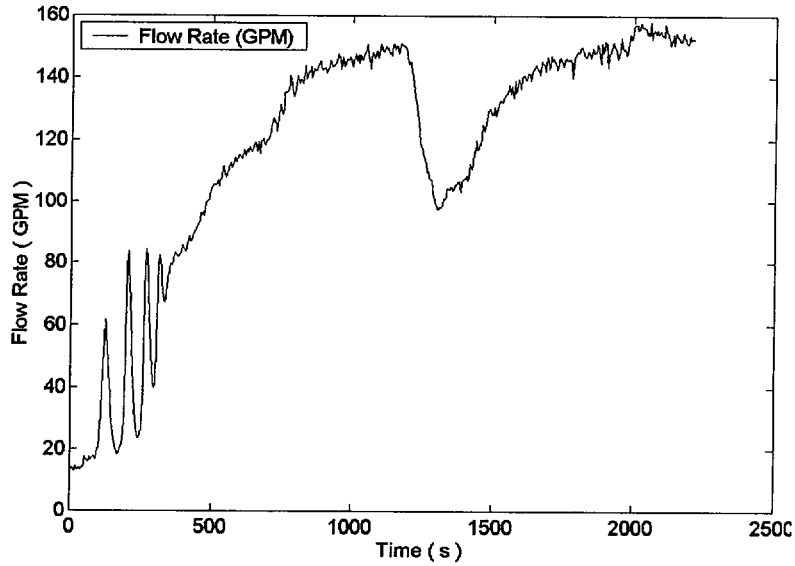

Figure C.17.2. Flow rate measurement

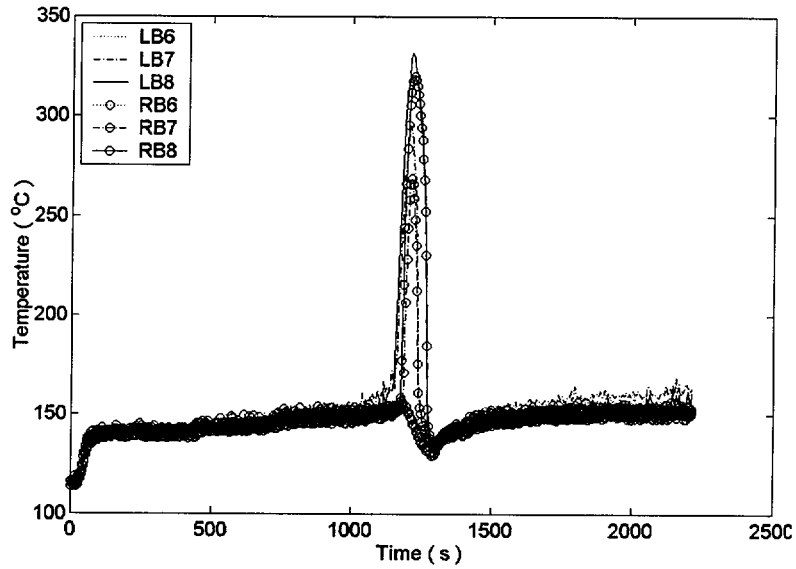

Figure C.17.3. Embedded thermocouple data in CHF-designed block (overall)

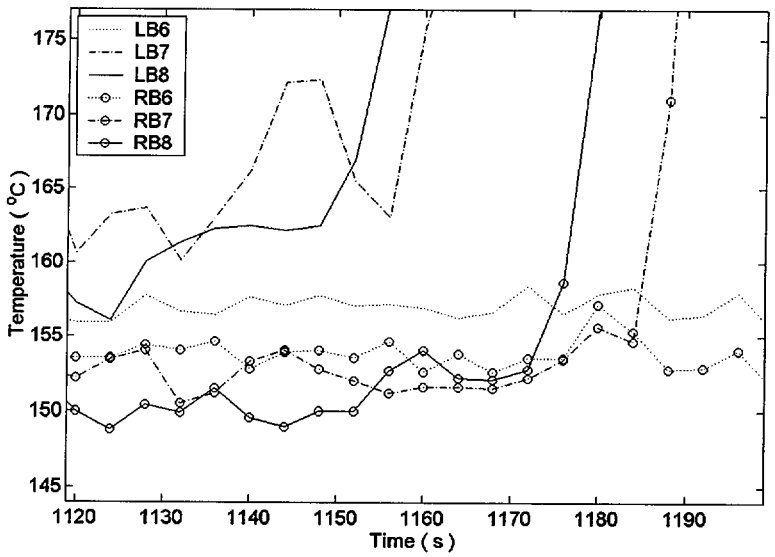

Figure C.17.4. Embedded thermocouple data in CHF-designed block (excursion)

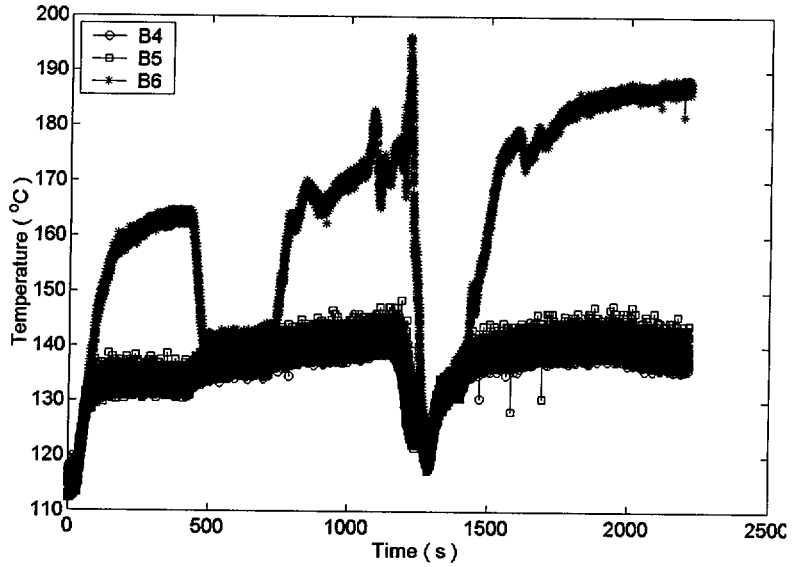

Figure C.17.5. Surface thermocouple data in CHF-designed block (overall)

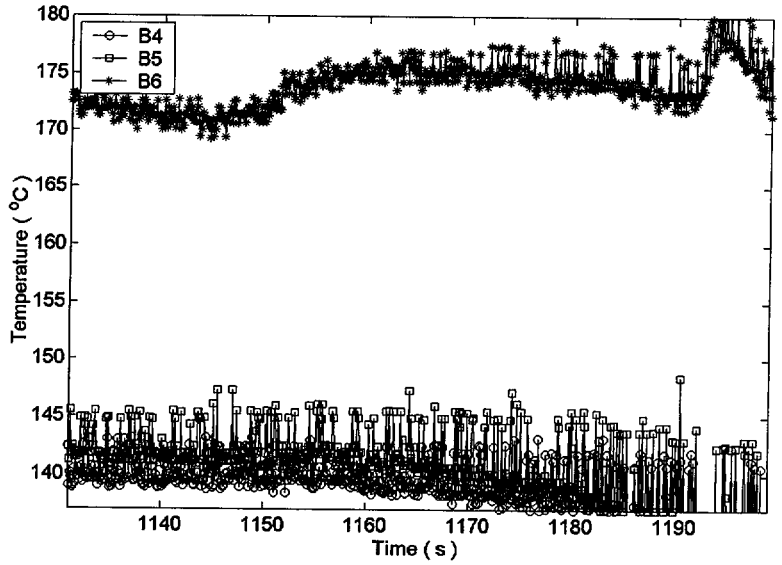

Figure C.17.6. Surface thermocouple data in CHF-designed block (excursion)

Run #18

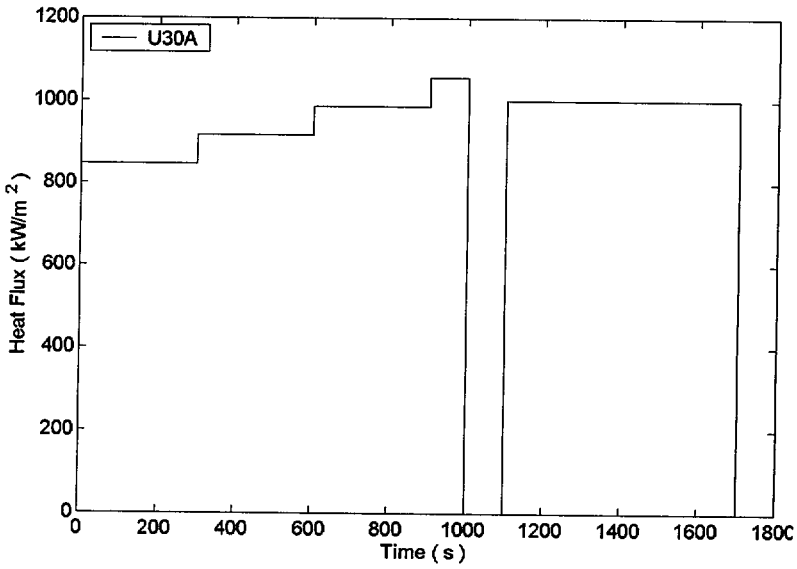

Figure C.18.1. Power history (heat flux) in the CHF-designed block B

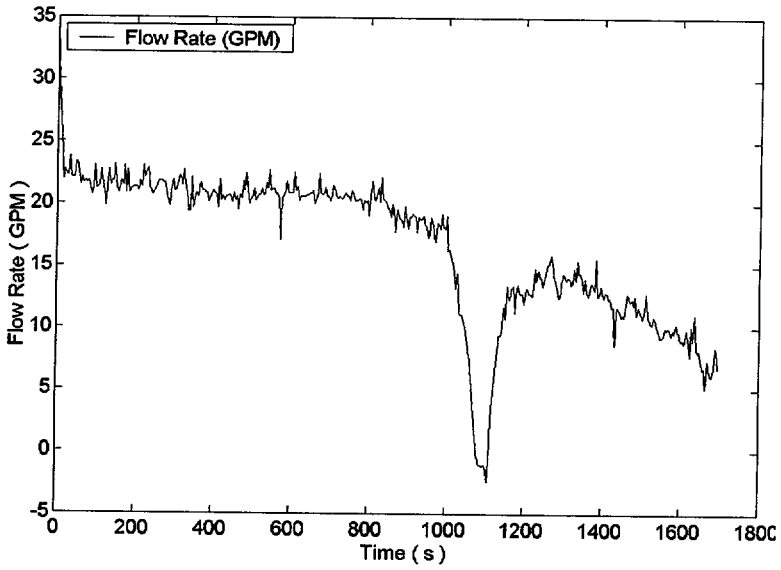

Figure C.18.2. Flow rate measurement

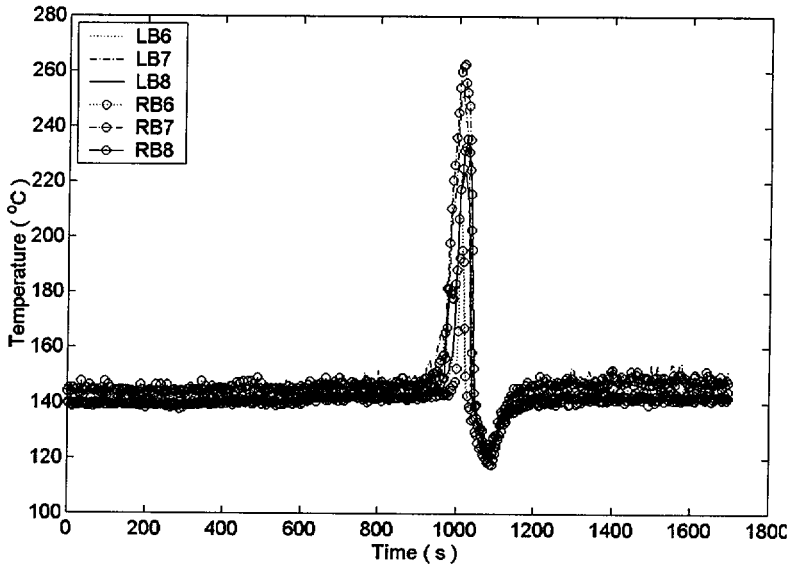

Figure C.18.3. Embedded thermocouple data in CHF-designed block (overall)

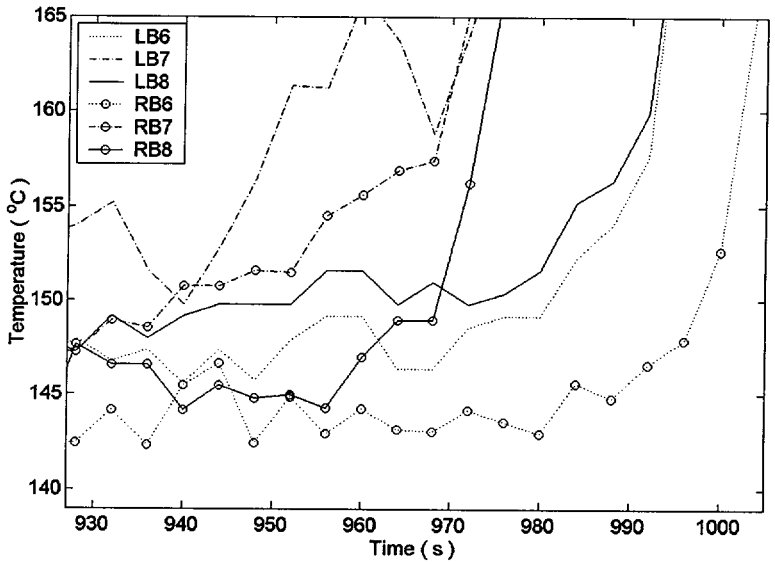

Figure C.18.4. Embedded thermocouple data in CHF-designed block (excursion)

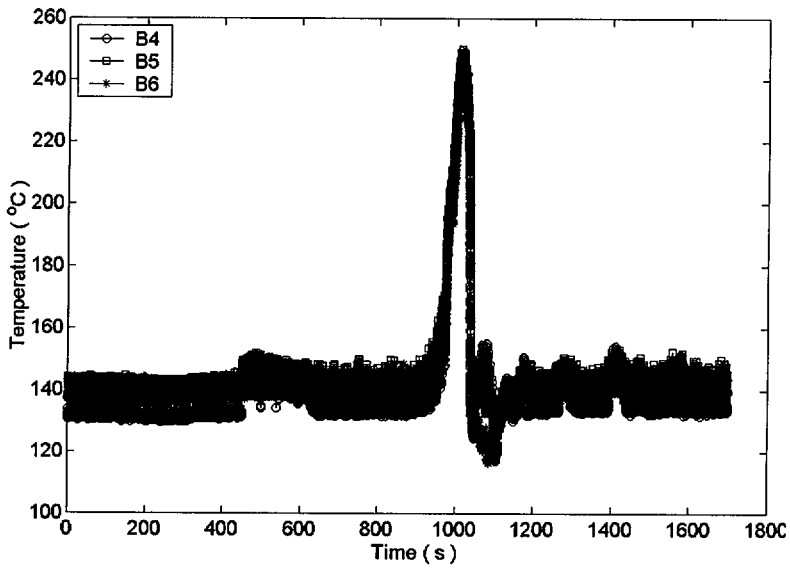

Figure C.18.5. Surface thermocouple data in CHF-designed block (overall)

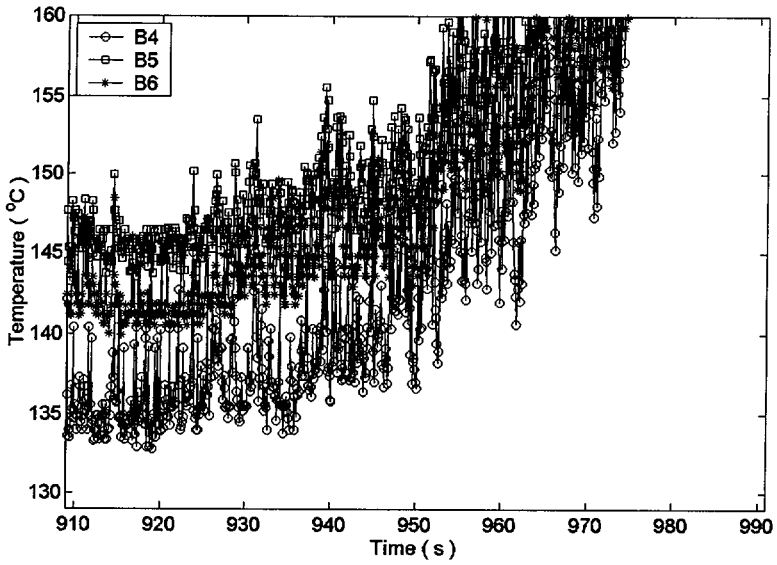

Figure C.18.6. Surface thermocouple data in CHF-designed block (excursion)

Run #19

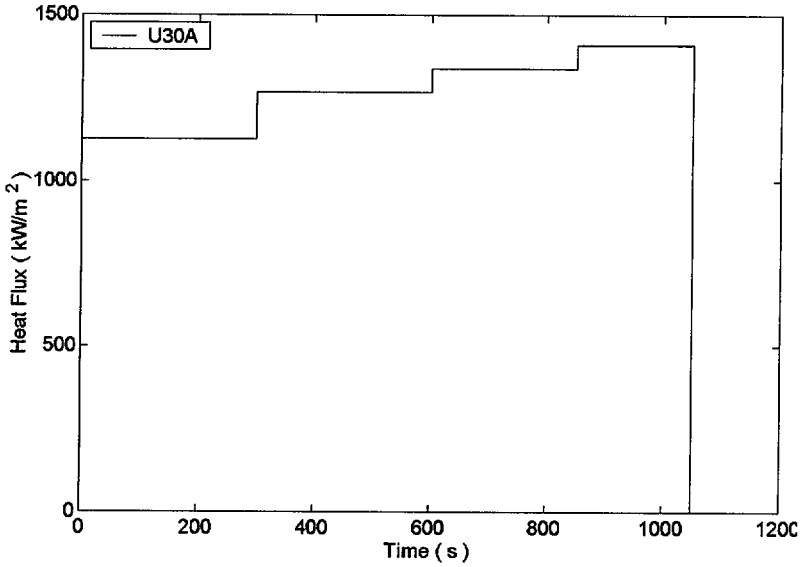

Figure C.19.1. Power history (heat flux) in the CHF-designed block C

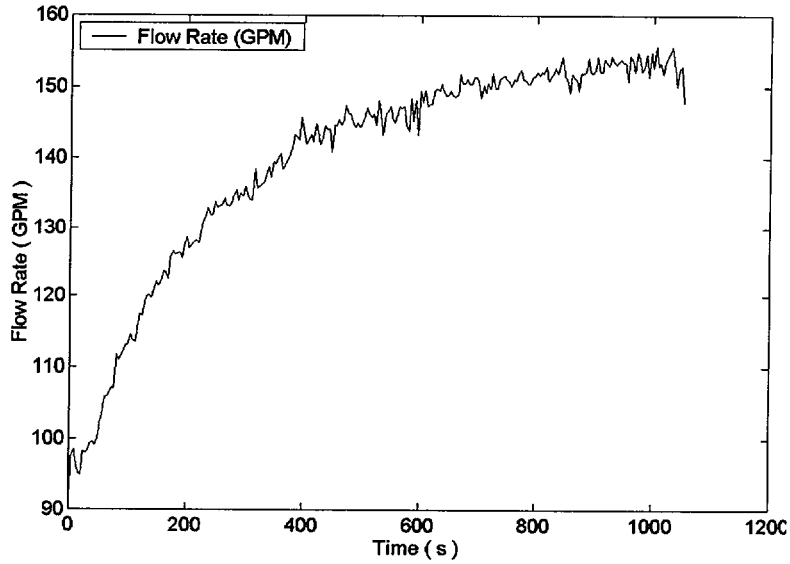

Figure C.19.2. Flow rate measurement

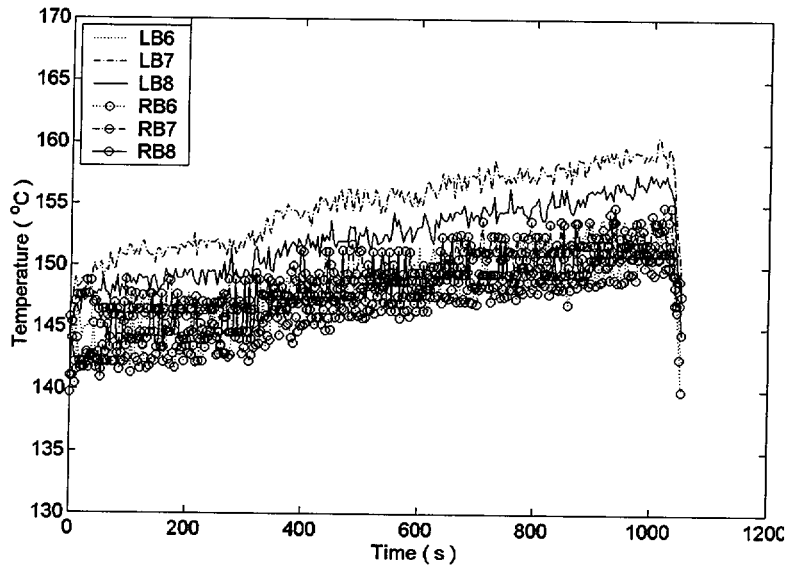

Figure C.19.3. Embedded thermocouple data in CHF-designed block (overall)

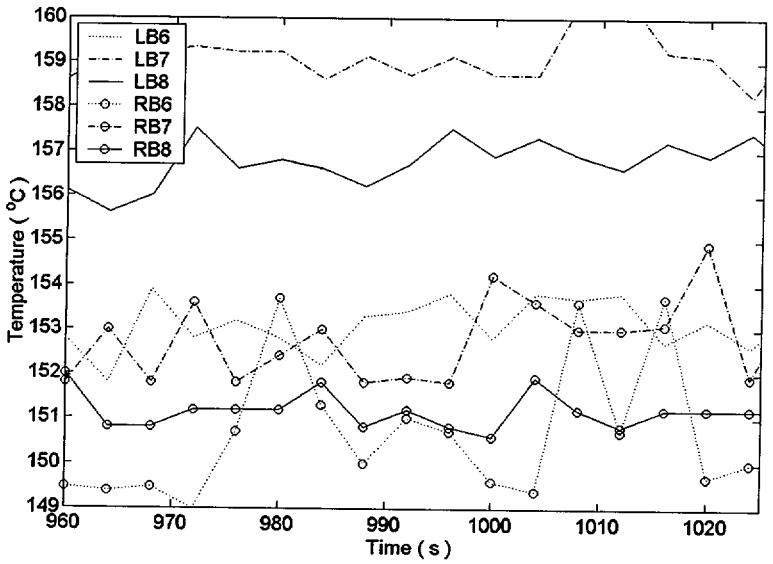

Figure C.19.4. Embedded thermocouple data in CHF-designed block (detail)

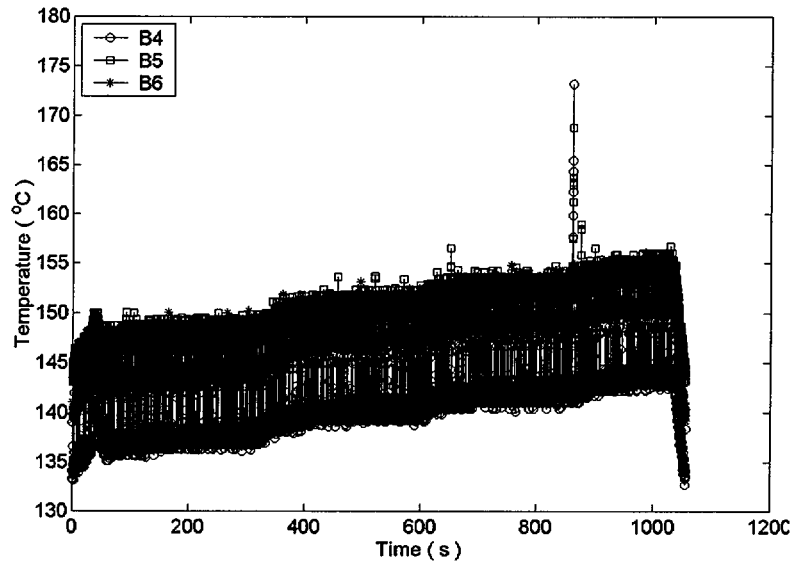

Figure C.19.5. Surface thermocouple data in CHF-designed block (overall)

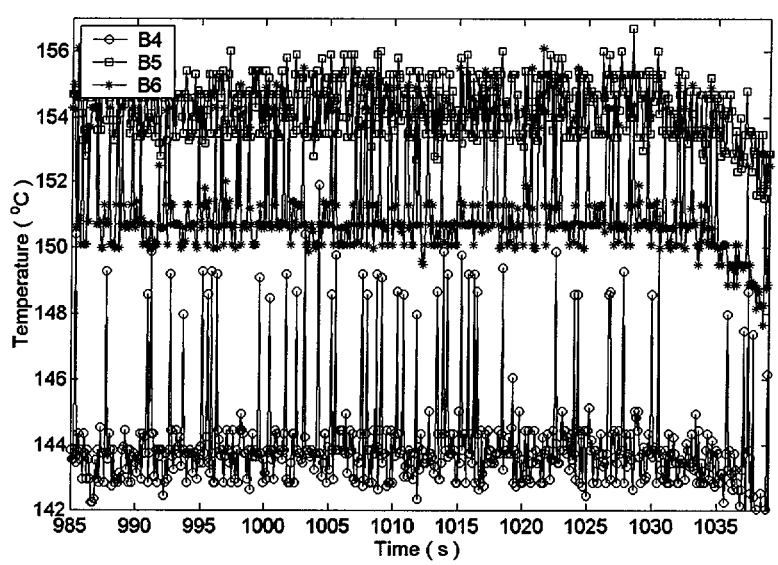

Figure C.19.6. Surface thermocouple data in CHF-designed block (detail)

Run #20

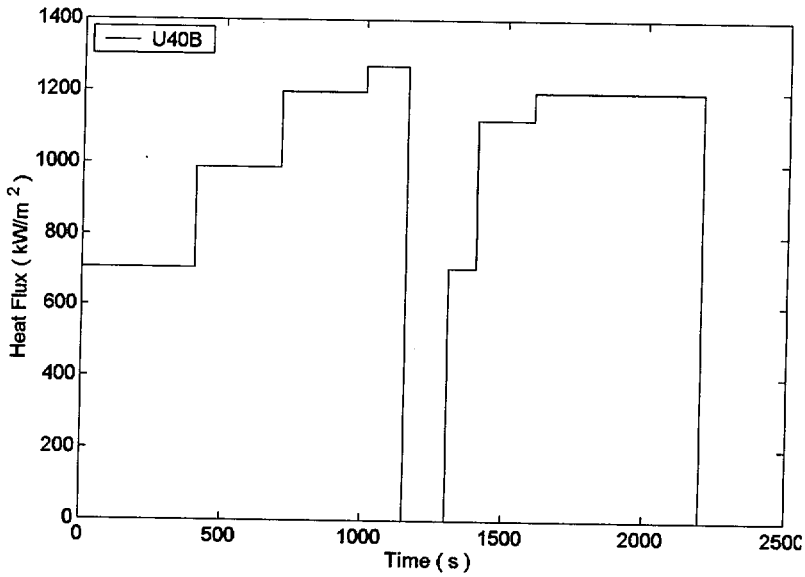

Figure C.20.1. Power history (heat flux) in the CHF-designed block C

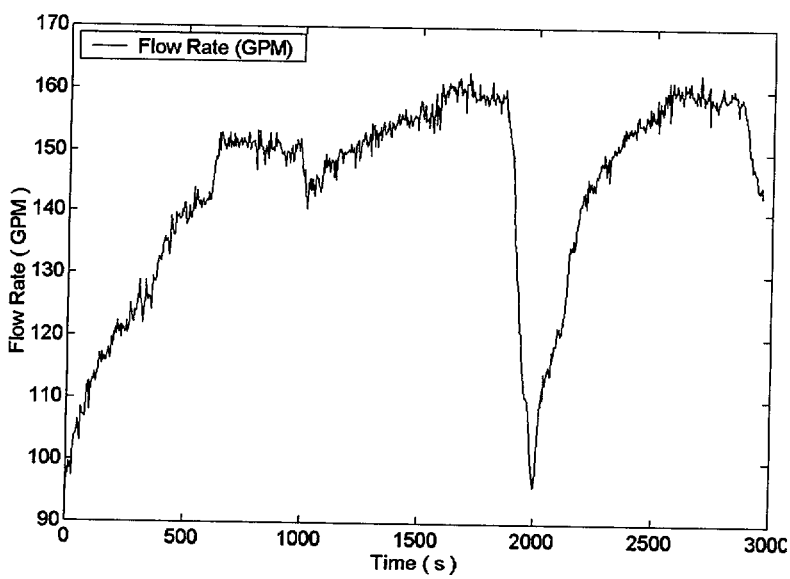

Figure C.20.2. Flow rate measurement

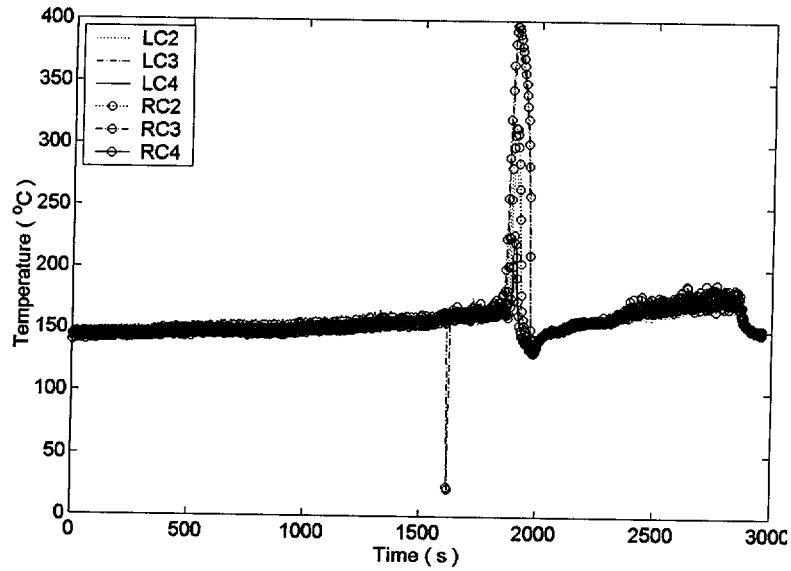

Figure C.20.3. Embedded thermocouple data in CHF-designed block (overall)

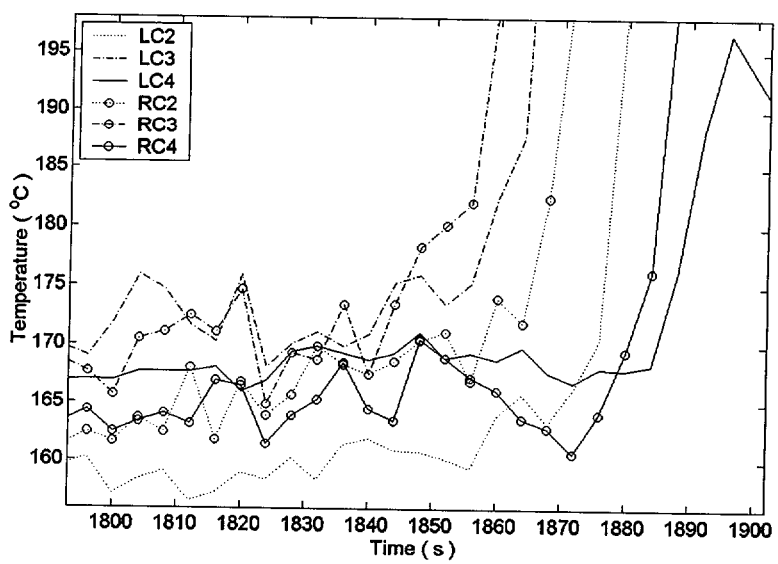

Figure C.20.4. Embedded thermocouple data in CHF-designed block (excursion)

Run #21

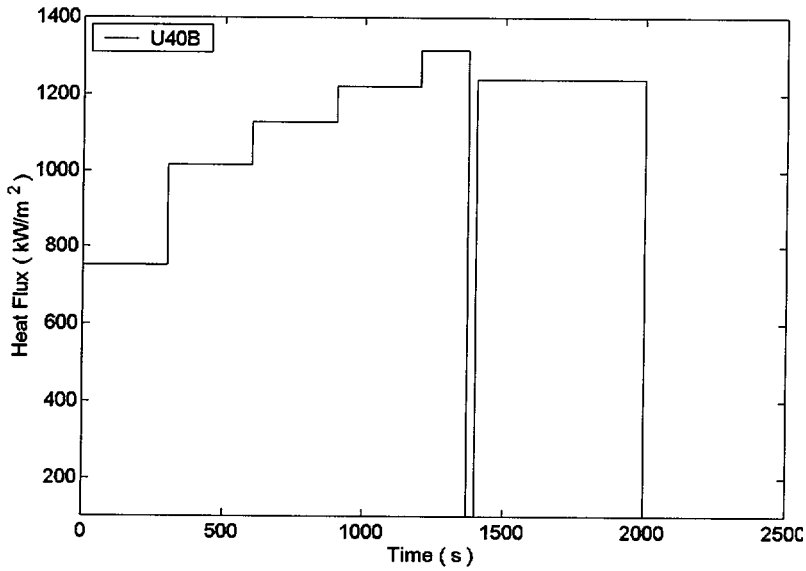

Figure C.21.1. Power history (heat flux) in the CHF-designed block C

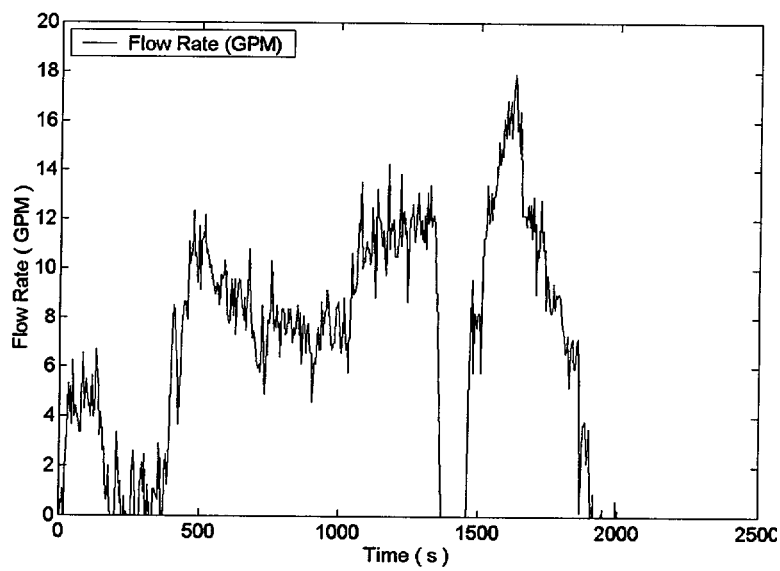

Figure C.21.2. Flow rate measurement

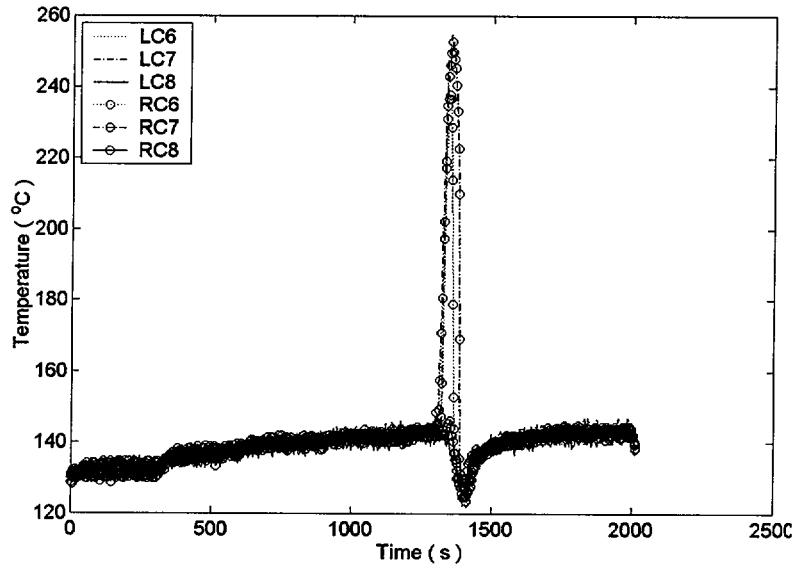

Figure C.21.3. Embedded thermocouple data in CHF-designed block (overall)

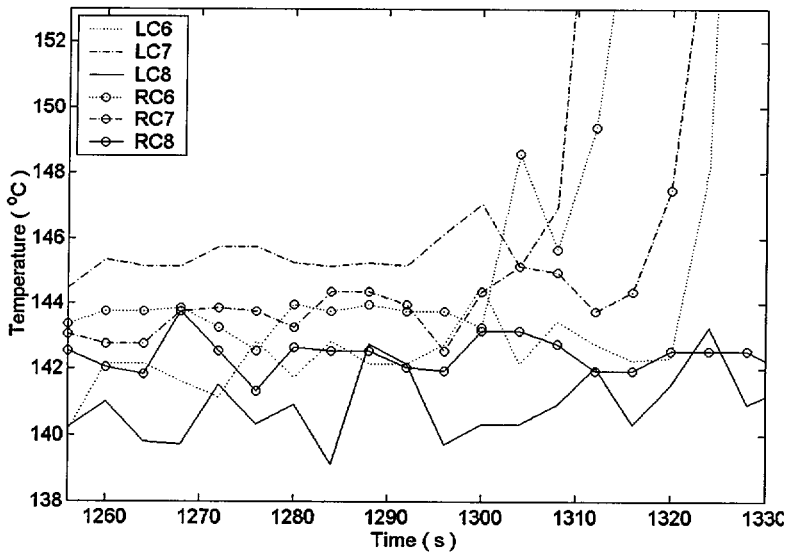

Figure C.21.4. Embedded thermocouple data in CHF-designed block (excursion)

Run #22

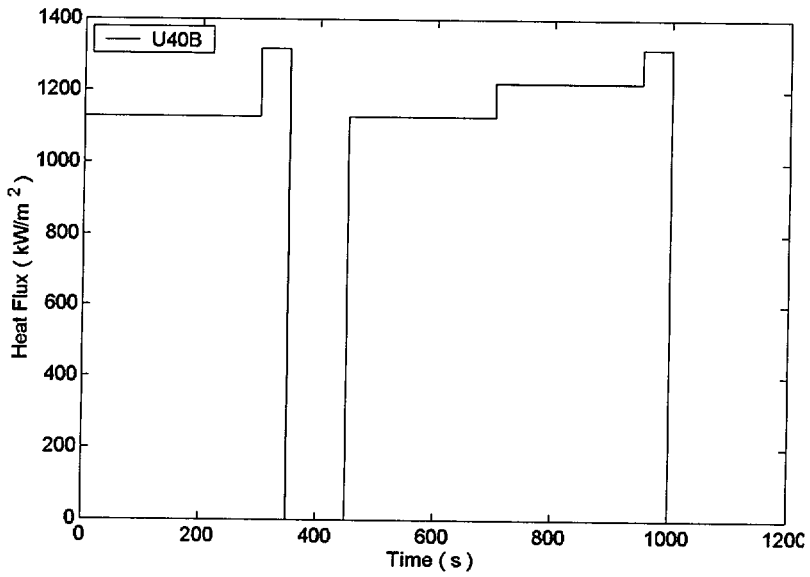

Figure C.22.1. Power history (heat flux) in the CHF-designed block C

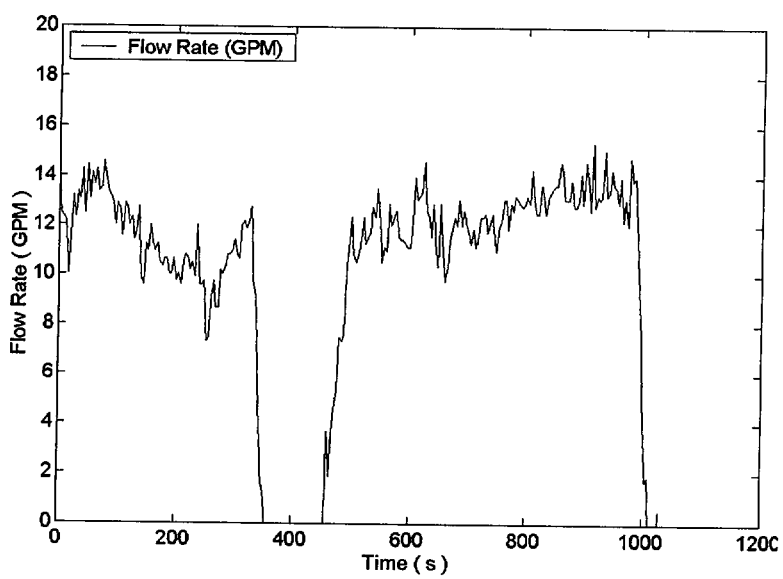

Figure C.22.2. Flow rate measurement

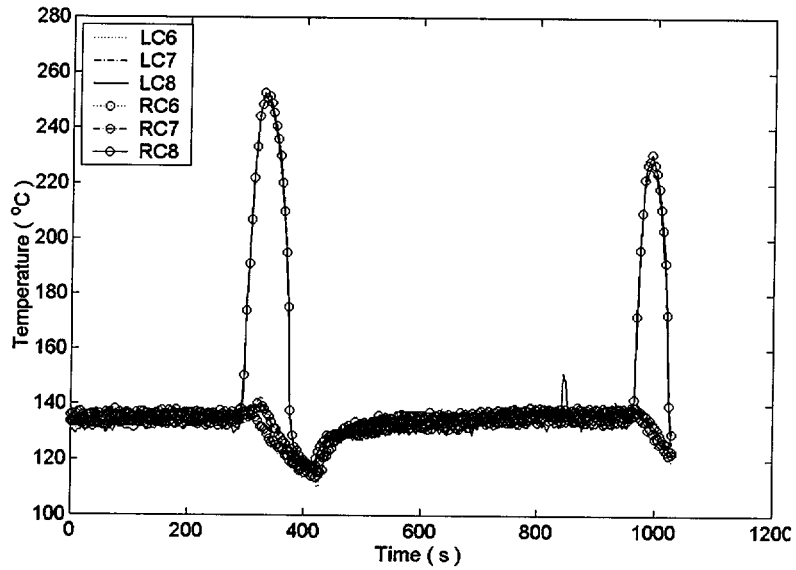

Figure C.22.3. Embedded thermocouple data in CHF-designed block (overall)

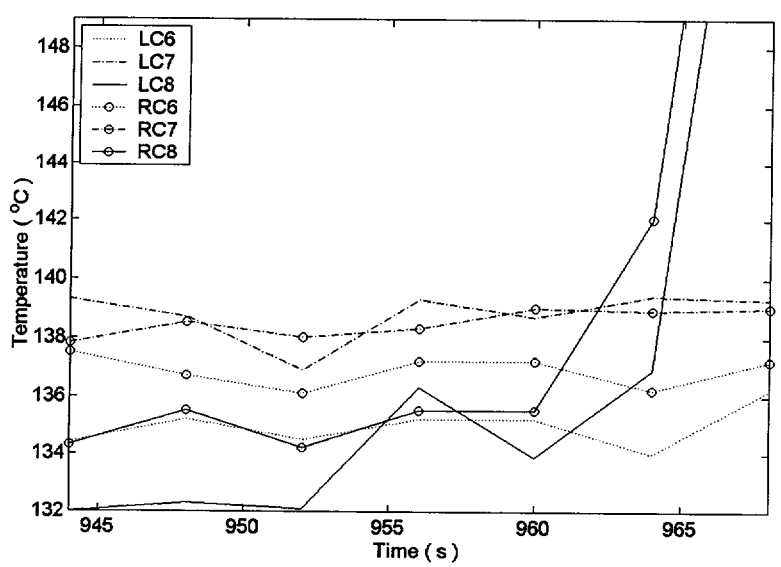

Figure C.22.4. Embedded thermocouple data in CHF-designed block (excursion)

Run #23

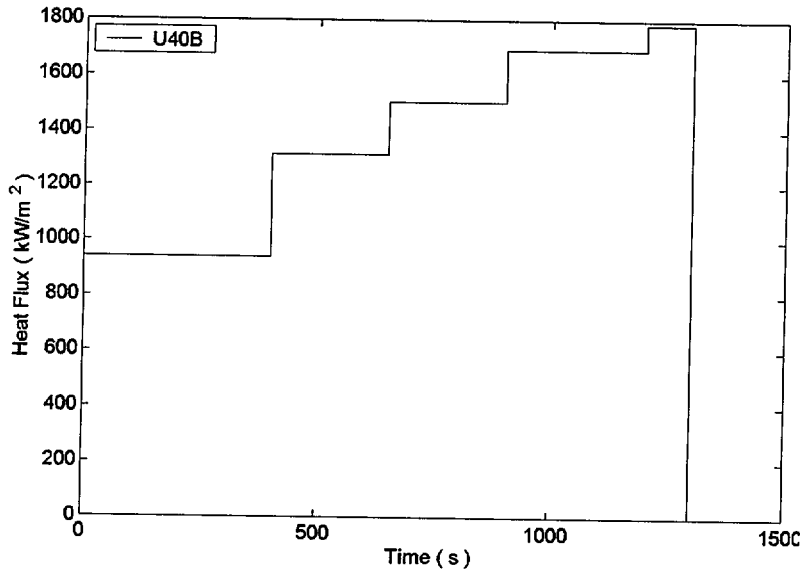

Figure C.23.1. Power history (heat flux) in the CHF-designed block C

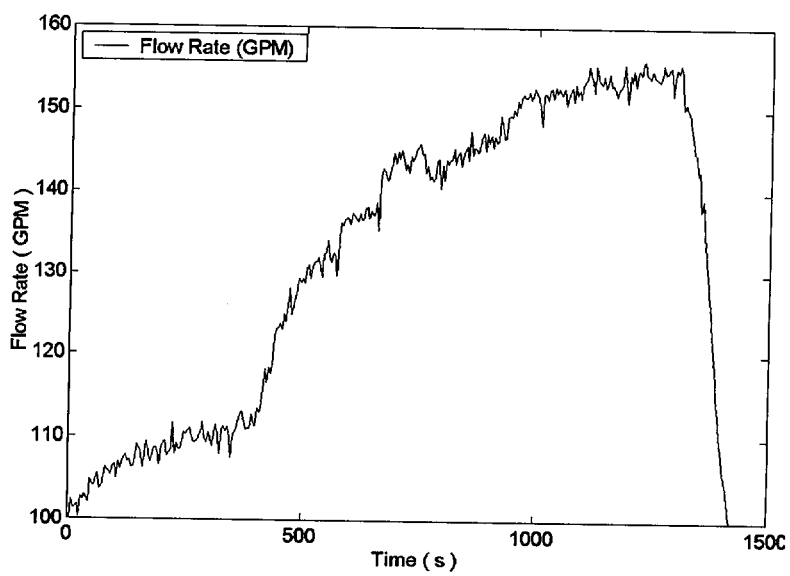

Figure C.23.2. Flow rate measurement

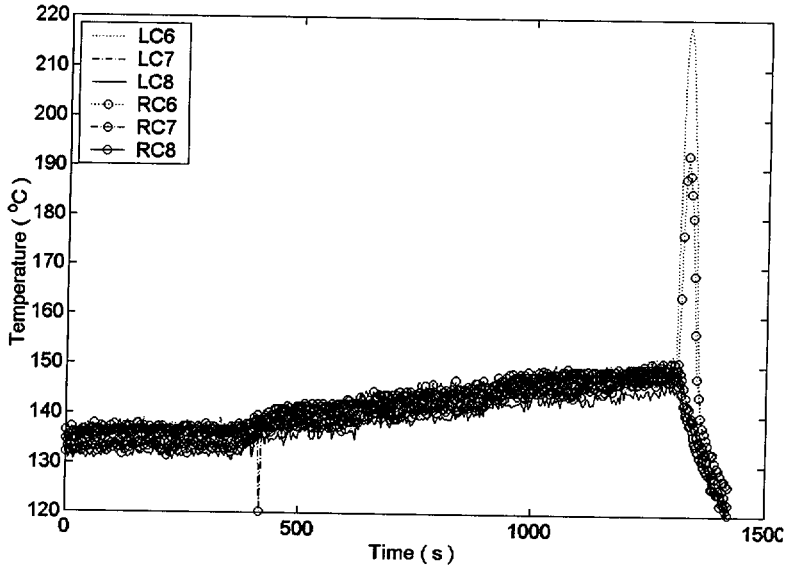

Figure C.23.3. Embedded thermocouple data in CHF-designed block (overall)

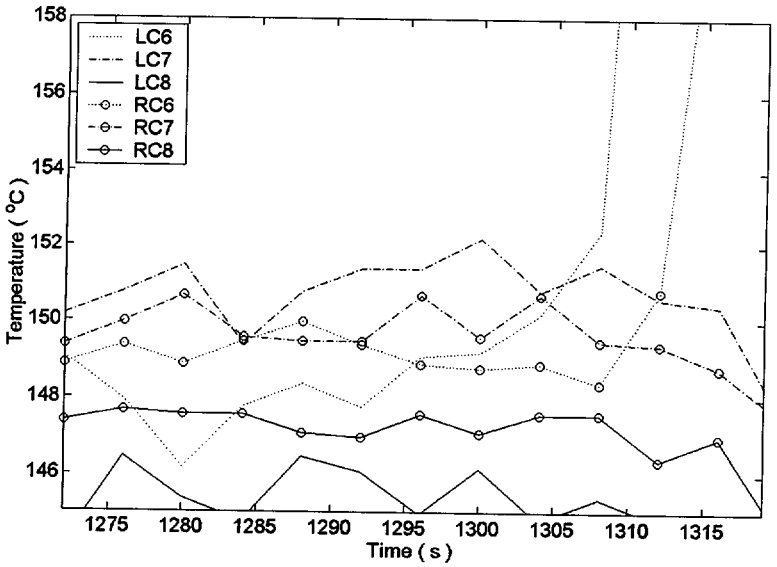

Figure C.23.4. Embedded thermocouple data in CHF-designed block (excursion)

Run #24

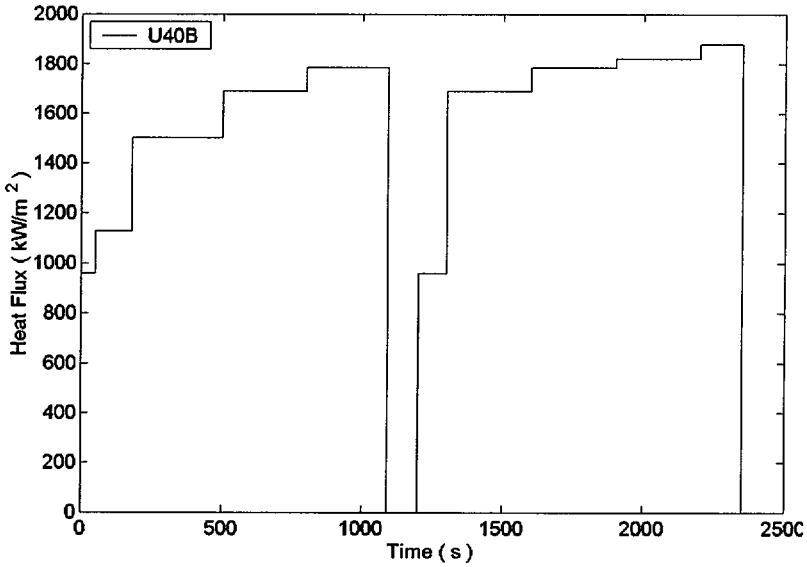

Figure C.24.1. Power history (heat flux) in the CHF-designed block C

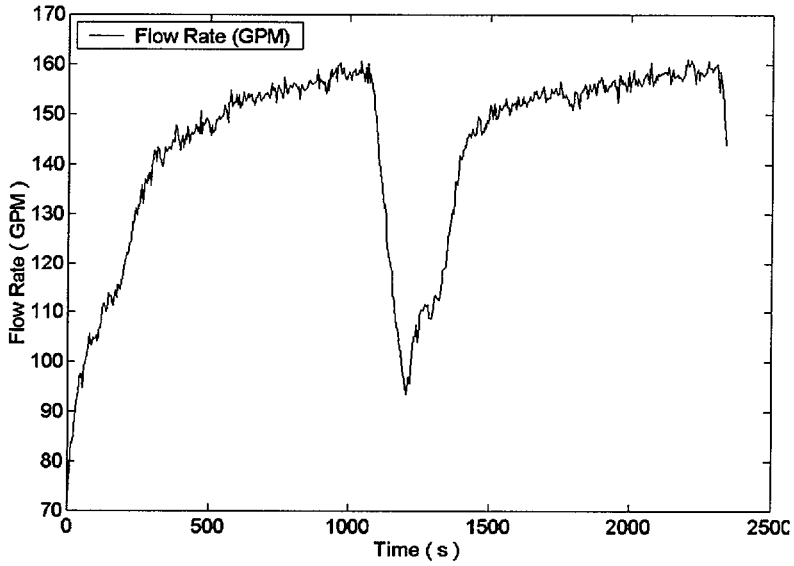

Figure C.24.2. Flow rate measurement

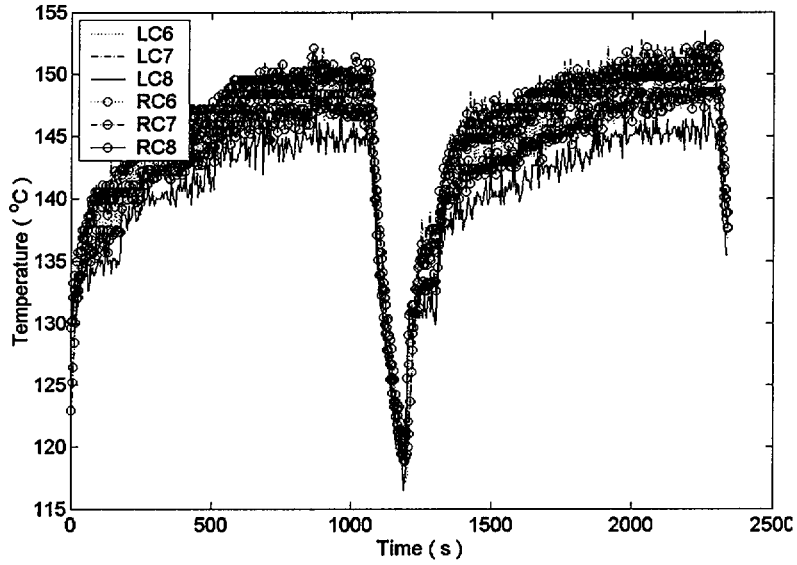

Figure C.24.3. Embedded thermocouple data in CHF-designed block (overall)

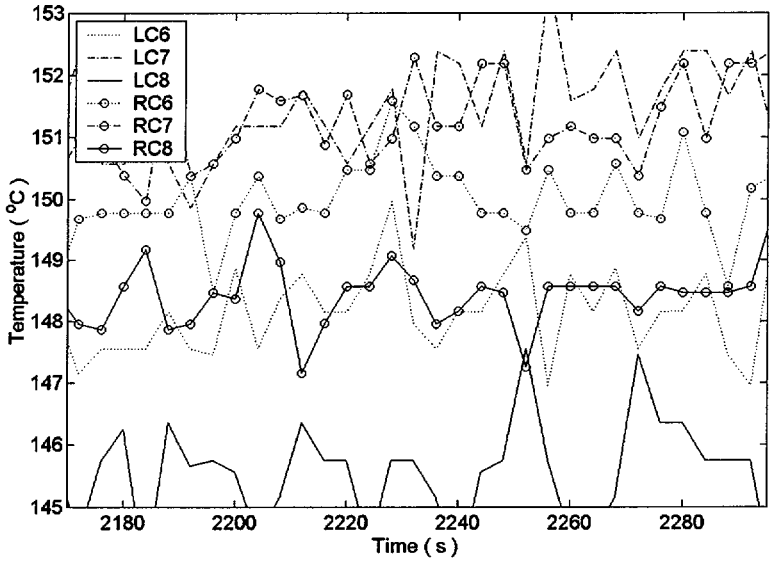

Figure C.24.4. Embedded thermocouple data in CHF-designed block (excursion)

Run #25

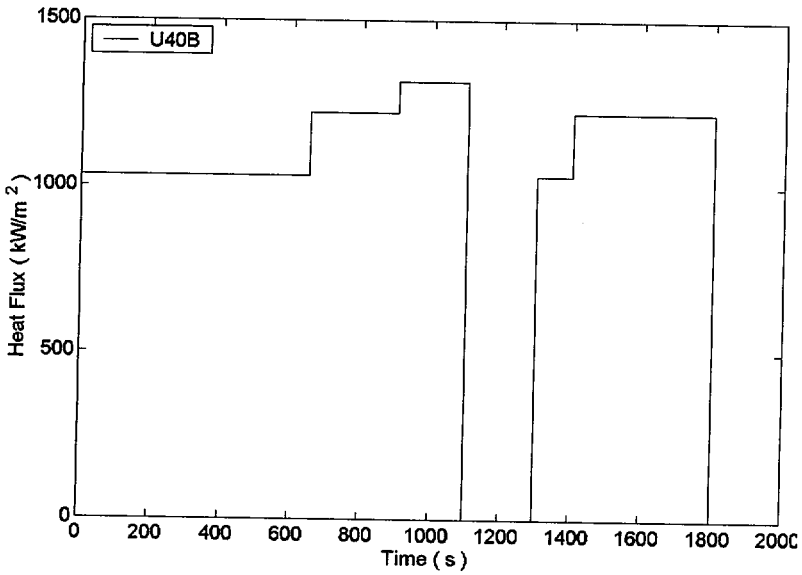

Figure C.25.1. Power history (heat flux) in the CHF-designed block C

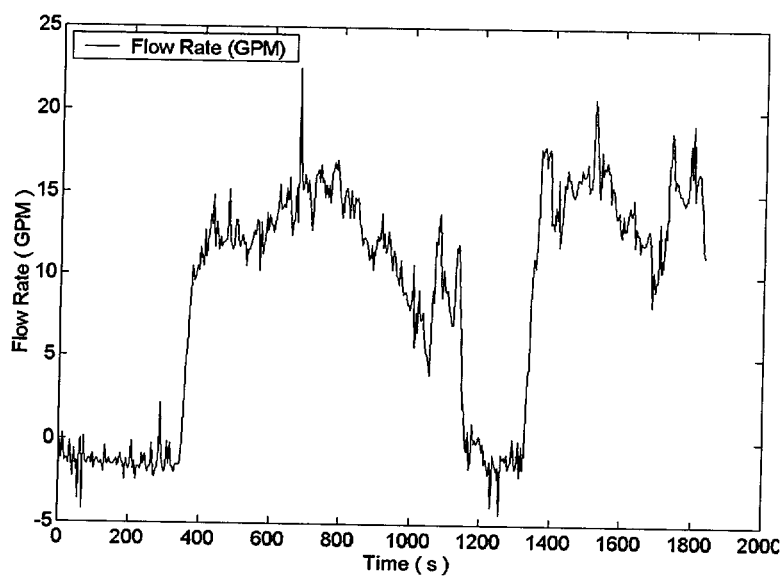

Figure C.25.2. Flow rate measurement

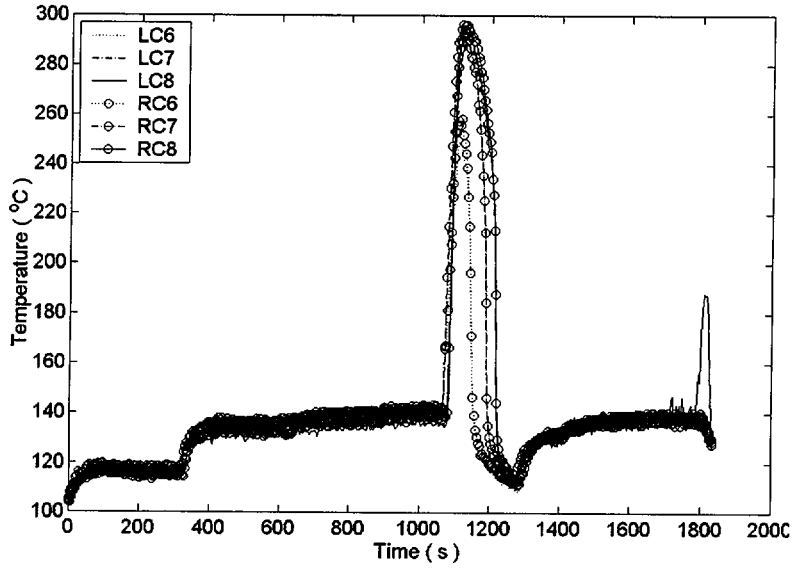

Figure C.25.3. Embedded thermocouple data in CHF-designed block (overall)

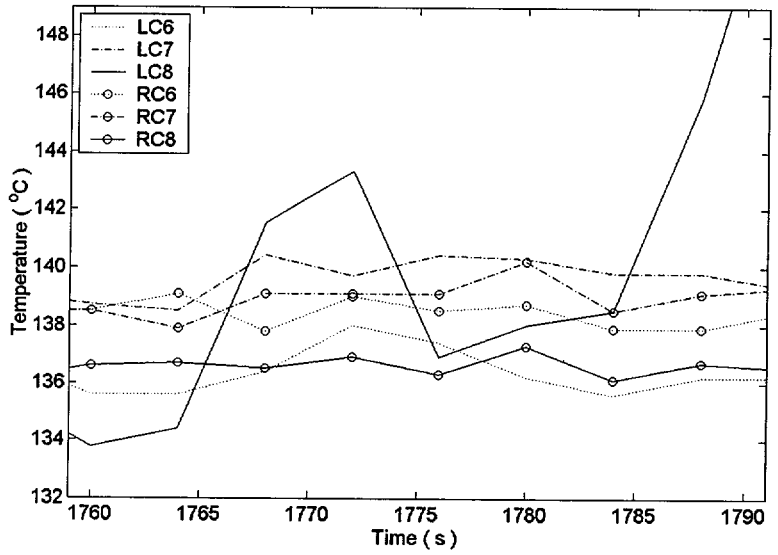

Figure C.25.4. Embedded thermocouple data in CHF-designed block (excursion)

Run #26

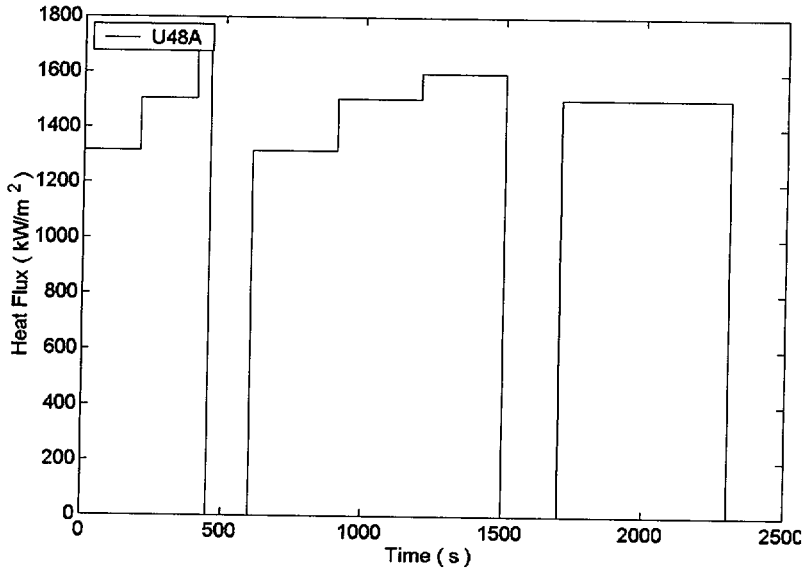

Figure C.26.1. Power history (heat flux) in the CHF-designed block C

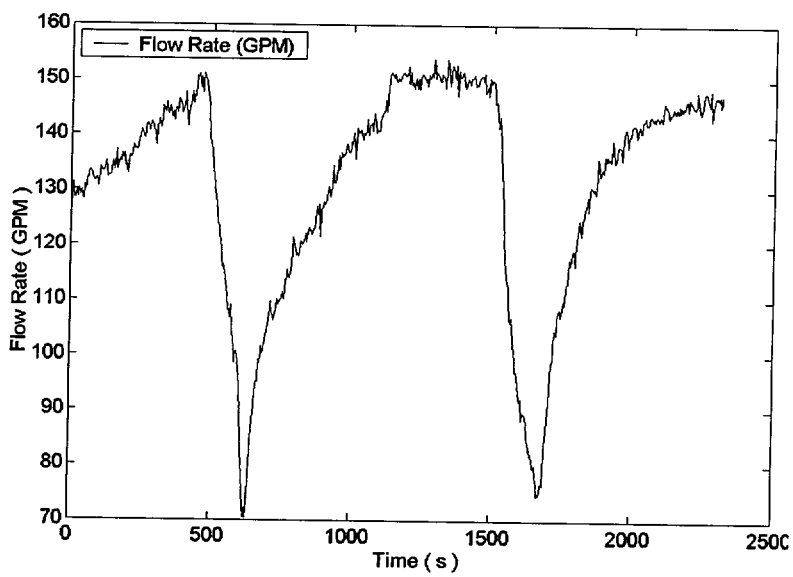

Figure C.26.2. Flow rate measurement

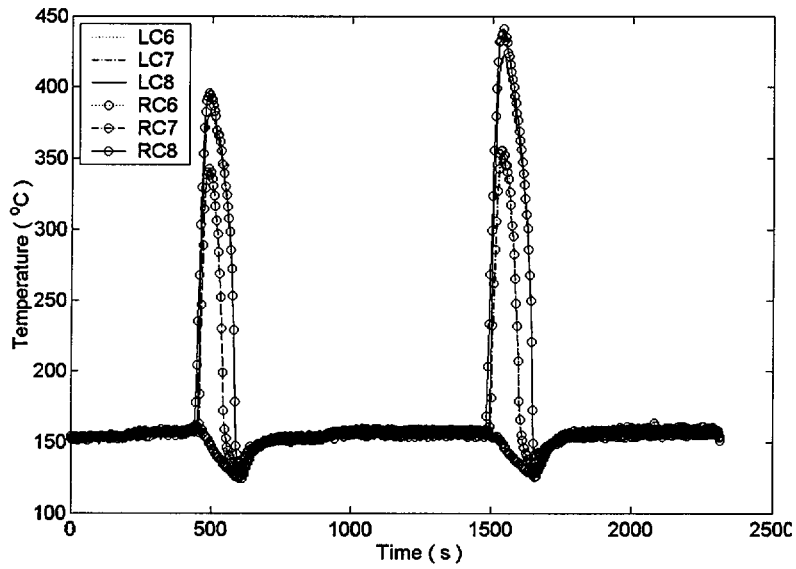

Figure C.26.3. Embedded thermocouple data in CHF-designed block (overall)

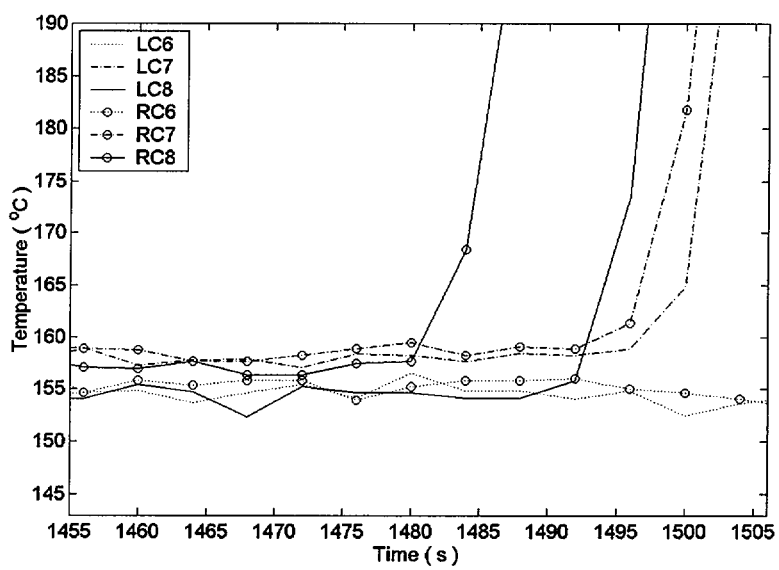

Figure C.26.4. Embedded thermocouple data in CHF-designed block (excursion)

Run #27

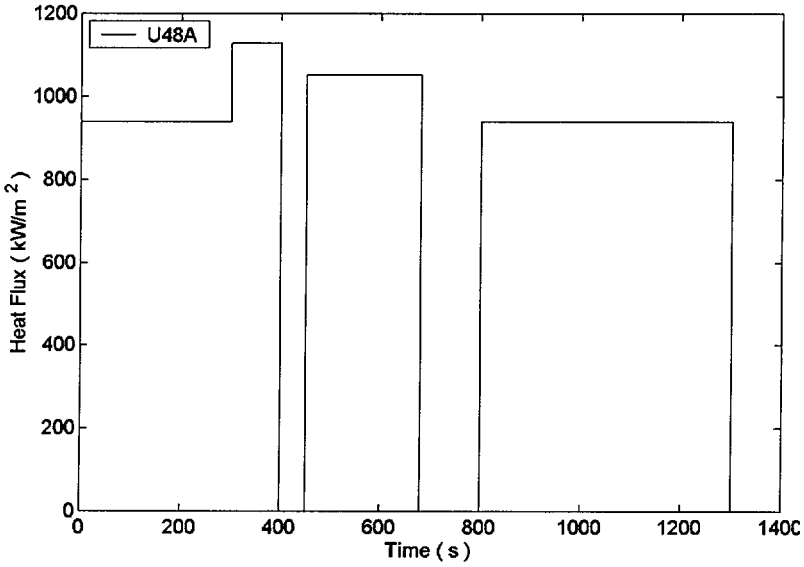

Figure C.27.1. Power history (heat flux) in the CHF-designed block C

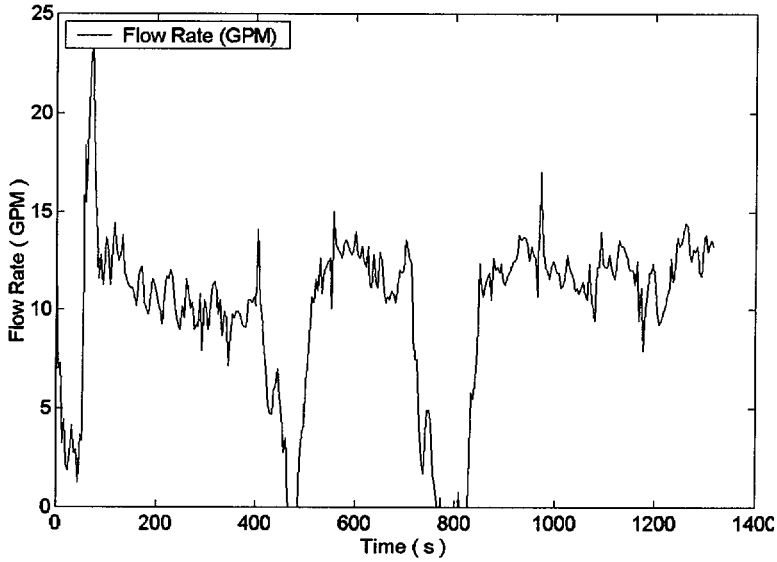

Figure C.27.2. Flow rate measurement

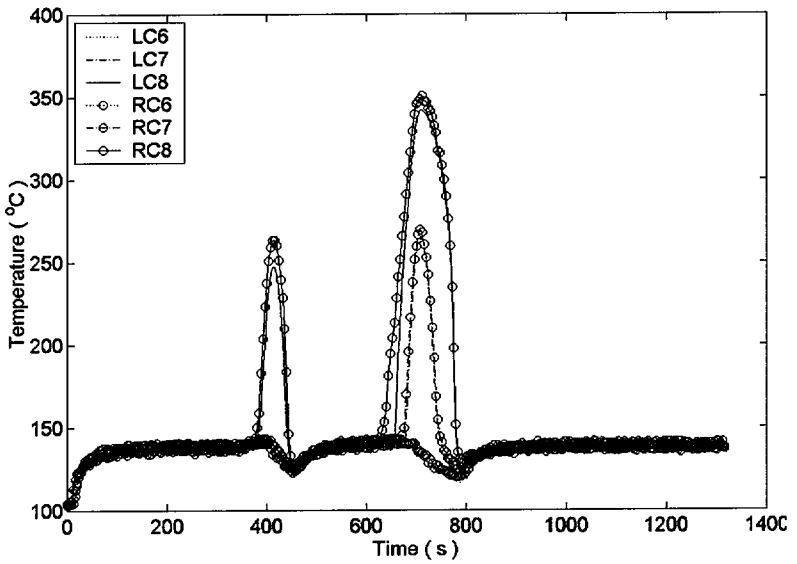

Figure C.27.3. Embedded thermocouple data in CHF-designed block (overall)

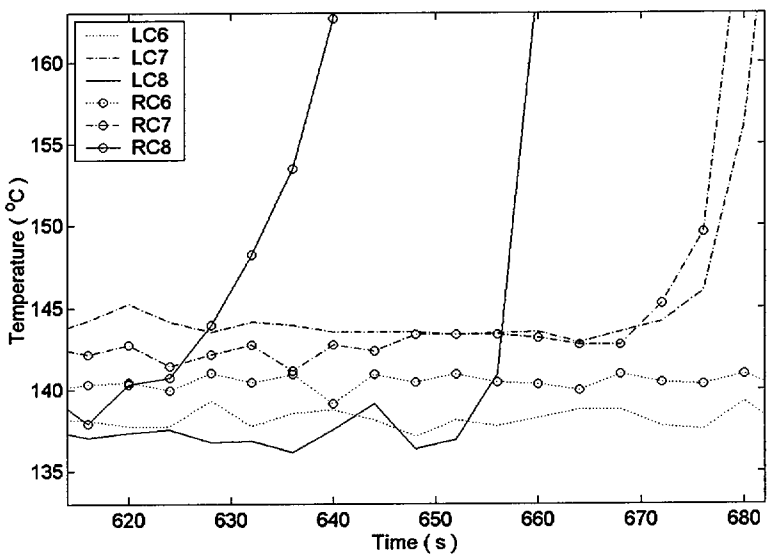

Figure C.27.4. Embedded thermocouple data in CHF-designed block (excursion)

Run #28

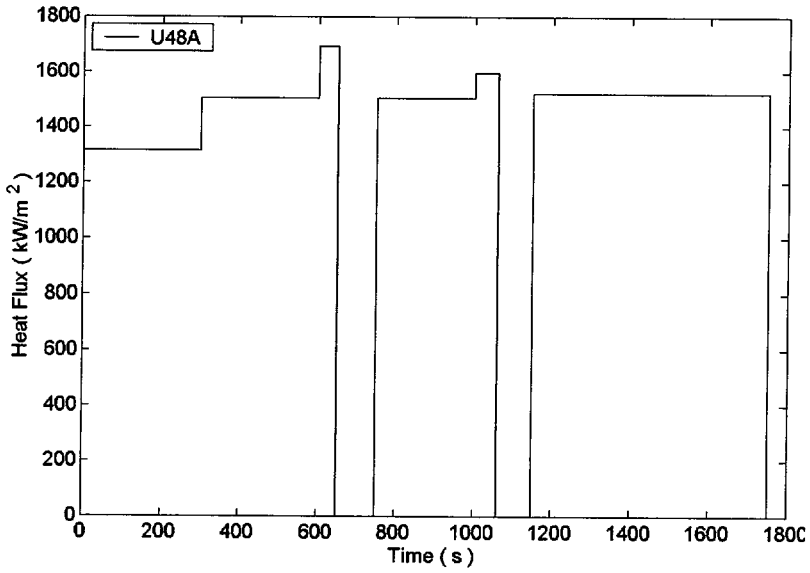

Figure C.28.1. Power history (heat flux) in the CHF-designed block C

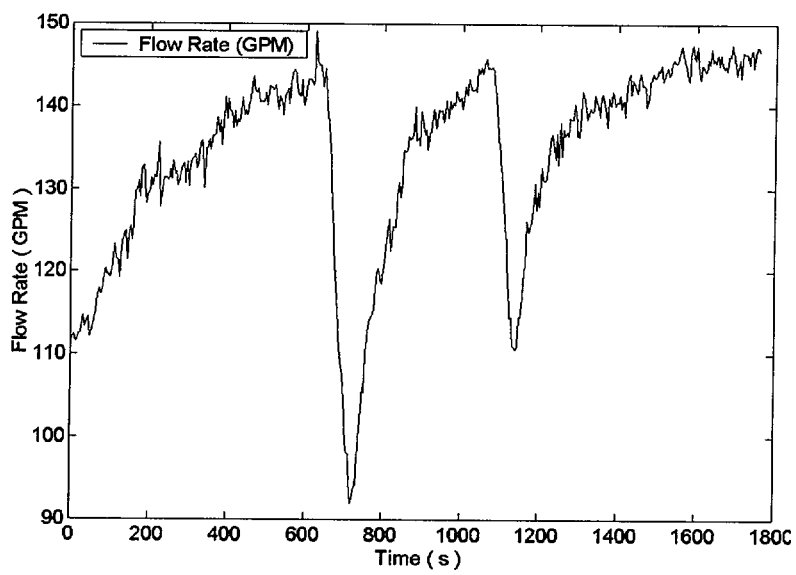

Figure C.28.2. Flow rate measurement

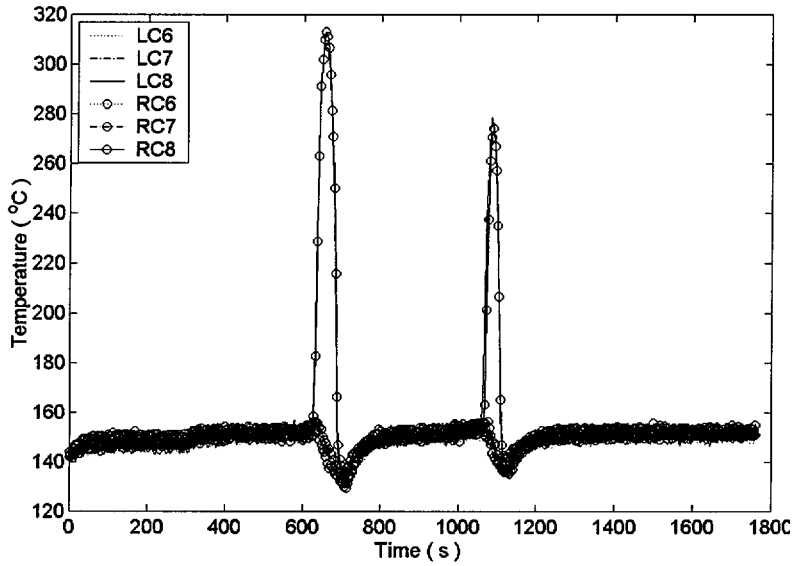

Figure C.28.3. Embedded thermocouple data in CHF-designed block (overall)

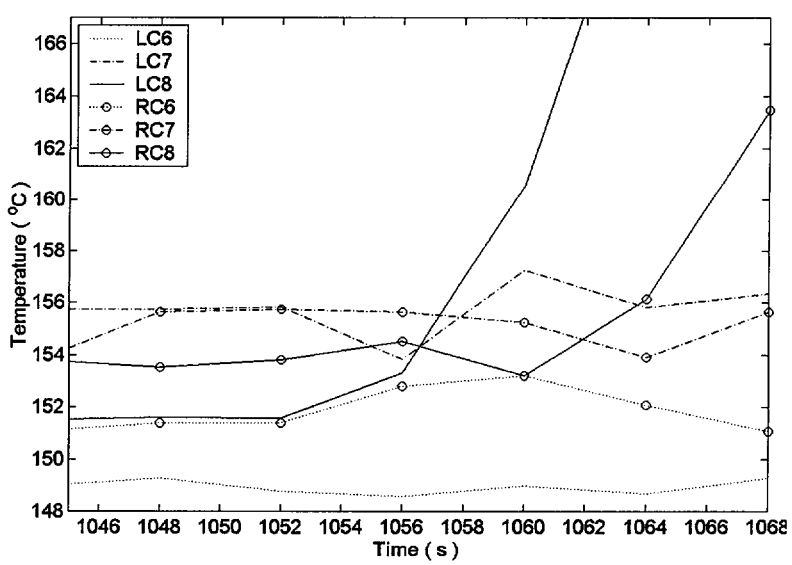

Figure C.28.4. Embedded thermocouple data in CHF-designed block (excursion)